NITROGEN CYCLING AND TRACE GAS DYNAMICS IN SHALLOW COASTAL AQUIFERS

by

CHARLES A. SCHUTTE

(Under the Direction of Samantha Joye)

ABSTRACT

Since the industrial revolution, human activity has doubled the amount of carbon in Earth's atmosphere and increased the rate of nitrogen supply to its biosphere by 40%. As a result, the climate is warming, sea level is rising, and fresh and saltwater resources are being threatened by eutrophication. Coastal areas are among the most vulnerable to these environmental challenges, and are economically critical zones that support tourism, fisheries, and half of the world's population. Primary production in coastal waters tends to be nitrogen limited, so anthropogenic nitrogen inputs results in eutrophication and degraded coastal water quality. Groundwater discharge is the dominant source of nitrogen to the South Atlantic Bight and rivals riverine nitrogen loading in many coastal ecosystems globally. However, groundwater must transit coastal aquifers prior to discharge where microbial communities have the potential to remove bioavailable nitrogen via coupled nitrification and denitrification or anammox. This microbial activity also generates methane and nitrous oxide, which are potent greenhouse gases. Thus, coastal groundwater influences both water quality and atmospheric chemistry.

The goal of this work was to quantify patterns and rates of microbial processes in shallow coastal aquifers that contribute to the production and consumption of bioavailable nitrogen and the greenhouse gases nitrous oxide and methane. High nitrification rates (0.78 ± 0.26 mmol m^{-2} day^{-1}) were found in shallow beach sand on a barrier island in coastal Georgia, USA. High nitrous oxide concentrations were also observed at this location (median = 282 nM, n = 32). Nitrous oxide production was supported by a nitrate loss rate of 11 mmol m^{-2} day^{-1}, which in turn, was too high to be supported by the observed nitrification rate alone, suggesting that nitrogen fixation was also important at this site. A hotspot of methane was observed in the freshwater lens near the center of Cabretta Island (median = 587 μM) supported by high rates of methanogenesis (22.2 ±10.6 mmol m^{-2} day^{-1}). However, most of this methane was consumed before it could be exported to the ocean due to active methanotrophy (18 ± 2.1 mmol m^{-2} day^{-1}) in surficial beach sand. Finally, submarine groundwater discharge was shown to export roughly the same quantity of greenhouse gases from salt marsh soils as direct efflux to the atmosphere, the only export pathway recognized previously in the literature.

INDEX WORDS: nitrification, denitrification, coastal aquifer, permeable sediment, beach, barrier island, groundwater discharge, greenhouse gas, nitrous oxide, methane

NITROGEN CYCLING AND TRACE GAS DYNAMICS IN SHALLOW COASTAL AQUIFERS

by

CHARLES A. SCHUTTE

B.S., The University of North Carolina at Chapel Hill, 2007

A Dissertation Submitted to the Graduate Faculty of The University of Georgia in Partial Fulfillment of the Requirements for the Degree

DOCTOR OF PHILOSOPHY

ATHENS, GEORGIA

2014

NITROGEN CYCLING AND TRACE GAS DYNAMICS IN SHALLOW COASTAL AQUIFERS

by

CHARLES A. SCHUTTE

Major Professor: Samantha B. Joye

Committee: Christof Meile
Mary Ann Moran
Alicia Wilson
Willard Moore
Bess Ward

Electronic Version Approved:

Julie Coffield
Interim Dean of the Graduate School
The University of Georgia
December 2014

DEDICATION

This work is dedicated to my parents, Brian and Deb Schutte, who inspired me to be a scientist.

ACKNOWLEDGEMENTS

My sincere thanks go to the following people, without whom this work would not have been possible:

- Dr. Virginia Schutte, Dr. Brian Schutte, Dr. Deb Schutte, Adelaide Schutte, and the rest of my family and friends for making sure that I am a person as well as a scientist.
- My advisor, Dr. Mandy Joye, for the opportunities she provided and for the freedom and support to pursue my own ideas.
- My committee, Dr. Christof Meile, Dr. Mary Ann Moran, Dr. Alicia Wilson, Dr. Billy Moore, and Dr. Bess Ward, for their excellent exam questions that I still ponder.
- Kim Hunter for her endless patience, even on Monday mornings, and for showing me how to hold a pipet.
- Dr. Marshall Bowles for taking me under his wing.
- Dr. Vladimir Samarkin for showing me that everything is possible.
- Daniel Saucedo for making me feel welcome on the island.
- All of the employees of the University of Georgia Marine Institute and the Georgia Coastal Ecosystems LTER for their logistical and moral support.
- All of the organizations that funded this work: the U.S. EPA, NSF, the Georgia Coastal Ecosystems LTER, and the UGA Graduate School.

Finally, I need to point out that Chapters 2-5 of this volume will be submitted for publication to scientific journals. Each of these manuscripts contains work that was done by my coauthors. In particular, the groundwater flow model presented in Chapter 2 and discussed in Chapters 3 and 4 was created by Tyler Evans at the University of South Carolina.

TABLE OF CONTENTS

Page

CHAPTER 1

INTRODUCTION AND LITERATURE REVIEW

Humans have created a massive disturbance of the global nitrogen cycle through industrial nitrogen fixation and fossil fuel burning, together amounting to 40% of the total nitrogen flux into the global biosphere each year [*Galloway et al.*, 2004]. Nitrogen-limited ecosystems such as estuaries and the coastal ocean are the most heavily impacted by this perturbation [*Howarth*, 1988] because relief from nitrogen limitation causes eutrophication, algal blooms, hypoxia, and fish kills [*Nixon*, 1995]. Sources of nitrogen to estuaries and the coastal ocean include riverine loading, atmospheric deposition, and submarine groundwater discharge (SGD). SGD is the dominant nitrogen source to the South Atlantic Bight in the southeastern United States [*Moore et al.*, 2002] and rivals riverine nitrogen loading at many other locations globally [*Slomp and Van Cappellen*, 2004].

Both globally [*Schlesinger*, 2009], and in coastal sediments [*Joye and Anderson*, 2008], the dominant sinks for bioavailable nitrogen are the microbial processes of denitrification and anammox. These processes reduce nitrate (NO_3^-) and nitrite (NO_2^-), respectively, to dinitrogen gas (N_2) and are active under anoxic conditions, although aerobic denitrification is also possible, particularly in permeable sediments [*Gao et al.*, 2010; *Rao et al.*, 2007]. Most coastal sediments are anoxic and highly reduced, trapping inorganic nitrogen in the form of ammonium (NH_4^+) [*Kroeger et al.*, 2007] and making it unavailable for denitrification and anammox. These processes must be coupled with

nitrification, the obligately aerobic process through which NH_4^+ is oxidized to NO_2^- and then NO_3^-. The coupling between nitrification and NO_3^- reduction processes is thought to be controlled by oxygen availability and is generally limited by the rate of oxygen and NO_3^- diffusion through the sediment [*Joye and Anderson*, 2008]. In permeable sediments like sand, however, high rates of porewater advection are driven by waves, tides, and interactions with bottom topography that generate pressure gradients within the sediment [*Huettel et al.*, 2014]. This porewater advection results in deep penetration of oxygen into the sediment [*Brotas et al.*, 1990; *de Beer et al.*, 2005] and oscillating redox conditions that accelerate coupled nitrification-denitrification in high permeability sediments [*Huettel et al.*, 2014] relative to other coastal sediment types [*Joye and Anderson*, 2008]. Therefore, high permeability, sandy coastal aquifers may act as efficient nitrogen sinks.

In **Chapter 2**, I explored the nitrogen cycling processes responsible for a hotspot of high porewater nitrate in the shallow aquifer on the upper beach of a barrier island in coastal Georgia, USA. I tested two hypotheses: 1) that deep oxygen penetration into the sand controlled nitrification rates, and 2) that beaches acted as natural nitrogen filters via tight coupling between nitrification and denitrification. To test these hypotheses, I recorded multiple high temporal resolution time series of in situ dissolved oxygen (DO) concentrations that extended over several months. These data revealed daily cycles in DO concentrations from near zero at night to near atmospheric saturation during the day. I then incubated beach sand across the observed range in DO concentrations to determine the influence of DO oscillations on rates of nitrogen cycling processes. Similar rates of nitrification and NO_3^- reduction via denitrification and/or anammox were present under oxic and anoxic conditions, respectively, indicating that the observed DO oscillations

coupled nitrogen oxidation and reduction processes and facilitated the removal of bioavailable nitrogen from beach groundwater.

Denitrification, nitrification, and dissimilatory nitrate reduction to ammonium (DNRA) all produce nitrous oxide (N_2O) as a byproduct. In **Chapter 3**, I further explored nitrogen cycling within this hotspot from the perspective of N_2O, which also exhibited extremely high concentrations at the same location where high NO_3^- concentrations were observed. I tested the hypothesis that beach sands were a nitrogen sink by using N_2O production as a proxy for bioavailable nitrogen removal. A hotspot of N_2O production was identified and three possible fates for this N_2O were investigated: in situ consumption, efflux to the atmosphere, and loss via groundwater discharge. A mass balance of these N_2O loss mechanisms was constructed in order to estimate the net N_2O production rate within the hotspot. Sand incubations indicted that very high rate of NO_3^- consumption drove the observed N_2O production, providing additional evidence that permeable barrier island sediments act as a nitrogen sink.

Nitrous oxide is also of interest because it is a potent greenhouse gas, meaning that any aquifer nitrogen sink may come at the expense of a source of N_2O to the atmosphere. Another strong greenhouse gas is methane (CH_4), which is produced primarily by microbial methanogenesis. This process is most active in anoxic, aquatic habitats [*Cicerone and Oremland*, 1988], making saturated, organic rich soils (e.g. marshes, rice paddies, landfills) the most important sites for CH_4 production globally [*Ciais et al.*, 2013]. Saline water can inhibit methanogenesis, so coastal environments are not thought of as significant CH_4 sources. However, groundwater discharge is the primary source of CH_4 to the coastal ocean [*Bugna et al.*, 1996; *Grunwald et al.*, 2009],

which drives much of the total marine CH_4 flux to the atmosphere [*Bange*, 2006]. This CH_4 is likely to be derived from aquifers in coastal uplands where a layer of fresh groundwater floats atop a layer of denser, saline groundwater [*Collins and Easley*, 1999]. These freshwater lenses form beneath barrier islands, which occupy 22,520 km of Earth's coastline [*Pilkey et al.*, 2009; *Stutz and Pilkey*, 2001], granting them the potential to be globally relevant sites of methanogenesis.

In **Chapter 4**, I investigated the processes that generated high CH_4 concentrations within the freshwater lens of the barrier island in order to test the hypotheses that 1) barrier islands export CH_4 to the atmosphere and/or coastal ocean, and 2) that the dominant fate for CH_4 produced within barrier islands was in situ consumption by methanotrophic microorganisms. I surveyed rates of methanogenesis and methanotrophy at multiple depths across the island center, and measured rates of CH_4 efflux to the atmosphere. High rates of methanogenesis within the fresh water lens were balanced by high rates of methanotrophy in shallow beach sands. The residence time of groundwater within an aquifer determined the exposure of dissolved CH_4 to methanotrophy. Therefore, the combination of groundwater residence time and methanotrophy controlled the groundwater-derived CH_4 flux to the coastal ocean.

In the southeastern United States, salt marshes dominate the coastal landscape behind barrier islands. These wetlands have gained attention recently for their ability to sequester "blue carbon" in soil, capturing carbon that would otherwise enter the atmosphere as carbon dioxide (CO_2), the primary greenhouse gas driving climate change. This carbon is captured through sedimentation of organic carbon-rich suspended solids from inundating tidal waters and high rates of net primary production that converts

atmospheric CO_2 into organic carbon [*Chmura et al.*, 2003; *McLeod et al.*, 2011]. The greenhouse gases CO_2, CH_4, and N_2O are all produced in salt marsh soils, however, and may be exported to the atmosphere, negating some of the climate benefit of carbon storage in marsh soils. Submarine groundwater discharge is an overlooked but potentially important second pathway for export of these gases from the marsh system.

In **Chapter 5**, I estimated the volumetric groundwater flux from four salt marsh sites on or around Sapelo Island, Georgia, USA using a radium mass balance approach. Marsh groundwater was enriched in radium relative to water in the tidal creeks flowing through these systems, so radium could be used as a tracer of groundwater discharge. The ratios of two radium isotopes were used to identify the groundwater monitoring wells at each site that sampled the aquifer that was discharging into the adjacent tidal creek. Dissolved inorganic carbon (DIC), CH_4, and N_2O concentrations in the groundwater from these wells was multiplied by the volumetric groundwater discharge to calculate the total groundwater-derived flux of these greenhouse gases, and these fluxes were then normalized to the area of salt marsh at each site. A comparison of groundwater-derived greenhouse gas fluxes with direct fluxes of these gases from the marsh surface to the atmosphere revealed that the groundwater-derived flux was an important pathway for export of these greenhouse gases from salt marsh ecosystems.

LITERATURE CITED

Bange, H. W. (2006), Nitrous oxide and methane in European coastal waters, *Estuarine Coastal and Shelf Science*, *70*(3), 361-374.

Brotas, V., A. Amorim-Ferreira, C. Vale, and F. Catarino (1990), Oxygen profiles in intertidal sediments of Ria Formosa (S. Portugal), *Hydrobiologia*, *207*(1), 123-130.

Bugna, G. C., J. P. Chanton, J. E. Cable, W. C. Burnett, and P. H. Cable (1996), The importance of groundwater discharge to the methane budgets of nearshore and continental shelf waters of the northeastern Gulf of Mexico, *Geochimica et Cosmochimica Acta*, *60*(23), 4735-4746.

Chmura, G. L., S. C. Anisfeld, D. R. Cahoon, and J. C. Lynch (2003), Global carbon sequestration in tidal, saline wetland soils, *Global Biogeochemical Cycles*, *17*(4).

Ciais, P., et al. (2013), Carbon and other biogeochemical cycles, in *Climate Change 2013: The Physical Science Basis. Contribution of Working Group I to the Fifth Assessment Report of the Intergovernmental Panel on Climate Change*, edited by T. F. Stocker, D. Qin, G.-K. Plattner, M. Tignor, S. K. Allen, J. Boschung, A. Nauels, Y. Xia, V. Bex and P. M. Midgley, Cambridge University Press, Cambridge, United Kingdom and New York, NY, USA.

Cicerone, R. J., and R. S. Oremland (1988), Biogeochemical aspects of atmospheric methane, *Global Biogeochemical Cycles*, *2*(4), 299-327.

Collins, W. H., and D. H. Easley (1999), Fresh-water lens formation in an unconfined barrier-island aquifer, *Journal of the American Water Resources Association*, *35*(1), 1-21.

de Beer, D., F. Wenzhöfer, T. G. Ferdelman, S. E. Boehme, M. Huettel, J. E. E. van Beusekom, M. E. Böttcher, N. Musat, and N. Dubilier (2005), Transport and

mineralization rates in north sea sandy intertidal sediments, Sylt-Rømø basin, Wadden sea, *Limnology and Oceanography*, *50*(1), 113-127.

Galloway, J. N., et al. (2004), Nitrogen cycles: past, present, and future, *Biogeochemistry*, *70*(2), 153-226.

Gao, H., F. Schreiber, G. Collins, M. M. Jensen, J. E. Kostka, G. Lavik, D. de Beer, H.-Y. Zhou, and M. M. Kuypers (2010), Aerobic denitrification in permeable Wadden Sea sediments, *The ISME Journal*, *4*, 417-426.

Grunwald, M., O. Dellwig, M. Beck, J. W. Dippner, J. A. Freund, C. Kohlmeier, B. Schnetger, and H. Brumsack (2009), Methane in the southern North Sea: sources, spatial distribution and budgets, *Estuarine Coastal and Shelf Science*, *81*(4), 445-456.

Howarth, R. W. (1988), Nutrient limitation of net primary production in marine ecosystems, *Annual Review of Ecology and Systematics*, *19*, 89-110.

Huettel, M., P. Berg, and J. E. Kostka (2014), Benthic Exchange and Biogeochemical Cycling in Permeable Sediments, in *Annual Review of Marine Science, Vol 6*, edited by C. A. Carlson and S. J. Giovannoni, pp. 23-51.

Joye, S. B., and I. C. Anderson (2008), Nitrogen cycling in coastal sediments, in *Nitrogen in the Marine Environment, 2nd Edition*, edited by D. G. Capone, D. A. Bronk, M. R. Mulholland and E. J. Carpenter, pp. 686-902, Elsevier.

Kroeger, K. D., P. W. Swarzenski, W. J. Greenwood, and C. Reich (2007), Submarine groundwater discharge to Tampa Bay: nutrient fluxes and biogeochemistry of the coastal aquifer, *Marine Chemistry*, *104*(1), 85-97.

McLeod, E., G. L. Chmura, S. Bouillon, R. Salm, M. Bjork, C. M. Duarte, C. E. Lovelock, W. H. Schlesinger, and B. R. Silliman (2011), A blueprint for blue carbon: toward an improved understanding of the role of vegetated coastal habitats in sequestering CO_2, *Frontiers in Ecology and the Environment*, *9*(10), 552-560.

Moore, W. S., J. M. Krest, G. Taylor, E. Roggenstein, S. B. Joye, and R. Lee (2002), Thermal evidence of water exchange through a coastal aquifer: Implications for nutrient fluxes, *Geophysical Research Letters*, *29*(14), 1704.

Nixon, S. W. (1995), Coastal marine eutrophication: a definition, social causes, and future concerns, *Ophelia*, *41*, 199-219.

Pilkey, O. H., J. A. G. Cooper, and D. A. Lewis (2009), Global distribution and geomorphology of fetch-limited barrier islands, *Journal of Coastal Research*, *25*(4), 819-837.

Rao, A. M. F., M. J. McCarthy, W. S. Gardner, and R. A. Jahnke (2007), Respiration and denitrification in permeable continental shelf deposits on the South Atlantic Bight: rates of carbon and nitrogen cycling from sediment column experiments, *Continental Shelf Research*, *27*(13), 1801-1819.

Schlesinger, W. H. (2009), On the fate of anthropogenic nitrogen, *Proceedings of the National Academy of Sciences*, *106*(1), 203-208.

Slomp, C. P., and P. Van Cappellen (2004), Nutrient inputs to the coastal ocean through submarine groundwater discharge: controls and potential impact, *Journal of Hydrology*, *295*, 64-86.

Stutz, M. L., and O. H. Pilkey (2001), A review of global barrier island distribution, *Journal of Coastal Research* (Special Issue 34), 15-22.

CHAPTER 2

INTENSE NITROGEN CYCLING IN PERMEABLE INTERTIDAL SEDIMENT REVEALED BY A NITROUS OXIDE HOTSPOT [1]

[1] Schutte, C.A., A.M. Wilson, T. Evans, W.S. Moore, K.L. Casciotti, and S.B. Joye. To be submitted to

ABSTRACT

Approximately 40% of the total global rate of nitrogen fixation is the result of human activities, and most of this anthropogenic nitrogen is used to fertilize agricultural fields. Approximately 23% of the applied agricultural nitrogen is delivered to the coastal zone, often reducing water quality and driving eutrophication. Microbial nitrogen cycling in coastal sediments can mitigate eutrophication by removing bioavailable nitrogen. However, some of these processes generate nitrous oxide, a potent greenhouse gas, as a byproduct. Here we report the discovery of a nitrous oxide production hotspot in shallow barrier island sands. Nitrous oxide concentrations, production and consumption rates, vertical diffusion fluxes, and flux to the atmosphere were measured across triplicate depth profiles. Using a mass balance approach, rates of net nitrous oxide production were estimated to be 40 μmol m^{-2} day^{-1}. This production was driven by a hotspot of nitrate consumption that removed bioavailable nitrogen from the coastal environment at a rate of 10 mmol m^{-2} day^{-1}, a rate that is comparable with the highest rates of denitrification reported for coastal sediments.

INTRODUCTION

The global rate of nitrogen fixation is now approximately two thirds higher than it was prior to the industrial revolution due to anthropogenic nitrogen fixation [*Galloway et al.*, 2004]. Much of this anthropogenic nitrogen is added to agricultural fields as fertilizer where crops assimilate it inefficiently, resulting in about 23% of fertilizer-nitrogen leaching into rivers that ultimately flow to the coast [*Schlesinger*, 2009]. Primary production in coastal waters tends to be nitrogen limited [*Howarth*, 1988], so this

anthropogenic nitrogen flux leads to eutrophication, which degrades coastal water quality [*Nixon*, 1995]. Nitrogen can enter coastal surface waters via riverine discharge, groundwater discharge, and atmospheric deposition. Of these, riverine discharge is the best studied, although groundwater nitrogen loading may rival riverine loading in some regions [*Slomp and Van Cappellen*, 2004], and is the dominant terrestrial nitrogen source to the South Atlantic Bight [*Moore et al.*, 2002].

Anammox and denitrification are microbial processes that convert nitrate (NO_3^-) and/or nitrite (NO_2^-) to dinitrogen gas (N_2) and, together, are the dominant sinks for bioavailable nitrogen globally [*Schlesinger*, 2009] and in coastal sediments [*Joye and Anderson*, 2008]. These processes, along with dissimilatory nitrate reduction to ammonium (DNRA), take place under anoxic conditions, though denitrification can also be active in the presence of oxygen [*Gao et al.*, 2010]. Nitrification is the autotrophic process by which ammonia is oxidized to NO_2^- and then NO_3^- in the presence of oxygen. Denitrification, nitrification, and DNRA all produce nitrous oxide (N_2O), a potent greenhouse gas. Because only denitrification and DNRA can produce N_2O under anoxic conditions, the presence of supersaturated N_2O in an anoxic water mass indicates NO_3^- reduction. Furthermore, a portion of the NO_3^- reduced is permanently removed from the environment as N_2 gas.

Coastal aquifers are known as subterranean estuaries where mixing of reduced and oxidized pore fluids creates steep chemical gradients that microorganisms harness to drive a variety of biogeochemical transformations [*Moore*, 1999]. Permeable sediments are particularly important because mixing is enhanced by rapid advection driven by waves, tides, buoyancy, and interactions with bottom topography [*Huettel et al.*, 2014;

Moore and Wilson, 2005]. This mixing traps marine particulate matter, increasing its mineralization, and intensifies biogeochemical reactions by simultaneously removing byproducts and increasing the supply of reactants [*Huettel et al.*, 2014]. Pore water advection also drives redox oscillations that allow permeable sediments to facilitate removal of bioavailable nitrogen [*Gao et al.*, 2010]; for example, nitrification under oxic conditions produces NO_2^- and NO_3^- that can be reduced to N_2 by anammox and denitrification under anoxic conditions. High permeability, sandy sediments cover the majority of Earth's continental shelves and beaches [*Boudreau et al.*, 2001]. These sediments intercept a great deal of nitrogen-rich groundwater prior to its discharge to the coastal zone, exposing the nitrogen in these fluids to anammox and denitrification. Therefore, coastal aquifers have the potential to attenuate groundwater nitrogen loading to estuaries and the coastal ocean.

Nitrogen cycling in permeable coastal sediments has garnered research interest recently, but most studies have focused on subtidal continental shelf sediment. We hypothesized that intertidal beach sands host high rates of microbial nitrogen cycling processes and are a sink for bioavailable nitrogen (NO_3^-, NO_2^-, NH_4^+, and dissolved organic nitrogen). This hypothesis was tested by using N_2O production as a proxy for bioavailable nitrogen removal. Groundwater geochemistry, including N_2O concentrations, was surveyed across a barrier island, and a hotspot of N_2O concentration was identified on the upper beach. Depth profiles of N_2O concentration and production and consumption rates were measured, and the diffusive flux from the production zone was estimated based on the concentration gradient while the advective flux was estimated based on a groundwater flow model. The total rate of N_2O production was estimated by

summing the three possible rates of N_2O loss from the system: consumption in nearby sediment, loss to the atmosphere, and lateral advection along groundwater flow paths. Sediment incubations were performed to show that the observed N_2O production was supported by a very high rate of NO_3^- consumption, representing a net sink for bioavailable nitrogen in permeable barrier island sediment.

METHODS

Cabretta Island is a small barrier island (~200 meters wide) located on the coast of Georgia, USA (Fig. 2.1) that experiences semidiurnal tides with a tidal range of 2-3 meters. Cabretta is a typical retrograding, Holocene-aged barrier island. A small tidal creek and salt marsh flank Cabretta on one side and a dune and beach system on the other. The beach side of the island has an unconfined surficial aquifer composed of fine sand. A relic marsh platform composed of mud and silt creates a confining unit beneath the sand. A transect of groundwater monitoring wells was installed across the island in 2008 (Fig. 2.1) in several clusters, such that each well within a cluster sampled a different depth between one and five meters beneath the sediment surface (Fig. 2.2a). While marine birds can be a source of nutrients to coastal habitats [*Mizota et al.*, 2012], no bird nesting was observed at this site.

An initial survey of Cabretta Island groundwater geochemistry was conducted from August 2008 – August 2010. Samples were collected from monitoring wells every other month throughout that time period. Prior to sampling, stagnant groundwater was removed from wells with a peristaltic pump. Freshly recharged groundwater was then collected into a disposable syringe using tygon tubing. The syringe and tubing were

rinsed with ~30 mL of groundwater prior to collecting three subsamples. Ten mL was injected into a 20 mL headspace vial with a butyl rubber septum that contained a sodium hydroxide pellet and a helium headspace. This sample was stored upside down until it was analyzed for N_2O concentration using a gas chromatograph with electron capture detector (Shimadzu GC-8A with Hayesep DB column). The N_2O detection limit was 31 nM (three times the standard deviation of 41 field blanks). The remaining subsamples were all filtered using a 0.2 μm syringe filter. A subsample for colorimetric analysis of hydrogen sulfide (H_2S) [*Cline*, 1969] was fixed with 20% (w/v) zinc acetate and stored at 4°C. A third subsample was stored frozen in an acid-washed Nalgene bottle until analysis for nitrite (NO_2^-) and NO_x ($NO_3^- + NO_2^-$). NO_x was measured using an Antek 745 vanadium reduction assembly coupled with an Antek 7050 chemiluminescent nitric oxide detector and NO_2^- was measured using standard colorimetric techniques [*Bendschneider and Robinson*, 1952]. The final 20 mL subsample was fixed with 0.05 mL of concentrated nitric acid until analysis for chloride and sulfate concentration via ion chromatography (Dionex ICS-2000).

Tidally-averaged groundwater flow rates were estimated using numerical models. Simulations of groundwater flow in Cabretta Island were conducted using SUTRA [*Voss and Provost*, 2002]. SUTRA is a finite element groundwater modeling program that simulates saturated-unsaturated, variable-density fluid flow and transport of a single solute, in this case salinity. The governing equation in the model is a form of the Richards equation:

$$\nabla \cdot [K(\Psi)\nabla h] = S_w S_s \frac{\partial h}{\partial t} + \varphi \frac{\partial S_w}{\partial t} - \alpha_s S_w \frac{\partial \sigma_T}{\partial t} \qquad \text{Equation 2.1}$$

where K is hydraulic conductivity, Ψ is negative pressure head, h is hydraulic head, S_w is water saturation, φ is porosity, σ_T is total stress and S_s is the specific storage,

$$S_s = \rho g(\alpha_s + \varphi\beta) \qquad \text{Equation 2.2}$$

where ρ is the density of water, g is gravity, α_s is sediment compressibility and β is fluid compressibility. Values for model parameters are listed in Table 2.1.

Boundary conditions for the model consisted of a no-flow boundary on the bottom, landward and seaward boundaries. The seaward boundary was assumed to be no-flow because the model domain was extended seaward far enough that the unconfined, surficial aquifer was always inundated and flow within it was negligible. A time-varying boundary condition was used along the upper boundary of the model. For portions of the upper boundary that were inundated, the pressure was specified based on the height of the column of seawater above the boundary. If a node along the surface of the domain was exposed and the sediment was fully saturated, a seepage face formed. This allowed groundwater to discharge if the water table intersected land surface. When exposed surface nodes had saturations less than 1, a specified flux boundary was applied to account for rainfall (50 inches per year). An idealized semi-diurnal tide with a period of 12 hours and range of 1.85 meters was used. Mean water level was set to 0 meters. Boundary conditions for solute transport were no flow for the bottom and seaward boundaries. The landward boundary was assigned a salinity of 0 ppt. Along the upper boundary, the salinity of water that entered was specified. In portions of the upper boundary that were inundated by the tide, the salinity of inflowing waters was 34 ppt. Rainfall that infiltrated above the level of the tide was assigned a salinity of 0 ppt. Where

flow was outward across the upper boundary, water leaving the flow domain carried its solutes with it.

Initial conditions were generated by running the simulation without tidal pumping, while accounting for infiltration of rainfall from the top boundary. For these preliminary simulations, an initial salinity of 0.034 ppt was assigned to all nodes within the model domain. This simulation was run until a steady-state distribution of salinity was established that matched salinities observed in the well transect closely. The results then served as the initial conditions for final simulations that included tidal fluctuations. Initial conditions did not affect the results because all transient simulations were allowed to reach a quasi-steady state, which required 110 years. Time steps of 10 min were required to effectively capture hydraulic responses to tidal fluctuations.

The model domain consisted of 11807 nodes and 11402 quadrilateral elements. Elements were approximately 0.3 by 0.3 meters in the uppermost 3 meters of the domain to overcome nonlinearities in pressure and solute solutions near the surface of the beach. Element size increased to a maximum dimension of 1 by 1 meter at approximately 6 meters depth, where high mesh density was not critical. Increasing the mesh density did not change the results.

Pore space gas equilibration chambers were constructed from PVC pipe and capped with butyl rubber stoppers. Large holes were drilled through the pipe and covered in a water-tight, gas-permeable, silicone rubber tube to allow exchange of N_2O between the gas inside the chamber and the gas or groundwater in the pore space outside the chamber (Fig. 2.3a) [*Jacinthe and Dick*, 1993]. Chambers were connected to a photoacoustic field gas monitor (Innova 1412, LumaSense Technologies Inc., Santa

Clara, CA) on the surface with two lengths of gas-tight, FEP tubing. Each chamber had an internal volume of 500 mL, which is large compared with the internal volume of the field gas monitor (60 mL). In this way, the field gas monitor was capable of circulating gas from the chamber to the monitor and back while measuring the concentration of N_2O with minimal dilution (<10%). Laboratory tests documented rapid equilibration of N_2O across the silicone rubber membrane. Five chambers were spiked with high concentrations (~15 times atmospheric) of N_2O. The concentration of N_2O within each chamber was measured periodically over the course of 24 hours. It took less than one day for the N_2O inside the chamber to re-equilibrate with the N_2O in the atmosphere (Fig. 2.3b).

Each equilibration chamber was placed within a 0.5-meter long section of 3" screened PVC pipe that allowed pore water or gas to enter the pipe and come into contact with the chamber membrane. Four chambers were stacked inside individual PVC housings, and these housings were coupled together to create a profiler covering the upper 2 meters of the sediment column (Fig. 2.3c). Equilibration chambers were separated from one another within the profiler by large butyl rubber stoppers, and the screened PVC was sealed over ~5 cm depth between chambers to prevent overlap between the pore volume sampled by adjacent chambers. Within each profiler, four individual gas concentration measurements could be made, each representing the average concentration across a 0.5-meter depth range. These average concentrations and values derived from them are reported as being located at the midpoint depth of each chamber throughout the paper.

Profilers were installed in triplicate on the upper beach of Cabretta Island near the spring high tide line at the sediment surface. Therefore, average N_2O concentrations were measured across 0-0.5, 0.5-1, 1-1.5 and 1.5-2 meter depth intervals (mid-point depths = 0.25, 0.75, 1.25 and 1.75 m, respectively). Concentration profiles were measured across multiple phases of the semidiurnal and lunar (spring/neap) tidal cycles during the winter (February) and summer (July-August) of 2012. A multilevel sampler was installed between two equilibration chamber profilers to collect pore water samples from a 2 cm interval centered on the midpoint depth of each chamber. Samples were collected to coincide with each N_2O profile measurement, and their chemical composition was analyzed as described above for the monitoring wells. In addition, a transect of small profilers containing two equilibration chambers each was installed from the high to the low tide lines on the beach perpendicular to the beach axis in October 2012. Following a 1-week equilibration period, a single set of N_2O concentration measurements was made, after which most profilers were destroyed by intense wave action.

From February to March of 2012, increasing N_2O concentration at 0.75 meters depth was correlated with groundwater temperature increasing from 14.7-17.0°C. N_2O concentrations approached summer concentrations above a critical temperature of 16.5 °C (Fig. 2.4a). The critical temperature was determined by splitting the N_2O concentration data into two groups above and below a specific temperature and performing a Student's t-test to test the null hypothesis that the two populations have the same mean. This test was repeated at 0.1°C intervals over a range of 15-17°C. The temperature with the lowest p-value was 16.5°C. This temperature was used as the cut-off between winter and summer data for all analyses presented here.

Rates of N_2O production and consumption were measured in laboratory incubations in July 2012. Sediment was collected using a hand auger from triplicate profiles, each within one meter of a different equilibration profiler, with individual samples taken from the midpoint of each equilibration chamber. These samples were returned to the lab and placed in 500 mL Schott bottles in 120 cc increments. All sediment retained its in situ porewater content such that sediment from the bottom 1.5 meters of each profile was saturated while sediment from the top 0.5 meters was undersaturated. Bottles were split into oxic and anoxic treatments and their headspaces were purged with air and nitrogen, respectively. Bottles from all treatments were then spiked with N_2O to approximate in situ concentrations in the top half meter of beach sand. Each treatment was carried out in triplicate at all four depths. After a 24-hour pre-incubation at in situ summer temperature (27°C), the headspace of each bottle was reset by purging with nitrogen or air and spiking the headspace with the same amount of N_2O. This allowed the sediment and porewater to equilibrate with the headspace N_2O concentration prior to the start of the experiment. Headspace N_2O concentrations were measured at approximately 0, 3, 6, 12, 24, and 48 hours using the field gas monitor. The linear rate of change in concentration was used to calculate the rate of N_2O production or consumption in 120 cc of sediment. These rates were then scaled up to the 0.5 m^3 of sediment that occupied one square meter of beach over a 0.5-meter depth interval centered on a pore gas equilibration chamber in order to convert rates from volumetric (cm^{-3}) to areal (m^{-2}) units.

Samples for isotopic analysis were collected from each equilibration chamber in October 2012 by displacing 125 mL of gas with saturated NaCl brine. Measurements of

$\delta^{15}N^{bulk}$, $\delta^{18}O$, and ^{15}N site preference (SP) in N_2O were made on a Delta PLUS XP isotope ratio mass spectrometer with custom-built purge and trap inlet [*McIlvin and Casciotti*, 2010]. The isotope ratios from each sample were normalized to parallel analyses of calibrated laboratory working gas according to procedures described previously [*Frame and Casciotti*, 2010], and atmospheric N_2O was analyzed after every nine samples as a quality control measure. The response of the mass spectrometer varied as a function of sample size so $\delta^{15}N^{bulk}$, $\delta^{18}O$, and ^{15}N site preference data were size-corrected to account for this instrument non-linearity [*McIlvin and Casciotti*, 2010].

The flux of N_2O from the sediment surface to the atmosphere was measured using cylindrical plexiglass flux chambers. One flux chamber was installed adjacent to each of the three equilibration chamber profilers on the upper beach immediately before or after concentration profiles were measured. Triplicate measurements were made of N_2O concentration within each flux chamber every 20-30 minutes over a 1-2 hour period using the field gas monitor [*Samarkin et al.*, 2010]. The rate of N_2O accumulation was calculated as a linear regression of these concentrations through time. The significance of each linear regression was calculated and fluxes were considered to be not significantly different from zero when the p-value was greater than 0.025.

Vertical diffusion of N_2O from zones of high to low concentration within saturated sand was calculated using equation 2.3, as described by Deurer et al. [2008]:

$$J_W = \varphi^{4/3} \cdot D_W \cdot \frac{\partial C}{\partial z} \qquad \text{Equation 2.3}$$

Where J_W is the vertical diffusive flux of N_2O (nmol m^{-2} day^{-1}), φ is sediment porosity (m^3 m^{-3}), D_w is the diffusion coefficient of N_2O in water (m^2 day^{-1}), and $\frac{\partial C}{\partial z}$ is the vertical concentration gradient of N_2O (nmol m^{-4}). Sediment porosity was assumed to be 0.43 at

0.75 and 1.25 meters deep (literature value for fine sand) and 0.53 at 1.75 meters deep (measured at this site). The higher porosity in the deepest sediment zone corresponds with a transition from sand to mud. The $\varphi^{4/3}$ term includes a tortuosity correction. D_w was assumed to be 0.000158 (m^2 day^{-1}) at 20°C and 0.000166 (m^2 day^{-1}) at 30°C [*Tamimi et al.*, 1994]. The diffusive flux was only calculated for sediment layers beneath 0.5 meters because they tended to be below the water table (Fig. 2.5) and were therefore saturated.

Transverse and longitudinal dispersion of N_2O from zones of high to low concentration within saturated sand were calculated using equations 2.4 and 2.5 [*Domenico and Schwartz*, 1998]:

$$J_T = D_T \cdot Q_{GW} \cdot \frac{\partial C}{\partial z} \qquad \text{Equation 2.4}$$

$$J_L = D_L \cdot Q_{GW} \cdot \frac{\partial C}{\partial x} \qquad \text{Equation 2.5}$$

Where J_T is the vertical flux of N_2O driven by transverse dispersion (µmol m^{-2} day^{-1}), D_T is the transverse dispersivity of sand (m), $\frac{\partial C}{\partial z}$ is the vertical concentration gradient of N_2O (µmol m^{-4}), J_L is the horizontal flux of N_2O driven by longitudinal dispersion (µmol m^{-2} day^{-1}), D_L is the longitudinal dispersivity of sand (m), and $\frac{\partial C}{\partial x}$ is the horizontal concentration gradient of N_2O (µmol m^{-4}). Q_{GW} is the groundwater flow velocity averaged across the tidal cycle derived from the model described above (m d^{-1}). The tidally-averaged velocity was used rather than the instantaneous velocity because the two values yield the same result as long as the groundwater flow direction does not reverse. Flow reversal was observed between low and high tide on the beach, and in this case, using the tidally-averaged velocity yielded a conservative estimate of the dispersive flux

of N_2O. Since the concentration gradient used in these calculations was averaged across tidal cycles, the tidally-averaged groundwater flow velocity was used as well.

The horizontal advective N_2O flux was calculated according to equation 2.6:

$$J_A = C_{GW} \cdot Q_{GW} \qquad \text{Equation 2.6}$$

where J_A is the flux of N_2O due to horizontal advection ($\mu mol\ m^{-2}\ day^{-1}$), C_{GW} is the groundwater N_2O concentration ($\mu mol\ m^{-3}$), and Q_{GW} is the tidally-averaged horizontal groundwater flow rate ($m\ day^{-1}$).

In June 2012, a separate set of sediment incubations were carried out to target the depth of maximum N_2O concentration. This depth was identified based on the observation that high N_2O concentrations were associated with high NO_3^- concentrations. The depth of maximum pore water NO_3^- concentration was located in shallow sand on the upper beach at Cabretta Island using an aquarium NO_3^- test kit (Aquarium Pharmaceuticals, Inc). Sand samples were collected from six holes spaced one meter apart at a depth of ~0.65 meters. Sand samples were collected from six holes at this depth spaced one meter apart. Sand was homogenized, stored in plastic bags under anoxic conditions at approximately in situ conditions, and transported back to the lab. Thirty cm^3 of sand was added to sixty 120 mL serum bottles. The headspace of each serum vial was purged with UHP N_2. Half of the bottles in each treatment were spiked with UHP O_2 to reach a headspace concentration of 21%. Bottles were incubated overnight at 27°C. The next day, 70 mL of artificial pore water (APW) with a salinity of 30 ppt that was purged with UHP N_2 was added to each serum vial. 24 bottles received APW amended with 50 $\mu M\ NH_4^+$, 24 bottles received APW with 150 $\mu M\ NO_3^-$ and 300 μM carbon (1:1:1 lactate:acetate:glucose molar carbon ratio), and 12 received APW with no nitrogen or

carbon source. The headspace of each bottle was purged with UHP N_2 again, and the same bottles that received O_2 the day before were spiked with O_2 again to the same concentration.

Each bottle was gently mixed and the first time point sample was collected immediately. Fluid samples were collected first by penetrating the septum with a needle and withdrawing 0.5 mL of APW to rinse the disposable syringe. After rinsing, 5.5 mL of APW was withdrawn and filtered through a 0.2 μm Target filter into a 15 mL centrifuge tube. 1.25 mL of the filtered sample was transferred into another tube containing 200 μL of phenol reagent [*Solorzano*, 1969] for subsequent analysis of NH_4^+. The remaining filtered sample was frozen for subsequent NO_3^- and NO_2^- analysis. Sixteen mL of 79% UHP N_2 and 21% UHP O_2 was then added to the serum bottle. Ten mL of headspace gas was then collected into a disposable syringe and injected into a 10 mL vacutainer for subsequent N_2O analysis.

Samples were incubated in the dark at 27°C, with gentle shaking at 25 rpm. Samples were collected as described above at 0, 24, 48, and 72 hours. Following the 72 hour sample, the headspace gas composition in every serum bottle was reset. The septum was removed from each bottle and the APW/sand mixture was purged very gently with UHP N_2. The septum was replaced and the headspace of the bottle was purged with UHP N_2. Within each APW treatment that received a nitrogen substrate, half of the bottles that had been incubated under oxic conditions and half that had been incubated under oxic conditions were reset back to the previous conditions. The other bottles were switched such that previously oxic bottles became anoxic and vice versa. A separate experiment confirmed that previously anoxic APW became saturated with oxygen in a matter of

hours when exposed to a 21% oxygen headspace. Within each new treatment, half were spiked with 50 μM H_2S and half were not. Each new treatment was applied to triplicate bottles. The headspaces of the control bottles (no inorganic N source) were reset, but none of them were switched from oxic to anoxic conditions or vice versa. Samples were collected at 0, 24, 48, 72, 96, and 144 hours following this reset. See Fig. 2.6 for a summary of experimental treatments.

In order to account for changes in both the dissolved and adsorbed NH_4^+ pools in this experiment, triplicate sediment cores were collected from the same location on the beach in October 2012. The cores were split into 5 cm sections and adsorbed NH_4^+ was extracted from each section using 2 M KCl. Dissolved NH_4^+ concentrations over the same depth interval were measured simultaneously by extracting pore water using Rhizon samplers. The average in situ dissolved:adsorbed NH_4^+ ratio was calculated and applied to dissolved NH_4^+ concentrations measured in the incubation experiment to estimate the total NH_4^+ content of each bottle at each time point.

RESULTS

The concentration of N_2O expected from equilibration of seawater (salinity = 35, temperature = 25°C) with the atmosphere is 6.38 nM [*Bange*, 2008]. The background concentration of dissolved N_2O in groundwater in all but one well across Cabretta Island from August 2008-August 2010 was indistinguishable from the detection limit of 31 nM, making it impossible to document whether groundwater in this aquifer was generally undersaturated or supersaturated with respect to the atmosphere. However, the median N_2O concentration of 225 nM (range = 145–5,500 nM, n=3) observed in a shallow well

near the spring high tide line on the beach (Fig. 2.2a) was two orders of magnitude higher than atmospheric equilibrium. This N_2O hotspot was characterized by highly elevated median concentrations of NO_3^- (675 μM, range = 141–1,210 μM) and nitrite (8.7 μM, range = 1.2–16 μM), important precursors for N_2O production by denitrifying and nitrifying microorganisms [*Bange*, 2008]. Surficial sediment contained low mean N_2O concentrations (14 ± 3.4 μM) elsewhere on the beach (Fig. 2.2b), demonstrating that the N_2O hotspot was restricted to the upper portion of the beach near the spring high tide line. This location is associated with a feature called the upper saline plume on many beaches [*Robinson et al.*, 2007], where seawater that is driven into shallow sands by waves and tides overlies fresher groundwater from the upland. However the upper saline plume was not observed at the study site, likely due to the shallow slope of the beach.

In the sandy, surficial, unconfined aquifer of Cabretta Island, groundwater generally flowed from the island upland towards a discharge point around the low tide line (225 meters from the creek in Fig. 2.2b). Groundwater flow was driven by precipitation on the upland, resulting in relatively slow flow rates (5 cm day^{-1}). On the intertidal portion of the beach, groundwater flow was faster (55 cm day^{-1}), driven by waves and tides. The high tide line on the beach, where the N_2O hotspot was located, marked the transition between these two groundwater flow regimes. Groundwater flow at this location likely alternated between high flow during spring tides when high tides regularly inundated the upper beach, and neap tides when the upper beach remained exposed for days at a time (Fig. 2.5). Averaged across spring/neap tidal cycles, the groundwater flow rate at the N_2O hotspot was around 30 cm day^{-1}.

In triplicate depth profilers installed at the location on the upper beach where high N_2O concentrations were observed in groundwater monitoring wells, maximum N_2O concentrations always occurred at 0.75 meters regardless of season (Fig. 2.7a). The groundwater temperature in shallow sands on the upper beach, recorded using buried temperature loggers and discrete groundwater samples from wells, was below 16.5°C only in January and February during the study period (Fig. 2.4b). The median N_2O concentration at 0.75 meters was 63 nM with an interquartile range (IQR) of 53–318 nM (n=11) when the temperature was below 16.5°C and 282 nM (IQR = 135–454 nM, n=32) when the temperature was above 16.5°C. Low N_2O concentrations were observed at all locations upstream of these profilers with respect to groundwater flow (Fig. 2.2). Therefore, the depth interval around 0.75 meters appeared to be a zone of N_2O production. Surprisingly, sediment incubations in February and July 2012 revealed no net N_2O production in this zone (Fig. 2.7b), and showed N_2O consumption under anoxic conditions. Sand was collected from a depth range of ~30 cm at the center of the 0.5-1 meter depth interval and obviously missed the layer of N_2O production. However, the more targeted incubations conducted in June 2012 used sand from a narrower depth range within the 0.5-1 meter depth interval that contained high NO_3^- concentrations similar to those associated with high N_2O concentrations in groundwater monitoring wells. These incubations showed net N_2O production at a rate of 64 ± 16 μmol m^{-2} day^{-1} (n=5) under anoxic conditions in the presence of NO_3^- and H_2S (Fig. 2.7b).

N_2O isotopic measurements were distinct from tropospheric N_2O ($\delta^{15}N$ -N_2O, +6.2 ‰, $\delta^{18}O$-N_2O +44.3 ‰) [*Croteau et al.*, 2010] throughout the depth profile, with $\delta^{15}N$-N_2O values lower than air and $\delta^{18}O$-N_2O values higher than air (Fig. 2.7c). The

most extreme isotopic values (highest $\delta^{18}O$-N_2O, up to +64 ± 1‰ and lowest $\delta^{15}N$ -N_2O, +1 ± 3‰) were observed at 0.75 meters (Fig. 2.7c). The ^{15}N site preference of N_2O in this depth range was higher than atmospheric N_2O, with a mean value of +27 ± 6‰ (not shown).

During the summer, N_2O concentrations at all other depths were at least one order of magnitude lower than the concentrations observed at 0.75 meters. This concentration gradient drove N_2O out of the production zone and into the underlying and overlying sands. The diffusive flux was calculated to be on the order of tens of nmol m^{-2} day^{-1} (Fig 2.7d). The vertical N_2O flux driven by transverse dispersion (J_T) was calculated to fall within the range 0.04–20 µmol m^{-2} day^{-1} (equation 2.4, Table 2.2). Transverse (rather than longitudinal) dispersion was used in this calculation because the numerical model showed that the bulk of groundwater flow was horizontal at this location (Fig. 2.2b). While the range in flux values was high, this calculation shows that transverse dispersion was likely to be a more important driver of vertical N_2O transport than diffusion.

A more accurate value for the vertical N_2O flux driven by transverse dispersion (J_{TM}) was calculated by constructing a N_2O mass balance for the 0.25 meter depth interval. The only N_2O source to this zone was upward dispersion of N_2O from the production zone at 0.75 meters. This N_2O source was balanced by consumption within the 0.25 meter layer and export to the atmosphere. The mean potential rate of N_2O consumption at 0.25 meters was 7.8 ± 3.0 µmol m^{-2} day^{-1} (n=3) under oxic conditions and 6.5 ± 5.3 µmol m^{-2} day^{-1} (n=3) under anoxic conditions (Fig. 2.7b). The consumption rate under oxic conditions (R_C) was used in this mass balance since the sand in this layer was unsaturated most of the time and was very low in organic carbon. Despite this

consumption, N_2O at 0.25 meters accumulated to a median concentration of 45 nM in the summer, around 7 times equilibrium with atmospheric N_2O. This positive concentration gradient combined with much faster diffusion in unsaturated sand above the water table in this zone resulted in a median flux of N_2O to the atmosphere (J_E) of 8.5 μmol m^{-2} day^{-1} (IQR = 3.2–13 μmol m^{-2} day^{-1}, n=49) in summer. No net flux of N_2O to the atmosphere occurred in the winter (n=31) when the vertical concentration gradient was reduced. Combined, the total rate of N_2O loss from the top 0.5 meters of sediment was 16 μmol m^{-2} day^{-1} (range = 8.0–24 μmol m^{-2} day^{-1}), which was supplied by an equivalent dispersive N_2O flux (J_{TM}) from the underlying production zone. This value is similar to the range of vertical dispersive fluxes calculated for this site (J_T = 0.04–20 μmol m^{-2} day^{-1}).

The diffusive fluxes across the saturated boundaries above and below the N_2O production zone were symmetrical (Fig. 2.7d). Because diffusion and dispersion are both described as Fickian processes with equations of the same form (equations 2.3 and 2.4), the dispersive flux was symmetrical as well. Therefore, the N_2O production zone at 0.75 meters supplied 16 μmol N_2O m^{-2} day^{-1} to both the overlying 0.25 meter depth interval and the underlying 1.25 meter interval via transverse dispersion. This downward flux was far exceeded by the mean potential N_2O consumption rates under anoxic conditions at 1.25 and 1.75 meters depth (71 ± 53 μmol m^{-2} day^{-1} and 46 ± 32 μmol m^{-2} day^{-1}, respectively; Fig. 2.7b), driving the N_2O concentration to the background concentration of ~20 nM in the bottom meter of these profiles.

In addition to the vertical movement of N_2O through the sediment column, some N_2O was lost from the production zone via horizontal dispersion and advection. The longitudinal (horizontal) dispersive flux was calculated from equation 2.5 to be 11 μmol

N_2O m^{-2} day^{-1} (range = 0.05–100 μmol m^{-2} day^{-1}). The advective flux of N_2O out of the production zone (J_{AO}) was calculated to be 35 μmol N_2O m^{-2} day^{-1} (range = 2.7–106 μmol m^{-2} day^{-1}) and the advective flux of N_2O into the production zone (J_{AI}) was calculated to be 2.3 μmol N_2O m^{-2} day^{-1} (range = 0.3–7.8 μmol m^{-2} day^{-1}) using equation 2.6. The median hotspot N_2O concentration (C_H = 121 μmol m^{-3}, IQR = 58-195 μmol m^{-3}) and the median background N_2O concentration (C_B = 7.7 μmol m^{-3}, IQR = 6-14 μmol m^{-3}) were used in place of C_{GW} to calculate J_{AO} and J_{AI} respectively. The net advection of N_2O out of the production zone (J_{AN}) was equal to the flux out (J_{AO}) minus the flux in (J_{AI}), or 34 μmol N_2O m^{-2} day^{-1} (range = 2.6–100 μmol m^{-2} day^{-1}). The parameters used to derive the dispersive and advective fluxes are displayed in Table 2.2. N_2O concentrations did not exceed the background value of ~20 nM in the shallow groundwater further down the beach in the direction of groundwater flow (Fig. 2.2b), suggesting that the majority of the combined horizontal dispersive and advective N_2O fluxes were consumed in adjacent beach sands.

The N_2O hotspot described was not unique to a specific location on Cabretta Island. Rather it occupied a ribbon of sand that stretched along the upper beach of two barrier islands in Georgia. A survey of the entire length of Cabretta Island and two locations on adjacent Sapelo Island revealed elevated NO_3^- concentrations in the shallow pore water of the upper beach (see Chapter 3). The zone of elevated NO_3^- concentrations had a median width (perpendicular to the beach) of 3.0 meters (IQR = 2.0–11 m, n=8, Table 2.3). While N_2O concentrations were not measured as part of this survey, a tight correlation between high NO_3^- and N_2O concentrations was observed at the study site and

the assumption was made that the spatial extent of the N_2O hotspot was similar to that observed for elevated NO_3^- concentrations.

The net rate of N_2O production (R_P) at 0.75 meters must balance the total export from this zone documented above according to equation 2.7:

$$R_P \cdot A_H = J_{AN} \cdot A_V + J_L \cdot A_V + 2 \cdot J_{TM} \cdot A_H \qquad \text{Equation 2.7}$$

Where J_{AN} is the net advective flux of N_2O out of the production zone (34 μmol m^{-2} day^{-1}, range = 2.6–100 μmol m^{-2} day^{-1}), J_L is the flux driven by longitudinal dispersion (11 μmol m^{-2} day^{-1}, range = 0.05–100 μmol m^{-2} day^{-1}), and J_{TM} is the flux driven by transverse dispersion (16 μmol m^{-2} day^{-1}, range = 8.0–24 μmol m^{-2} day^{-1}). This mass balance assumes that each equilibration chamber represents a prism with its depth (z) equal to 0.5 m (representing one equilibration chamber), its width (x) equal to the median width of the hotspot (3.0 m, IQR = 2.0–11 m), and its length representing 1 meter of coastline. Therefore, the vertical surface area of this prism (A_V) is 0.5 m^2 and its horizontal surface area (A_H) is 3.0 m^2 (IQR = 2.1–11 m^2). The values of the parameters used to solve equation 2.7 for R_P and their derivation are located in Table 2.2. This N_2O mass balance (Fig. 2.8) yielded a net N_2O production rate (R_P) within the production zone (at 0.75 meters depth) of 40 μmol m^{-2} day^{-1} (range = 17–57 μmol m^{-2} day^{-1}).

In a sediment incubation experiment, the only treatment with sufficient net N_2O production to match the in situ rate presented above was that containing both NO_3^- and H_2S (64 ± 16 μmol m^{-2} day^{-1}; Fig. 2.9), where N_2O production was associated with NO_3^- consumption and NH_4^+ production. Approximately one third of the NO_3^- reduced was converted to NH_4^+ and thus retained within the barrier island system as bioavailable nitrogen. The remaining two thirds of the NO_3^- that was consumed was permanently

removed from the sediment as either N_2O or N_2 gas. On average, the ratio of N_2O production to permanent NO_3^- removal as N_2O or N_2 gas was 0.004 ± 0.001 (n=5), meaning that 0.8 ± 0.2% of this NO_3^- was removed as N_2O and the remainder was converted to N_2. Dividing the rate of N_2O production (40 μmol m^{-2} day^{-1}) by the measured N_2O to NO_3^- ratio yields a rate of NO_3^- consumption of 10 mmol NO_3^- m^{-2} day^{-1} (range = 3.3–19 mmol NO_3^- m^{-2} day^{-1}).

DISCUSSION

The maximum N_2O concentration measured in the 2-meter depth profile was 4,670 nM, a concentration that exceeds 77% of those reported in a review of N_2O concentrations in pore fluids across a range of environments including forests, grasslands, and agricultural fields [*Clough et al.*, 2005]. The concentrations of N_2O and NO_3^- dissolved in Cabretta Island groundwater rival those observed in a NO_3^- contaminated coastal aquifer [*LaMontagne et al.*, 2003], although Cabretta Island is a pristine environment with little anthropogenic nitrogen loading. These high N_2O concentrations yielded high N_2O fluxes from the beach surface to the atmosphere, with a median value of 8.5 μmol m^{-2} day^{-1} (IQR = 3.2–13 μmol m^{-2} day^{-1}) when groundwater temperatures exceeded 16.5 °C. This temperature threshold was surpassed in every month but January and February (Fig. 2.4b), for a total of ~300 days per year. Taking this seasonality into account, the annual N_2O efflux from the beach was 5.1 mmol N m^{-2} yr^{-1} (IQR = 1.9–7.8 mmol m^{-2} yr^{-1}), falling within the range observed in other intertidal coastal sediments [*Middelburg et al.*, 1995].

The rate of N_2O production in Cabretta Island beach sands estimated by mass balance (14–57 μmol m^{-2} day^{-1}) and measured in incubations (64 ± 16 μmol m^{-2} day^{-1}) were in close agreement. These production rates were higher than the fluxes of 6.74 ± 3.84 μmol N_2O m^{-2} day^{-1} reported for continental shelf sediments [*Seitzinger and Nixon*, 1985] or 0.68–14 μmol N_2O m^{-2} day^{-1} reported for estuarine sediments [*Middelburg et al.*, 1995]. In sediment incubations, net N_2O production was associated with NO_3^- reduction and not NH_4^+ oxidation (Fig. 2.9). However, the most probable source of the NO_3^- required to fuel N_2O production was microbial nitrification (see Chapter 3) that took advantage of overlapping NH_4^+ and dissolved O_2 availability in the 0.5-1.5 meter depth window (Fig. 2.10). Other potential sources of this NO_3^- include atmospheric deposition [*Paerl et al.*, 2002], infiltration of seawater enriched with NO_3^- from the Altamaha River [*Weston et al.*, 2009], and coupled nitrogen fixation, remineralization, and nitrification [*An and Joye*, 2001; *Steppe and Paerl*, 2005] taking place at another location on the island such that NO_3^- was transported to the N_2O production zone. Sediment incubations demonstrated the potential activity of nitrification within the N_2O production zone (Fig. 2.9). While nitrification was likely a source of N_2O at this site [*Conrad*, 1996], this process did not drive net N_2O production.

The isotopic signature of N_2O within the production zone was distinct from atmospheric N_2O, indicating fractionation by the processes producing and consuming N_2O within the sediment. The high $\delta^{18}O$ of N_2O in the production zone (Fig. 2.7c) is consistent with N_2O production by denitrifying microorganisms, while the low site preference suggests N_2O production by nitrifying microorganisms [*Casciotti and Buchwald*, 2012]. Furthermore, consumption of N_2O produced at 0.75 meters depth in

deeper strata should be associated with increasing $\delta^{15}N$, $\delta^{18}O$, and site preference of N_2O in these deeper layers [*Casciotti and Buchwald*, 2012], a pattern that does not exist in the data (Fig. 2.7c). It is possible that the lack of increased isotopic enrichment with depth is the result of complete N_2O consumption within microzones in the sediment. However, it is also possible that the processes that produced and consumed N_2O within the 0.5-1 meter depth range took place over a narrower depth range than could be resolved by the 0.5 meter long equilibration chambers. In this case, the unique isotopic signature of N_2O within this depth range was the result of the integration of multiple production and consumption processes and this isotopically distinct N_2O was transported out of the production zone and where it mixed with N_2O derived from the atmosphere.

N_2O accumulation in beach sand was driven by NO_3^- reduction. In sediment incubations, the rate of NO_3^- reduction increased when H_2S was added (Fig. 2.9). Even though denitrification is inhibited by H_2S, it is known to stimulate denitrification-linked N_2O production [*Joye*, 2002]. Another possibility is that autotrophic denitrifying microorganisms couple NO_3^- reduction with H_2S oxidation in beach sand [*Cardoso et al.*, 2006]. The average H_2S concentration (0.4 ± 0.2 μM, n=7) observed at 0.75 meters depth (Fig. 2.10a) was lower than the concentration used in these incubations. However, these measurements were made during the day when high concentrations of dissolved oxygen (>100 μM) were observed in porewater from this depth zone (see Chapter 3). It is possible that higher concentrations of H_2S accumulated at night in the absence of dissolved oxygen. The high variability in N_2O concentrations observed at this site may have resulted from the balance between N_2O production and consumption shifting in response daily or tidal timescale fluctuations in porewater geochemistry.

Regardless of the NO_3^- reduction mechanism, the rate of permanent NO_3^- removal from Cabretta Island (10 mmol m^{-2} day^{-1}, range = 3.3–19 mmol m^{-2} day^{-1}) was comparable with the highest denitrification rates reported for permeable coastal sediments [*Huettel et al.*, 2014] and for coastal sediments in general [*Joye and Anderson*, 2008]. This rate is substantially higher than the 2.07 ± 0.3 mmol m^{-2} day^{-1} nitrogen loss rate reported for sandy intertidal sediment in the Wadden Sea [*Gao et al.*, 2012]. It is possible that the rate of NO_3^- loss reported for Cabretta Island was an overestimate since some of the NO_3^- could have been retained within the system by microbial assimilation [*Middelburg and Nieuwenhuize*, 2000]. Even if a high percentage of the measured NO_3^- loss was due to assimilation, however, the rate of NO_3^- loss from denitrification and/or anammox would still be substantial.

The high rates of nitrogen loss observed in beach sands add to the growing body of evidence that permeable sediments are important for coastal nitrogen budgets [*Huettel et al.*, 2014]. Nitrogen cycling in beach sand is not as well studied as permeable continental shelf sediment because beaches occupy a smaller area globally. However, beaches are extremely valuable resources because of their intense use in tourism [*Houston*, 2008], contributing over $300 billion to the U.S. economy alone in 2007. Harmful algal blooms can diminish the economic benefits of beaches [*Hoagland and Scatasta*, 2006], however, and nitrogen loading increases the incidence of these blooms [*Paerl*, 1997]. Microbial processes in undisturbed beach sand mitigate this nitrogen loading and thus provide a valuable ecosystem service. The impact of anthropogenic disturbances such as beach nourishment, scraping, and smoothing on microbial processes is largely unknown and represents an important topic for future research.

The strength of the nitrogen sink associated with beach sand will shift in response to external drivers such as a warming global climate, sea level rise, and coastal eutrophication. Annual nitrogen loss rates are likely to increase in response to climate change as more coastal aquifers spend greater portions of the year above the threshold temperature for N_2O production documented above. This increase has the potential to be more important at higher latitudes where temperatures are currently below this threshold for a greater proportion of the year. The response to sea level rise and eutrophication is likely more complex, but both processes have the potential to increase H_2S production via sulfate reduction. Eutrophication will increase rates of primary production and consequently the availability of organic carbon substrate for sulfate reducing microorganisms, allowing them to produce more H_2S. Sea level rise will increase concentrations of sulfate, the other substrate that sulfate reducers require in order to produce H_2S, in coastal aquifers by injecting sulfate-replete seawater into previously freshwater aquifers. Given that the presence of H_2S in sand from the N_2O hotspot increased rates of both N_2O production and NO_3^- reduction, sea level rise and eutrophication may further increase the magnitude of the barrier island nitrogen sink.

LITERATURE CITED

An, S., and S. Joye (2001), Enhancement of coupled nitrification-denitrification by benthic photosynthesis in shallow estuarine sediments, *Limnology and Oceanography*, *46*(1), 62-74.

Anderson, J. L. (2011), Field and numerical observations of groundwater dynamics within Cabretta Island, a barrier island off the coast of Georgia, M.S. thesis, 1–62 pp., University of South Carolina, Columbia, SC.

Bange, H. W. (2008), Gaseous nitrogen compounds (NO, N_2O, N_2, NH_3) in the ocean, in *Nitrogen in the Marine Environment*, edited by D. G. Capone, D. A. Bronk, M. R. Mulholland and E. J. Carpenter, pp. 51-94, Elsevier, Burlington, MA.

Bendschneider, K., and R. J. Robinson (1952), A new spectrophotometric method for the determination of nitrite in sea water, *Journal of Marine Research*, *11*(1), 87-96.

Boudreau, B. P., M. Huettel, S. Forster, R. A. Jahnke, A. McLachlan, J. J. Middelburg, P. Nielsen, F. Sansone, G. Taghon, and W. Van (2001), Permeable marine sediments: overturning an old paradigm, *EOS, Transactions American Geophysical Union*, *82*(11), 133-140.

Cardoso, R. B., R. Sierra-Alvarez, E. R. Flores, J. Gómez, and J. A. Field (2006), Sulfide oxidation under chemolithoautotrophic conditions, *Biotechnology and Bioengineering*, *95*(6), 1148-1157.

Casciotti, K. L., and C. Buchwald (2012), Insights on the marine microbial nitrogen cycle from isotopic approaches to nitrification, *Frontiers in Microbiology*, *3*.

Cline, J. D. (1969), Spectrophotometric determination of hydrogen sulfide in natural waters, *Limnology and Oceanography*, *14*(3), 454-458.

Clough, T. J., R. R. Sherlock, and D. E. Rolston (2005), A review of the movement and fate of N_2O in the subsoil, *Nutrient Cycling in Agroecosystems*, *72*, 3-11.

Conrad, R. (1996), Soil microorganisms as controllers of atmospheric trace gases (H_2, CO, CH_4, OCS, N_2O, and NO), *Microbiological reviews*, *60*(4), 609-640.

Croteau, P., E. L. Atlas, S. M. Schauffler, D. R. Blake, G. S. Diskin, and K. A. Boering (2010), Effect of local and regional sources on the isotopic composition of nitrous oxide in the tropical free troposphere and tropopause layer, *Journal of Geophysical Research-Atmospheres*, *115*.

Deurer, M., C. von der Heide, J. Böttcher, W. H. M. Duijnisveld, D. Weymann, and R. Well (2008), The dynamics of N_2O near the groundwater table and the transfer of N_2O into the unsaturated zone: a case study from a sandy aquifer in Germany, *Catena*, *72*(3), 362-373.

Domenico, P. A., and F. W. Schwartz (1998), *Physical and chemical hydrogeology*, Wiley New York.

Frame, C. H., and K. L. Casciotti (2010), Biogeochemical controls and isotopic signatures of nitrous oxide production by a marine ammonia-oxidizing bacterium, *Biogeosciences*, *7*(9), 2695-2709.

Freeze, R. A., and J. A. Cherry (1979), *Groundwater*, Prentice-Hall, Englewood Cliffs, NJ.

Galloway, J. N., et al. (2004), Nitrogen cycles: past, present, and future, *Biogeochemistry*, *70*(2), 153-226.

Gao, H., F. Schreiber, G. Collins, M. M. Jensen, J. E. Kostka, G. Lavik, D. de Beer, H.-Y. Zhou, and M. M. Kuypers (2010), Aerobic denitrification in permeable Wadden Sea sediments, *The ISME Journal*, *4*, 417-426.

Gao, H., et al. (2012), Intensive and extensive nitrogen loss from intertidal permeable sediments of the Wadden Sea, *Limnology and Oceanography*, *57*(1), 185-198.

Gelhar, L. W., C. Welty, and K. R. Rehfeldt (1992), A critical review of data on field-scale dispersion in aquifers, *Water Resources Research*, *28*(7), 1955–1974.

Heiss, J. W., and H. A. Michael (2014), Saltwater-freshwater mixing dynamics in a sandy beach aquifer over tidal, spring-neap, and seasonal cycles, *Water Resources Research*, *50*, 6747–6766.

Hoagland, P., and S. Scatasta (2006), The economic effects of harmful algal blooms, in *Ecology of harmful algae*, edited, pp. 391-402, Springer.

Houston, J. R. (2008), The economic value of beaches—a 2008 update, *Shore & Beach*, *76*(3), 22-26.

Howarth, R. W. (1988), Nutrient limitation of net primary production in marine ecosystems, *Annual Review of Ecology and Systematics*, *19*, 89-110.

Huettel, M., P. Berg, and J. E. Kostka (2014), Benthic Exchange and Biogeochemical Cycling in Permeable Sediments, in *Annual Review of Marine Science, Vol 6*, edited by C. A. Carlson and S. J. Giovannoni, pp. 23-51.

Jacinthe, P. A., and W. A. Dick (1993), Use of silicone tubing to sample nitrous oxide in the soil atmosphere, *Soil Biology and Biochemistry*, *28*(6), 721-726.

Joye, S. B. (2002), Denitrification in the marine environment, in *Encyclopedia of Environmental Microbiology*, edited by G. Bitton, Wiley, New York, NY.

Joye, S. B., and I. C. Anderson (2008), Nitrogen cycling in coastal sediments, in *Nitrogen in the Marine Environment, 2nd Edition*, edited by D. G. Capone, D. A. Bronk, M. R. Mulholland and E. J. Carpenter, pp. 686-902, Elsevier.

LaMontagne, M. G., R. Duran, and I. Valiela (2003), Nitrous oxide sources and sinks in coastal aquifers and coupled estuarine receiving waters, *The Science of the Total Environment*, *309*, 139-149.

McIlvin, M. R., and K. L. Casciotti (2010), Fully automated system for stable isotopic analyses of dissolved nitrous oxide at natural abundance levels, *Limnology and Oceanography-Methods*, *8*, 54-66.

Middelburg, J. J., and J. Nieuwenhuize (2000), Nitrogen uptake by heterotrophic bacteria and phytoplankton in the nitrate-rich Thames estuary, *Marine Ecology Progress Series*, *203*.

Middelburg, J. J., G. Klaver, J. Nieuwenhuize, R. M. Markusse, T. Vlug, and F. J. W. A. van der Nat (1995), Nitrous oxide emissions from estuarine intertidal sediments, *Hydrobiologia*, *311*, 43-55.

Mizota, C., K. Noborio, and Y. Mori (2012), The Great Cormorant (*Phalacrocorax carbo)* colony as a "hot spot" of nitrous oxide (N_2O) emission in central Japan, *Atmospheric Environment*, *57*, 29-34.

Moore, W. S. (1999), The subterranean estuary: a reaction zone of ground water and sea water, *Marine Chemistry*, *65*, 111-125.

Moore, W. S., and A. M. Wilson (2005), Advective flow through the upper continental shelf driven by storms, buoyancy, and submarine groundwater discharge, *Earth and Planetary Science Letters*, *235*(3), 564-576.

Moore, W. S., J. M. Krest, G. Taylor, E. Roggenstein, S. B. Joye, and R. Lee (2002), Thermal evidence of water exchange through a coastal aquifer: Implications for nutrient fluxes, *Geophysical Research Letters*, *29*(14), 1704.

Nixon, S. W. (1995), Coastal marine eutrophication: a definition, social causes, and future concerns, *Ophelia*, *41*, 199-219.

Paerl, H. W. (1997), Coastal eutrophication and harmful algal blooms: Importance of atmospheric deposition and groundwater as" new" nitrogen and other nutrient sources, *Limnology and oceanography*, *42*(5), 1154-1165.

Paerl, H. W., R. L. Dennis, and D. R. Whitall (2002), Atmospheric deposition of nitrogen: implications for nutrient over-enrichment of coastal waters, *Estuaries*, *25*(4B), 677-693.

Robinson, C., L. Li, and D. A. Barry (2007), Effect of tidal forcing on a subterranean estuary, *Advances in Water Resources*, *30*(4), 851-865.

Samarkin, V. A., M. T. Madigan, M. W. Bowles, K. L. Casciotti, J. C. Priscu, C. P. Mckay, and S. B. Joye (2010), Abiotic nitrous oxide emission from the hypersaline Don Juan Pond in Antarctica, *Nature Geoscience*, *3*(5), 341-344.

Schlesinger, W. H. (2009), On the fate of anthropogenic nitrogen, *Proceedings of the National Academy of Sciences*, *106*(1), 203-208.

Seitzinger, S. P., and S. W. Nixon (1985), Eutrophication and the rate of denitrification and N_2O production in coastal marine sediments, *Limnology and Oceanography*, *30*(6), 1332-1339.

Slomp, C. P., and P. Van Cappellen (2004), Nutrient inputs to the coastal ocean through submarine groundwater discharge: controls and potential impact, *Journal of Hydrology*, *295*, 64-86.

Smith, A. J. (2004), Mixed convection and density-dependent seawater circulation in coastal aquifers, *Water Resources Research*, *40*(8), W08309.

Solorzano, L. (1969), Determination of ammonia in natural waters by the phenolhypochlorite method, *Limnology and Oceanography*, *14*(5), 799-801.

Steppe, T. F., and H. W. Paerl (2005), Nitrogenase activity and nifH expression in a marine intertidal microbial mat, *Microbial Ecology*, *49*(2), 315-324.

Tamimi, A., E. B. Rinker, and O. C. Sandall (1994), Diffusion coefficients for hydrogen sulfide, carbon dioxide, and nitrous oxide in water over the temperature range 293-368 K, *Journal of Chemical and Engineering Data*, *39*(2), 330-332.

Voss, C. I., and A. M. Provost (2002), A model for saturated-unsaturated, variable-density ground-water flow with solute or energy transport, *U.S. Geological Survey Water Resources Investigations Report*, 02-4231.

Weston, N. B., J. T. Hollibaugh, and S. B. Joye (2009), Population growth away from the coastal zone: thirty years of land use change and nutrient export in the Altamaha River, GA, *Science of the Total Environment*, *407*(10), 3347-2256.

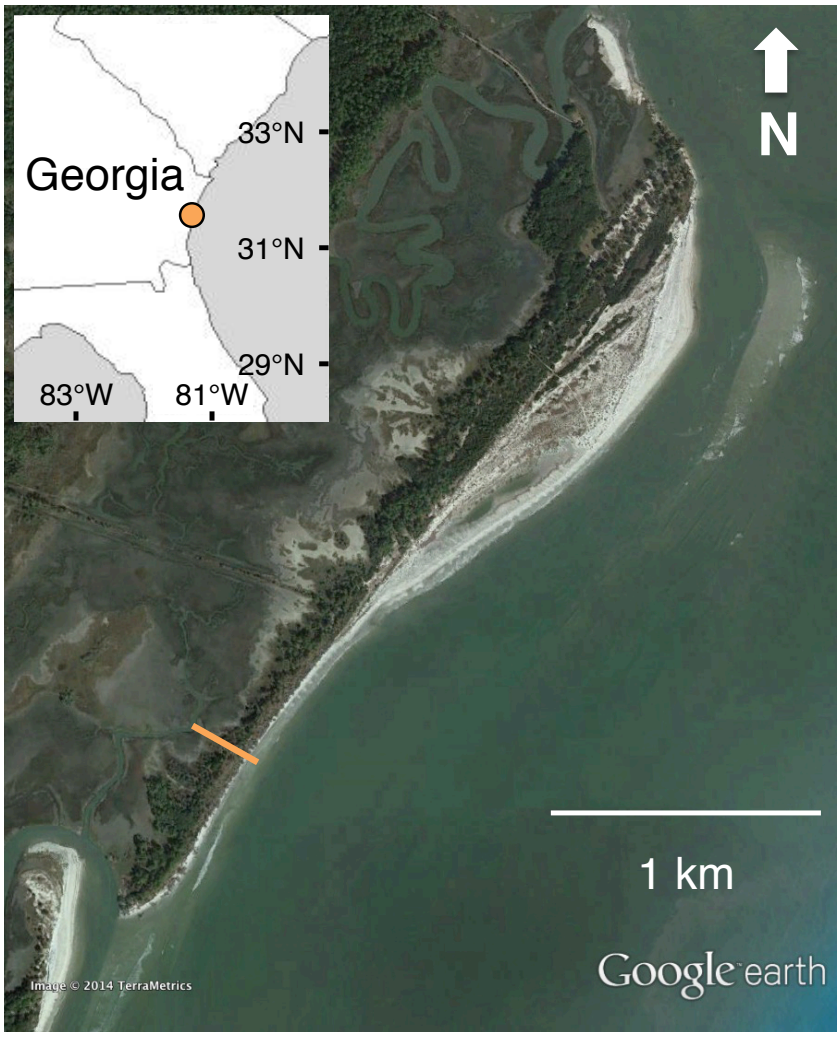

Figure 2.1. The orange dot on the inset map shows the location of Cabretta Island on the coast of Georgia, USA. The orange line shows the position of the groundwater monitoring well transect on Cabretta Island.

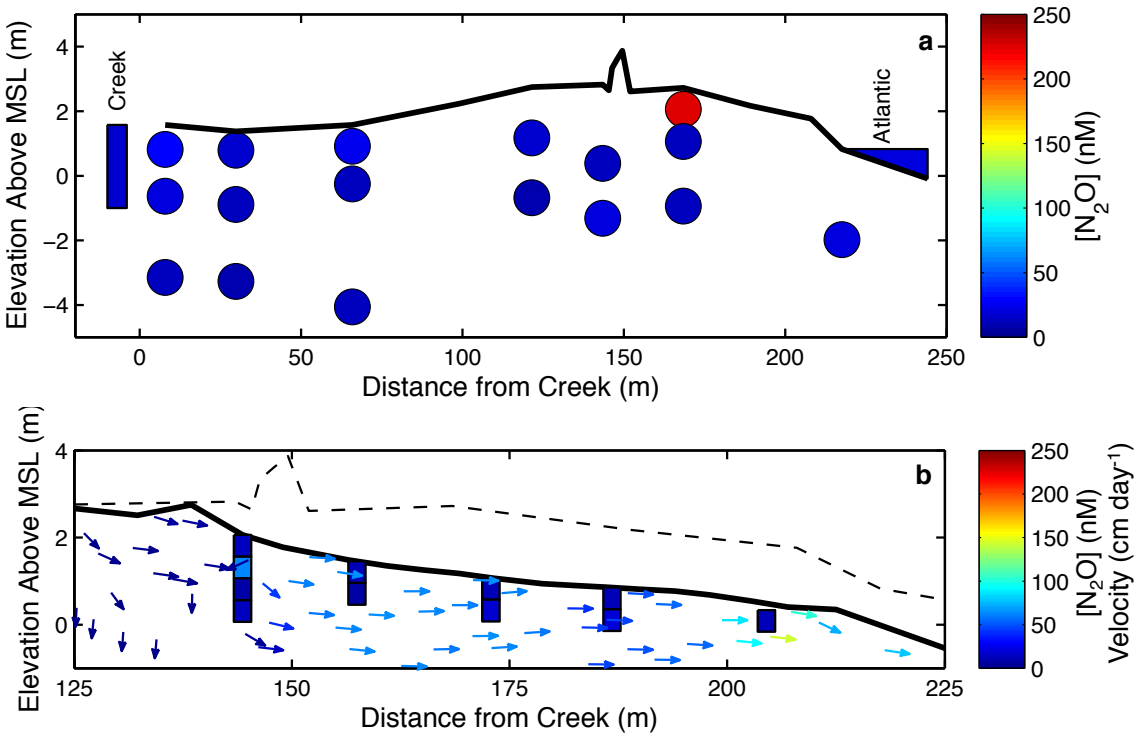

Figure 2.2. Cross section (10:1 vertical exaggeration) of median N_2O concentrations across a transect of groundwater monitoring wells on Cabretta Island sampled every other month from August 2008 – August 2010 (n=13, except the well highlighted red where the well was lost to erosion after the first three measurements) (a). N_2O concentrations measured in a transect of equilibration chambers (5:1 vertical exaggeration) installed perpendicular to the axis of the beach in October 2012 (b). The arrows show the velocity of groundwater flow averaged across tidal cycles estimated from the numerical flow model. In both panels, the heavy black line shows the sediment surface at the time that samples were collected. In panel (b), the dashed black line is the sediment surface from 2008-2010, matching the heavy black line in panel (a).

Table 2.1. Model parameters. Permeability values were calculated by Anderson [2011] and were similar to those found in Freeze and Cherry [1979]. Dispersivity values were within the range used by Smith [2004] and Gelhar et al. [1992] for similar aquifers. The flow field generated by the model showed a negligible impact in response to increasing dispersivity values by an order of magnitude.

Sediment Type	Permeability (m^2)	Porosity	Longitudinal Dispersivity (m)	Transverse Dispersivity (m)
Sand	2×10^{-11}	0.43	1	0.1
Mud	5×10^{-15}	0.72	1	0.1

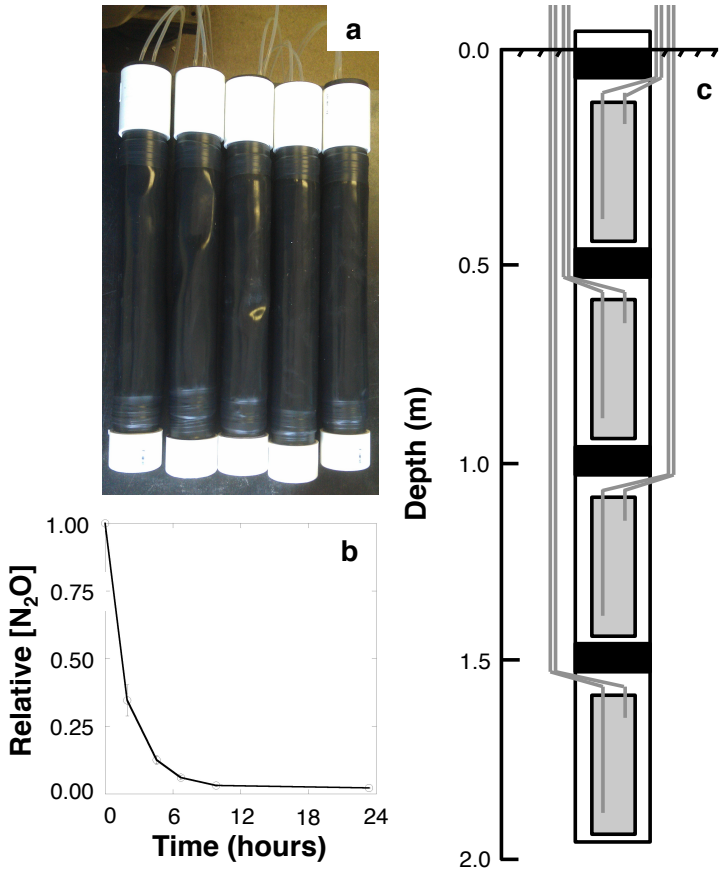

Figure 2.3. Photo of individual equilibration chambers (a). Time required for the N_2O concentration within an equilibration chamber to return to equilibrium with the atmosphere following an addition of N_2O (b). Schematic diagram of four equilibration chambers stacked into a profile to measure gas concentrations at 0.5 m intervals (c).

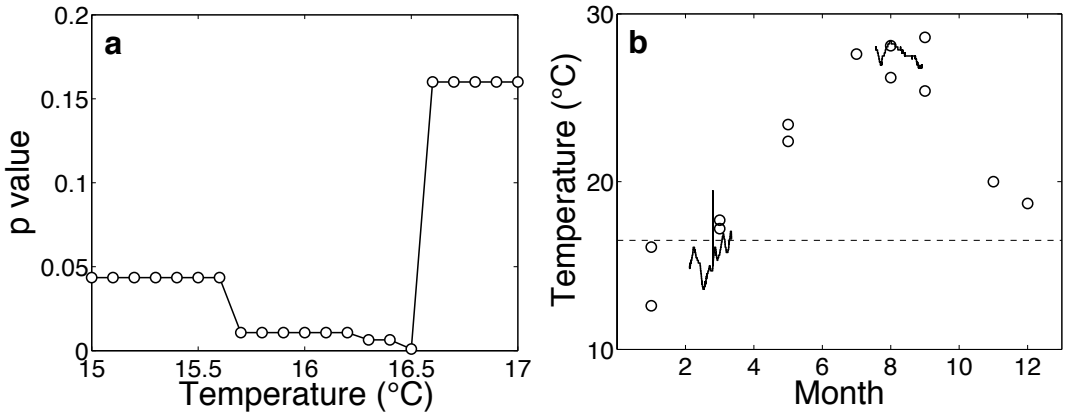

Figure 2.4. p values returned by a series of Student's t-tests that tested the null hypothesis that two groups of N_2O concentration data shared the same mean (a). Concentration data were collected during winter 2012 from the 0.5-1 m depth interval of the profile on the upper beach. For each test, N_2O data that were split into two groups above or below a threshold temperature, and this temperature was varied from 15° to 17° at 0.1° intervals. Groundwater temperatures measured throughout the year (b) in monitoring wells (open circles) and by loggers installed 0.75 m deep on the upper beach adjacent to N_2O concentration profiles (144 meters from the creek; black lines). The dashed line represents the critical temperature threshold of 16.5°C.

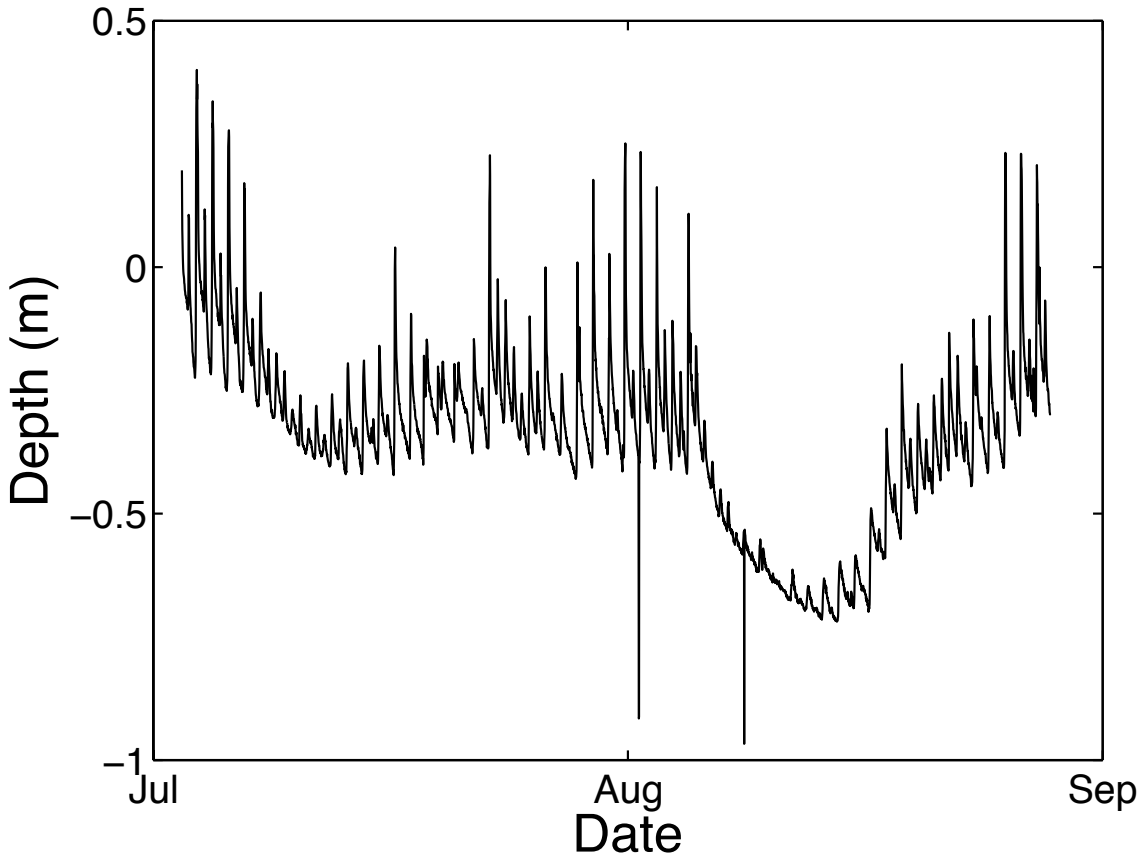

Figure 2.5. Depth of the water table below the sediment surface on the upper beach near the location of the N_20 equilibration profilers (144 meters from the creek) during the summer of 2012. Positive values indicate tidal inundation.

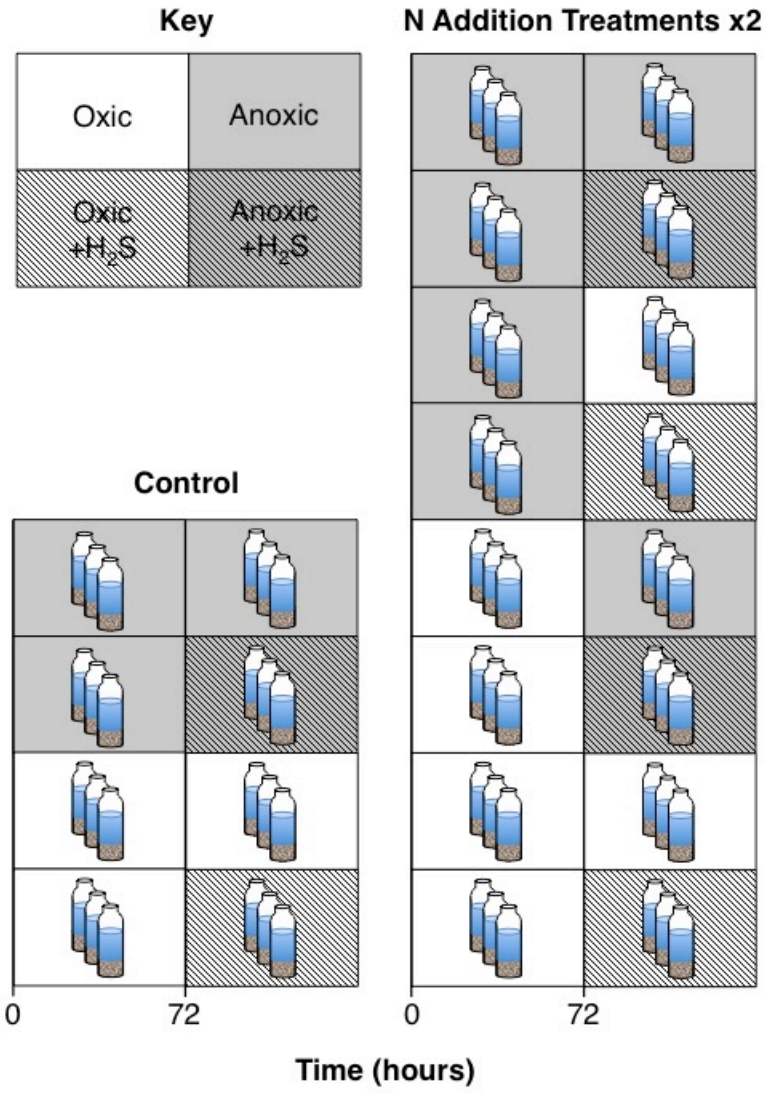

Figure 2.6. Summary diagram of the treatments used in the N_2O hotspot sediment incubations. The controls received no additional nitrogen or carbon substrate. There were two sets of nitrogen addition treatments: one received 50 µM NH_4^+, the second received 150 µM NO_3^- and 300 µM organic carbon (1:1:1 lactate:acetate:glucose molar carbon ratio).

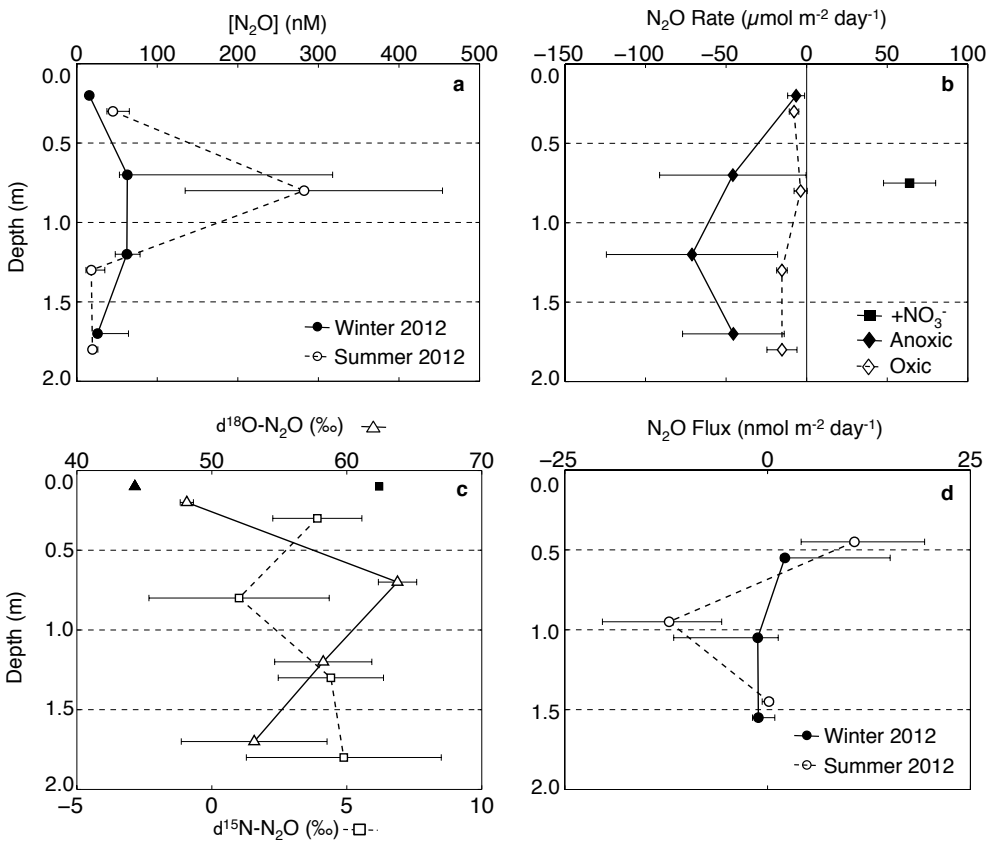

Figure 2.7. Median N_2O concentrations from equilibration chambers (a). Mean net potential rates of N_2O production and consumption under oxic and anoxic conditions (b). The mean potential N_2O production rate when NO_3^- and H_2S were added ($+NO_3^-$) is also displayed (data from June 2012). Mean bulk $\delta^{15}N$-N_2O and $\delta^{18}O$-N_2O (c). Pore space isotopic composition is represented by open symbols and tropospheric composition by closed symbols. Median diffusive flux of N_2O between sediment layers represented by equilibration chambers with positive values representing upward fluxes and negative values representing downward fluxes (d). Error bars show the interquartile range (a and d) or one standard deviation (b and c). Winter and summer data were collected in February and July-August 2012, respectively (a, b, d), while isotopic data were collected in October 2012 (c).

Table 2.2. Values and units for the input and output variables in equations 2.4, 2.5, 2.6, and 2.7. C_{GW} in equation 2.6 was replaced with C_H (representing the N_2O concentration of the hotspot) or C_B (representing the background N_2O concentration from the rest of the site). These values were derived from the median and quartiles of the entire N_2O concentration data set from summer 2012 (n = 32). Transverse dispersivity (D_T) values were conservative estimates based on Heiss and Michael [2014], Smith [2004], and Gelhar et al. [1992]. The rate of horizontal groundwater flow averaged across a tidal cycle (Q_{GW}) was derived from the numerical model.

Variable	Low Est.	Mid. Est.	High Est.	Derivation
C_H (nM)	135	282	454	Median ± IQR from equilibration chambers (0.75 meters, summer)
C_B (nM)	14	18	33	Median ± IQR from equilibration chambers (1.25 and 1.75 meters, summer)
φ (m^3 m^{-3})	0.43	0.43	0.43	Literature
C_H (µmol m^{-3})	58	121	195	C_H (nM) x φ
C_B (µmol m^{-3})	6.0	7.7	14	C_B (nM) x φ
z (m)	0.5	0.5	0.5	Equilibration chambers
x (m)	11	3	2	C. A. Schutte et al., manuscript in preparation, 2014
$\frac{\partial C}{\partial z}$ (µmol m^{-4})	77	197	358	Median ± IQR from equilibration chambers (median, summer)
$\frac{\partial C}{\partial x}$ (µmol m^{-4})	9.5	76	181	Estimated as $(C_H-C_B)/(0.5x)$
D_L (m)	0.1	0.5	1	See caption
D_T (m)	0.01	0.05	0.10	See caption
J_T (µmol m^{-2} d^{-1})	0.04	3.0	20	Equation 4
J_E (µmol m^{-2} d^{-1})	3.2	8.6	13	Median ± IQR from efflux measurements
R_C (µmol m^{-2} d^{-1})	4.8	7.8	11	Mean ± SD from potential rate measurements (0.25 meters, summer)
J_{TM} (µmol m^{-2} d^{-1})	8.0	16	24	$J_E + R_C$
J_L (µmol m^{-2} d^{-1})	0.05	11	100	Equation 5
Q_{GW} (m d^{-1})	0.05	0.3	0.55	Numerical model
J_{AI} (µmol m^{-2} d^{-1})	0.30	2.3	7.8	Equation 6 (using C_B)
J_{AO} (µmol m^{-2} d^{-1})	2.9	36	107	Equation 6 (using C_H)
J_{AN} (µmol m^{-2} d^{-1})	2.6	34	100	$J_{AO} - J_{AI}$
A_V (m^2)	0.50	0.50	0.50	Equilibration chambers
A_H (m^2)	2.0	3.0	11	C. A. Schutte et al., manuscript in preparation, 2014
R_P (µmol m^{-2} d^{-1})	17	40	57	Equation 7
f	0.005	0.004	0.003	Sediment incubations
R_N (mmol m^{-2} d^{-1})	3.3	10	19	$(R_P/f)/1000$

Table 2.3. Spatial distribution of high pore water nitrate concentrations on the upper beach of Cabretta Island (Locations 1-10) and Sapelo Island (Locations 11-12).
* Location of pore gas equilibration chambers used in this study

Location	**Latitude** (°)	**Longitude** (°)	**Depth** (m)	**Width** (m)	**Max.** $[NO_3^-]$ (μM)
1*	31.42512	81.24694	1.05	4.05	1200
2	31.42371	81.24798	0.91	2.00	635
3	31.42609	81.24612	0.77	12.00	1912
7	31.42774	81.24441	1.01	10.50	2954
8	31.43192	81.23798	0.91	16.00	548
10	31.43609	81.23576	1.10	2.00	183
11	31.40616	81.25732	1.67	2.00	105
12	31.39003	81.26453	1.08	2.00	314
Mean	N/A	N/A	1.06	6.32	981
Std. Dev.	N/A	N/A	0.27	5.65	997

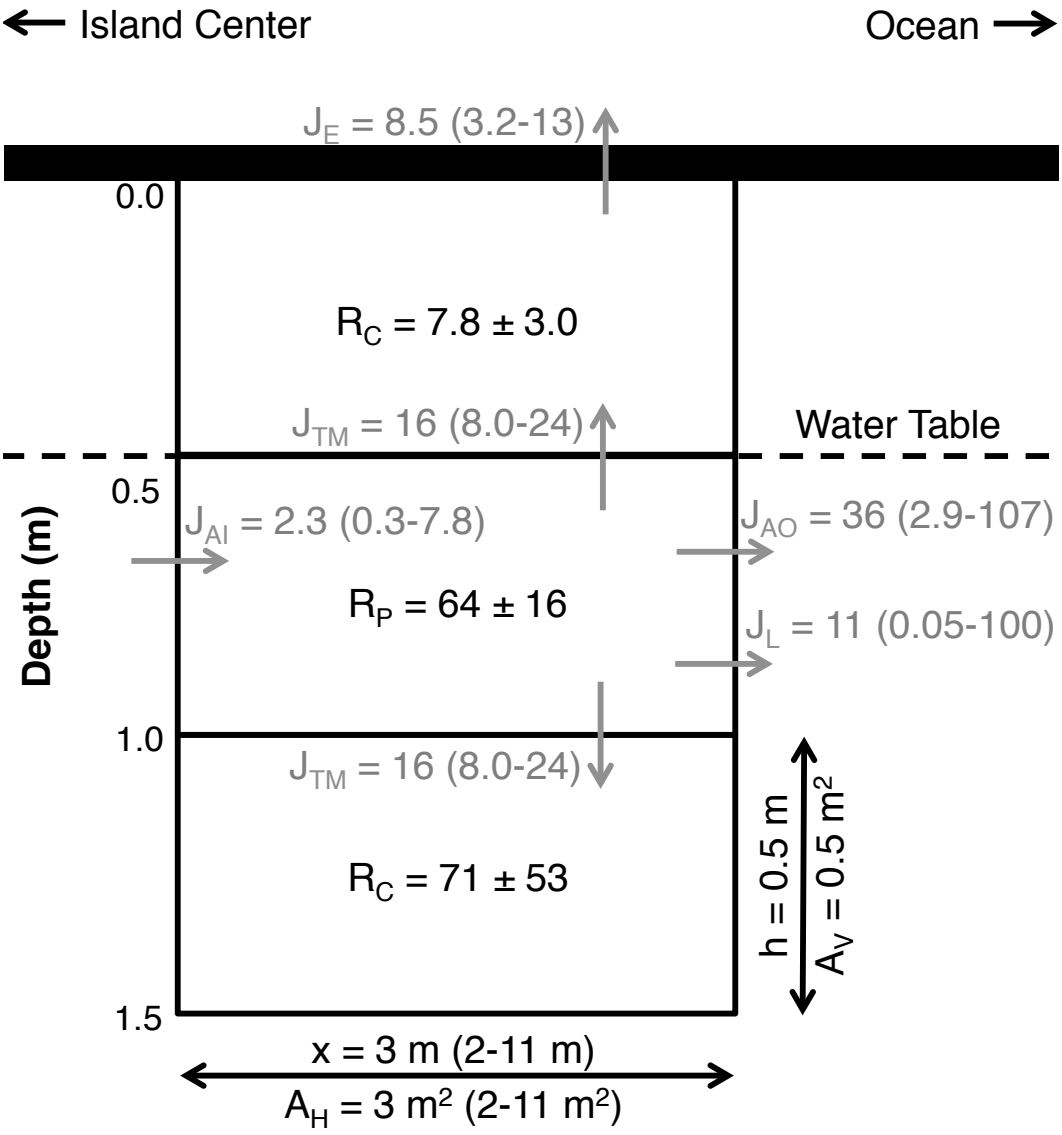

Figure 2.8. Nitrous oxide mass balance for a cross section of the beach. Each box represents a prism with a width equivalent to one meter of coastline, the length of the hotspot (x), and a depth of 0.5 m (h, the height of an equilibration chamber). Production and consumption rates are displayed in black (mean ± 1 standard deviation). Fluxes associated with transport processes including advection (J_{AI} and J_{AO}), longitudinal dispersion (J_L), and transverse dispersion (J_T) are displayed in gray and labeled with middle (and low-high) estimates. The median value (and IQR) are displayed for the atmospheric loss term (J_E). All rates and fluxes are expressed in units of μmol N_2O m^{-2} day^{-1}. Advection was not calculated in the top interval because it was assumed to be unsaturated and therefore had no groundwater flow. Advection was ignored in the bottom depth interval because there was no horizontal concentration gradient to drive a net flux in or out of the box. The 1.5-2.0 meter depth interval is not displayed in this diagram because there was no N_2O concentration gradient in either the horizontal or vertical directions, so were no N_2O fluxes in or out of that zone.

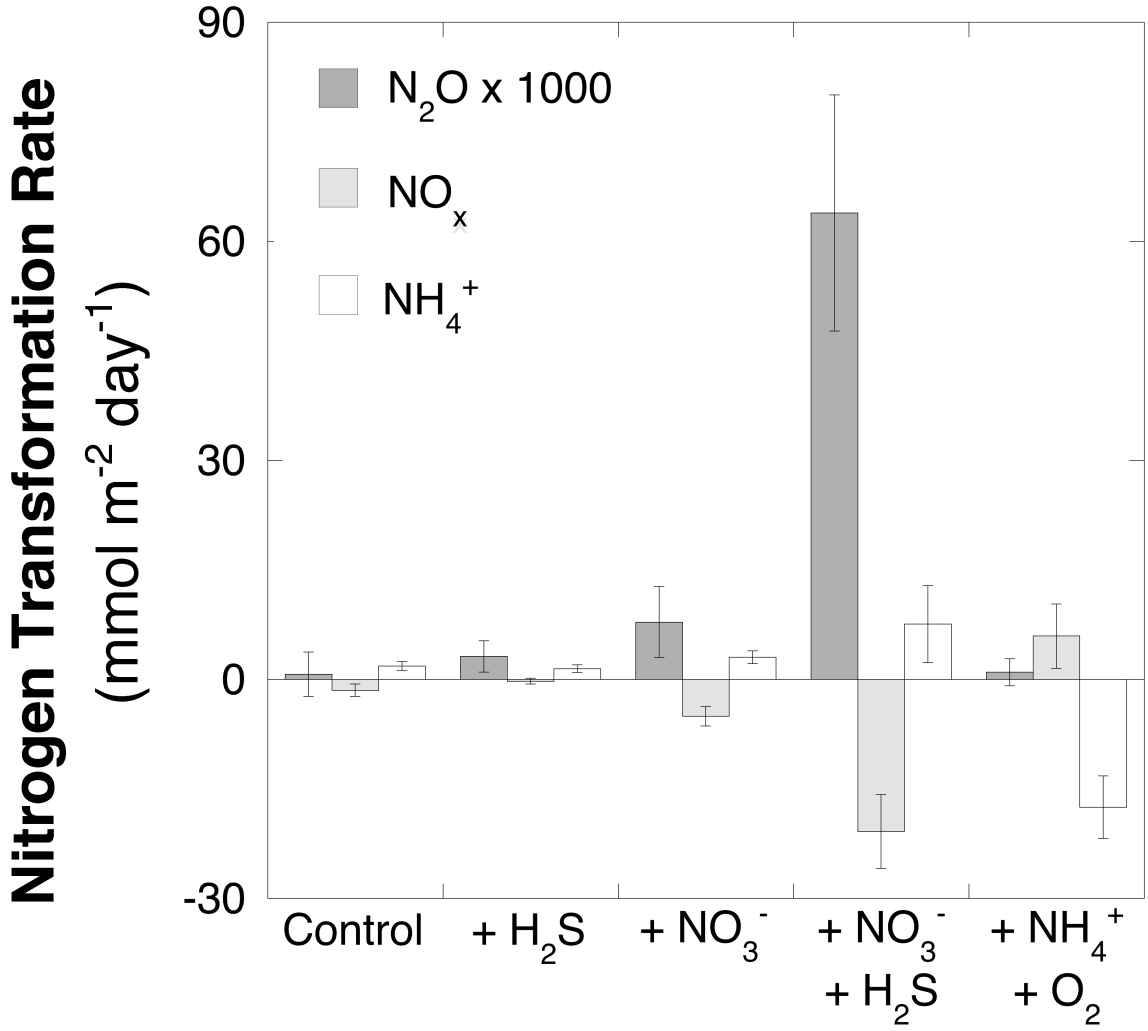

Figure 2.9. Mean nitrogen transformation rates in a bottle incubation experiment in the 24 hours following the addition of H_2S. Negative rates represent consumption and positive rates represent production. Error bars are plus or minus one standard deviation. NH_4^+ rates were calculated based on the change in the sum of the dissolved and adsorbed pools.

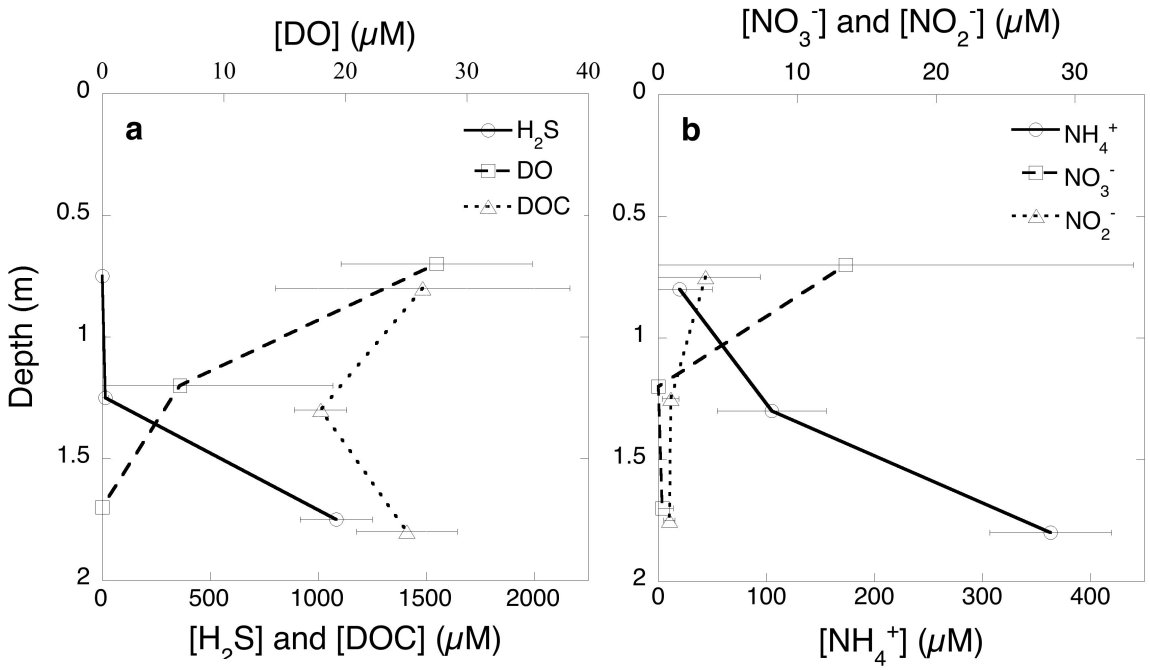

Figure 2.10. Concentration profiles of dissolved oxygen and sulfide (a) and nitrate, nitrite, and ammonium (b) adjacent to equilibration chambers in summer 2012. No data is available in the 0-0.5 m interval because the pore space was unsaturated except at extreme high tides.

CHAPTER 3

DEEP OXYGEN PENETRATION DRIVES NITRIFICATION IN INTERTIDAL BEACH SANDS[2]

[2] Schutte, C.A., A.M. Wilson, T. Evans, W.S. Moore, and S.B. Joye. To be submitted to *Limnology and Oceanography*.

ABSTRACT

The global nitrogen cycle is undergoing a massive perturbation, with around 40% of the global flux of fixed nitrogen into the biosphere coming from human activity. Primary production in coastal water bodies tends to be nitrogen limited, so this anthropogenic nitrogen loading can have far reaching ecosystem impacts such as eutrophication, algal blooms, hypoxia, and fish kills. Groundwater can be an important pathway for this nitrogen to enter coastal waters. As nitrogen-rich groundwater flows through coastal aquifers, however, microbial processes such as coupled nitrification-denitrification can remove nitrogen, potentially limiting its groundwater-driven flux into adjacent surface waters. However, nitrification is often limited by oxygen availability in reduced coastal aquifers, making this coupling inefficient. We discovered a zone of elevated nitrate concentration (median = 431 μM) in the shallow beach sands of a barrier island in coastal Georgia, USA. Porewater dissolved oxygen concentrations at this location varied from near zero at night to near atmospheric saturation during the day. Beach sand incubated across this range in dissolved oxygen concentration showed high nitrification rates under oxic conditions (0.78 ± 0.26 mmol m^{-2} day^{-1}) that were similar to rates of net nitrate removal when averaged across oxic/anoxic oscillations (1.2 ± 1.7 mmol m^{-2} day^{-1}). Therefore, dissolved oxygen oscillations linked nitrogen oxidation and reduction pathways such that nitrogen was removed from beach sand.

INTRODUCTION

Through the invention of the Haber-Bosch process, by which gaseous nitrogen in the atmosphere is fixed industrially into a bioavailable form, humans began a massive

global experiment on the nitrogen cycle. Anthropogenic nitrogen fixation now accounts for 40% of the fixed nitrogen flux into the global biosphere each year [*Galloway et al.*, 2004]. This excess nitrogen has a strong impact on nitrogen-limited ecosystems such as estuaries and the coastal ocean [*Howarth*, 1988], where it relieves nitrogen limitation and causes eutrophication, which results in algal blooms, hypoxia, and fish kills [*Nixon*, 1995]. Upwelling is an important nitrogen source in some coastal marine systems, but other sources, including riverine loading, atmospheric deposition, and submarine groundwater discharge (SGD), generally dominate in estuaries and the coastal ocean. Though riverine nitrogen inputs are by far the most studied, SGD inputs can rival riverine inputs in many cases [*Slomp and Van Cappellen*, 2004], and SGD is the dominant nitrogen source to the South Atlantic Bight adjacent to the southeastern United States [*Moore et al.*, 2002].

Sinks for these nitrogen inputs are necessary in order to maintain functional coastal ecosystems. Bioavailable nitrogen is removed from coastal waters by the microbial processes of denitrification and anammox, which reduce nitrate (NO_3^-) and nitrite (NO_2^-), respectively, to dinitrogen gas (N_2) [*Joye and Anderson*, 2008]. These processes are active under anoxic conditions, though aerobic denitrification has been observed at some locations [*Gao et al.*, 2010; *Rao et al.*, 2007]. Coastal sediments tend to be anoxic and are important sites for microbial NO_3^- reduction. However, due to the reduced nature of these sediments, inorganic nitrogen in the porewater tends to be present as ammonium (NH_4^+) [*Kroeger et al.*, 2007], limiting the oxidized nitrogen substrate that is required by denitrification and anammox. Therefore, another microbial nitrogen cycling process is necessary to optimize the sediment nitrogen sink. Nitrification is the

aerobic oxidation of NH_4^+ to NO_2^- and then NO_3^-. Together, coupled nitrification-denitrification constitutes an important nitrogen sink in coastal sediments [*Joye and Anderson*, 2008]. Coupled nitrification-anammox has also been documented, but so far only in pelagic settings [*Lam et al.*, 2007].

The dominant paradigm is that the oxidative and reductive processes of the nitrogen cycle are coupled by diffusion. Nitrification is active in shallow sediments where oxygen is available. This NO_3^- then diffuses into anoxic sediments where denitrification or anammox reduces it to N_2. However, this coupling is much stronger in permeable sediment where porewater advection can rapidly deliver NO_3^- from zones of nitrification to denitrification [*Huettel et al.*, 2014]. Coupled nitrification-denitrification is well documented in subtidal permeable sediments such as continental shelves where rates of nitrogen removal are high relative to other coastal sediments. Intertidal permeable sediments are less well studied, but tides and waves have been shown to drive changes in oxygen concentration [*Brotas et al.*, 1990; *de Beer et al.*, 2005], which in turn can strongly influence rates of nitrogen cycling processes.

Beaches are composed of intertidal sand by definition and are increasingly recognized as biogeochemical reactors [*Anschutz et al.*, 2009; *Boudreau et al.*, 2001]. This globally important landform accounts for around 75% of Earth's coastline that is not covered in ice [*Brown*, 2001]. Coastal aquifers, including those beneath beaches, are dynamic systems where upland-derived groundwater mixes with seawater that is circulated through the porespace by waves and tides in what is known as what is known as the subterranean estuary [*Moore*, 1999]. This mixing creates geochemical gradients that microorganisms exploit to drive metabolic processes that can influence

biogeochemical cycles. Studies of beach biogeochemistry have focused primarily on carbon and oxygen cycling as beaches trap and mineralize marine particulate organic matter and export inorganic nutrients back to the ocean [*Anschutz et al.*, 2009; *Charbonnier et al.*, 2013]. However, beaches are likely to support active cycling throughout an entire cascade of biogeochemical processes, including nitrogen cycling processes.

Beaches are also incredibly important for the tourism industry, accounting for $300 billion in profits in the United States alone in 2007 [*Houston*, 2008]. The usability of this resource is negatively impacted by poor water quality, however, and events like harmful algal blooms have the potential to decrease the economic productivity of beaches [*Hoagland and Scatasta*, 2006]. Nitrogen loading is a key cause of harmful algal blooms in the coastal ocean [*Paerl*, 1997]. Therefore, if beach sands have the capacity to filter nitrogen out of porewater prior to discharge, they may help to prevent harmful algal blooms. In this way, intact beaches may increase the resilience of coastal ecosystems to anthropogenic perturbations such as excessive nitrogen loading.

We tested the hypotheses that oxygen penetration into intertidal beach sand drives nitrification and that nitrification is coupled to denitrification such that beaches act as natural reactors that filter fixed nitrogen from porewater prior to discharge to the ocean. A hotspot of elevated NO_3^- concentration in beach porewater was identified where nitrification was likely to be active. The variability in porewater dissolved oxygen (DO) concentration at this location was assessed, and beach sand was incubated across the observed range in DO to determine its impact on rates of nitrogen transformation processes. While nitrification was active in the presence of in situ DO concentrations, its

rate was too low to support the observed rate of NO_3^- reduction via denitrification and/or anammox. This decoupling of nitrification and denitrification indicated another NO_3^- source and additional geochemical evidence suggested that this source may be in situ nitrogen fixation.

METHODS

The study site was located on Cabretta Island (hereafter Cabretta), a small, Holocene barrier island on the coast of Georgia, USA (Fig. 3.1a) that is ~200 meters wide and extends across a salt marsh, forested upland, dune system, and sandy beach. Cabretta is separated from the larger Sapelo Island by a small tidal creek. The beach on Cabretta extends for ~2.5 km and is separated from the beach on the southern end of Sapelo Island by an inlet (Fig. 3.1b). These islands are exposed to semidiurnal tides with a tidal range of ~1.5 meters on neap tides and ~3 meters on spring tides. A surficial, unconfined aquifer composed primarily of fine sand extends across part of the forested upland and across the dunes and beach.

A transect of 17 groundwater monitoring wells was installed across the entire width of Cabretta in June 2008. Wells were clustered such that groundwater could be sampled from several depths at the same location (Fig. 3.2). An initial survey of groundwater geochemistry was conducted by collecting samples from these wells every two months from August 2008 through August 2010. Prior to sample collection, stagnant groundwater was purged from each well using a peristaltic pump. Freshly recharged groundwater was collected with a disposable syringe and tygon tubing. The syringe and tubing were rinsed with ~30 mL of sample and four subsamples were collected for

different analytes. 10 mL of unfiltered groundwater were collected into a He-purged, 20-mL headspace vial, fixed with a base pellet, and sealed with a butyl rubber stopper. This sample was acidified with 0.5 mL of concentrated HCl prior to analysis for dissolved inorganic carbon (DIC) on a Shimadzu GC-2010 gas chromatograph with Carbosphere column, methanizer, and flame ionization detector. All remaining subsamples were filtered with a 0.2 μm Target® filter. The first subsample was fixed with zinc acetate and used to measure the concentration of sulfide (H_2S) [*Cline*, 1969]. Another subsample was stored frozen in an acid-washed Nalgene bottle and analyzed for dissolved organic carbon and nitrogen (DOC and DON, respectively), nitrite (NO_2^-) and NO_x ($NO_3^- + NO_2^-$). DOC and total dissolved nitrogen (TDN) were measured using a Shimadzu TOC-5000 with a TN unit. NO_x was measured using an Antek 745 vanadium reduction assembly coupled with an Antek 7050 chemiluminescent nitric oxide detector and NO_2^- was measured using standard colorimetric techniques [*Bendschneider and Robinson*, 1952]. Another 5 mL subsample was fixed with 200 μL of phenol reagent [*Solorzano*, 1969] and stored at 4°C for subsequent colorimetric analysis of NH_4^+. NO_3^- concentration was calculated as the difference between NO_x and NO_2^-, and DIN as the sum of NO_x and NH_4^+, and DON as the difference between TDN and the sum of NO_x and NH_4^+. 20 mL of groundwater were filtered into an acid-washed 20 mL scintillation vial and fixed with 50 μL of concentrated nitric acid. Dissolved inorganic phosphorus (DIP) was measured as phosphate by spectrophotometry [*Strickland and Parsons*, 1972] and total dissolved iron (Fe) was measured using atomic adsorption spectroscopy.

In October 2012, shallow porewater from twelve locations (10 on Cabretta Island and 2 on Sapelo Island) was surveyed for NO_3^-. At each location, the approximate spring

high tide line was found by marking the highest wrack deposit on the beach that was still beneath the dune. A wrack-free spot nearby was selected and a hole drilled through the dry sand on the surface of the beach using a hand auger to a depth of approximately 50 cm. A stainless steel pushpoint sampler was inserted into the sand at the bottom of the hole. Porewater was collected into a disposable syringe from as near to the top of the water table as possible. A subsample was tested for NO_3^- using an aquarium test kit (Aquarium Pharmaceuticals, Inc.). A second subsample was collected for the more precise NO_3^- analysis described above. Holes were drilled and samples collected at 2-meter intervals up and down the beach until a hole with no detectable NO_3^- was sampled on either side. Additional samples were collected at approximately 15 cm depth intervals from an existing hole at the center of the NO_3^- zone. The latitude and longitude of this central hole were measured using a handheld GPS unit.

The speed and direction of groundwater flow beneath the beach on Cabretta Island were modeled using SUTRA (see Chapter 2). Groundwater flow was driven by the pressure gradient between the water table and oscillating sea level with a wavelength of 12 hours and an amplitude of 1.85 meters (representing an idealized spring tide at this location). Groundwater flow was also influenced by the stratigraphy of the island, which was composed of two layers, determined using electrical resistivity tomography surveys and coring during groundwater monitoring well installation, with very different permeabilities. An unconfined surface layer of fine-grained, isotropic sand with a permeability of 2×10^{-11} m^2 [*Anderson*, 2011] was underlain by a relic marsh mud layer with a permeability of 5×10^{-15} m^2.

In June and July 2011 and July and August 2012, porewater dissolved oxygen (DO) concentrations were monitored in the shallow porewater near the spring high tide line on the beach (near monitoring well cluster TT-6, Fig. 3.2). Porewater containing high NO_3^- concentrations was located as described above for surveys. Duplicate mini-piezometers were installed at that location, spaced two meters apart. These mini-piezometers were constructed from 0.5" PVC pipe with a 2 cm screened interval. The screened interval was sealed with a tight-fitting hose barb and connected to a length of gas-impermeable FEP-lined polyethylene tubing. A sample was collected from each mini-piezometer to ensure that it was installed within a zone of NO_3^--rich porewater. Mini-piezometers were installed at the shallowest depth at which water could still be pumped from them (~65 cm deep). Each mini-piezometer was connected via FEP-lined tubing to a peristaltic pump and then a YSI 600XLM-V2 sonde equipped with a ROX optical DO sensor and installed in a flow-through cell. The pumps were run very slowly such that porewater was pumped continuously from each mini-piezometer past the sonde sensors at a rate of 3.6-4.5 L hr^{-1}. Each pump and sonde were housed in a shelter behind the dunes, approximately 5 meters from the mini-piezometer. Two simultaneous time series of groundwater salinity, temperature, pH, and DO concentrations were measured for 4-6 weeks during the summers of 2011 and 2012. Each time series encompassed multiple consecutive spring and neap tides. Sondes collected data at 15-minute intervals throughout each time series. The depth to the water table was measured in a nearby groundwater monitoring well using a pressure logger throughout the low flow pump tests. Water level data for nearby Doboy Sound and meteorological data from Sapelo Island

were downloaded from the Georgia Coastal Ecosystems LTER website (https://gce-lter.marsci.uga.edu/portal/monitoring.htm).

In June 2012, just prior to the low flow pump tests described above, sand was collected from 6 holes spaced at 1-meter intervals along the spring high tide line on the beach, near where the mini-piezometers were installed later in the summer. Sand was homogenized and 30 cm^3 was added to thirty 120 mL serum bottles. Half of the bottles were kept under a N_2 atmosphere, and half under a 21% oxygen (O_2) 79% N_2 mix. Following a 24-hour preincubation at 27°C, 70 mL of an anoxic artificial pore water (APW) with a salinity of 30 ppt was added to each serum vial. Six bottles received APW with no nitrogen or carbon source, 12 bottles were amended with 50 μM NH_4^+, and 12 bottles were amended with 150 μM NO_3^- and 300 μM carbon (1:1:1 lactate:acetate:glucose molar carbon ratio). Within each treatment, half the bottles were kept anoxic and the other half oxic. Each bottle was immediately sampled for analysis of NH_4^+ and NO_3^- as described above, and the sample volume was replaced with UHP N_2 for anoxic bottles and a mix of N_2 and O_2 for oxic bottles. Samples were collected at 0, 24, 48, and 72 hours. Between sampling, bottles were placed on a shaker table at 25 rpm inside a dark incubator set at 27°C.

Following the 72-hour sample, each bottle was opened and the APW/sand mixture was purged very gently with UHP N_2. Bottles were resealed and half of the bottles from each nitrogen-amended treatment were set back to their original oxic or anoxic state. The other half were switched such that previously anoxic bottles became oxic and vice versa. Following this reset, samples were collected at 0, 24, 48, 72, 96, and 144 hours. A linear regression of the change in NH_4^+ and NO_3^- concentrations through time was performed

for each bottle. The average of the slopes from triplicate bottles for each treatment was used to estimate the net potential rate of NH_4^+ and NO_3^- production and consumption. A schematic representation of the experimental procedure is provided in Figure 3.3.

In October 2012, triplicate sediment cores were collected from approximately the same location on the beach where sand for the experiment described above was collected. Each core was sectioned into 5 cm increments, and adsorbed NH_4^+ was extracted from each using 2 M KCl. A depth profile of Rhizon samplers was installed at the same location and sampled for dissolved NH_4^+. The in situ dissolved: adsorbed NH_4^+ concentration ratio was calculated from these data and applied to the dissolved NH_4^+ concentrations in the experiment above in order to account for changes in both the dissolved and adsorbed NH_4^+ pools.

RESULTS

Groundwater NO_3^- concentrations were uniformly low across most of Cabretta (Fig. 3.2a), with a median NO_3^- concentration of 0 μM and an interquartile range (*IQR*) of 0.0–0.4 μM (n = 207). The exception was the well installed one meter deep on the upper part of the beach near the spring high tide line. This well was only sampled three times before it was washed away. NO_3^- concentrations at this location were between 140 μM and 1200 μM, at least two orders of magnitude higher than the concentration observed anywhere else on the island. This same well also had the lowest median NH_4^+ concentration on the island (2.3 μM, range = 2.0–3.1 μM, n = 3) compared to a median NH_4^+ concentration in other wells of 105 μM (*IQR* = 49–323 μM, n = 207). Ammonium concentrations were generally much higher and more variable across the island than NO_3^-

with the highest concentrations in deep wells near the center of the island and the lowest concentrations in shallow wells that were inundated regularly with surface or creek water (Fig 3.2b).

This nitrate hotspot was not limited to a single location. A survey along the entire extent of Cabretta Island (Fig. 3.1c) as well as two locations on adjacent Sapelo Island (Fig. 3.1d) revealed elevated NO_3^- concentrations near the spring high tide line on the beach everywhere except the extreme tips of Cabretta Island. The maximum NO_3^- concentrations observed at each location were extremely variable, but the median value was 431 μM (*IQR* = 120–1,200, *n* = 10). The highest concentrations tended to be near the middle of the island (along its Northeast-Southwest axis), with concentrations decreasing towards its northern and southern ends (Fig. 3.1c). A similar trend was observed with the width of the NO_3^- feature: it was narrowest near the extremes of the island and widest near the island center. This width varied between 2 and 16 meters, with a median of 2 meters and a mean of 6.3 meters. Maximum NO_3^- concentrations were observed near the top of the water table and decreased rapidly between 10 and 20 cm deeper, though concentrations remained elevated above the median groundwater NO_3^- concentration up to 50 cm below the depth where the maximum concentration was observed (Fig. 3.4).

This NO_3^- hotspot also had higher DIN concentrations than were found in most other monitoring wells across Cabretta Island (Table 3.1), resulting in high DIN to DIP ratios ranging from 29–226 (Table 3.2). The *IQR* for the well with the next highest DIN:DIP (TT-1, 1 meter) was 23-57. High DIN:DIP in the marsh well was driven by very low DIP concentrations rather than very high DIN concentrations, however (Table 3.1). The high median Fe:DIP of 8.0 (*IQR* = 0.7-34) indicates that DIP was mostly

removed from solution through the formation of Fe-P minerals [*Slomp and Van Cappellen*, 2004]. This, in turn, was only possible because insufficient H_2S was present to remove the Fe from solution through the formation of Fe-S minerals (Table 3.1).

On the upper part of the beach near where elevated groundwater NO_3^- concentrations were observed, groundwater flow patterns shifted drastically between low and high tide. At low tide, groundwater flow was uniformly down the beach with speeds less that 100 cm day^{-1} on the upper beach (Fig 3.5a). At high tide, groundwater flow directions reversed across most of the beach. Groundwater flowing down from the island upland converged with beach groundwater flowing back toward the island center near the high tide line (Fig. 3.5b), which moved higher on the beach during spring tides relative to neap tides. The location with elevated NO_3^- concentrations was only inundated on spring high tides and was situated at the groundwater flow convergence at those times. It is possible that when the beach was inundated at high tide, oxic seawater was advected through beach sands, driving oxygen into the aquifer.

Indeed, large oscillations in groundwater DO concentrations were observed from 62-64 cm depth on the upper part of the beach where maximum NO_3^- concentrations were found (Fig. 3.6). However, these DO oscillations were not consistently in phase with oscillations in tidal height in nearby surface waters or with the depth of the water table on the upper beach. Instead, DO peaks always occurred during the day when photosynthetically available radiation (PAR) was high, and DO minima always occurred at night. Therefore, the source of the observed groundwater DO was in situ photosynthesis rather than tidally driven import of oxygen-rich seawater. The full DO, PAR, and water level datasets are presented in Figure 3.7. Dissolved oxygen

concentrations were generally less than 30 μM at night and peaked at 193 ± 61 μM (n = 19) during the day (Fig. 3.6). DO concentrations crashed rapidly between daily maxima and nightly minima, indicating that oxygen was consumed at a rate of 161 ± 65 mmol m^{-3} day^{-1} (n = 16, calculated using the Matlab findpeaks function).

Incubation experiments from June 2012 demonstrated that the microbial community in beach sands from the zone of high NO_3^- concentration (65 cm deep near the high tide line) rapidly switched between different nitrogen cycling modes in response to shifts in DO (Fig. 3.8). When sand was incubated under oxic conditions with additional NH_4^+, NO_x (NO_3^- + $NO_2^{-)}$ was produced at an average rate of 9.1 ± 1.6 mmol m^{-3} day^{-1} (n = 3). Following the switch from oxic to anoxic conditions, the NO_x that was produced in the presence of oxygen was consumed at an average rate of 8.7 ± 1.6 mmol m^{-3} day^{-1}. Averaged across all oxic NH_4^+ addition treatments (n = 12), the rate of NH_4^+ consumption (32 ± 5.5 mmol m^{-3} day^{-1}) was substantially higher than the simultaneous rate of NO_x production (7.7 ± 1.5 mmol m^{-3} day^{-1}, n = 12). In NO_3^- and DOC addition treatments, NO_x was consumed universally, though the consumption rate was higher in anoxic (22 ± 16 mmol m^{-3} day^{-1}, n = 12) than oxic bottles (7.8 ± 4.9 mmol m^{-3} day^{-1}, n = 12). This NO_x consumption was associated with a smaller rate of NH_4^+ production (4.8 ± 1.2 mmol m^{-3} day^{-1}, n = 3), likely from dissimilatory reduction of NO_3^- to NH_4^+. In the NH_4^+ addition treatment in which NO_x was produced during the initial oxic phase of the experiment, NO_x was consumed during the following anoxic phase at a lower rate (8.7 ± 1.6 mmol m^{-3} day^{-1}) than was observed in other treatments in which both NO_3^- and labile DOC were present (22 ± 16 mmol m^{-3} day^{-1}).

DISCUSSION

While most subterranean estuaries have low NO_3^- relative to NH_4^+ concentrations [*Kroeger et al.*, 2007], beach porewater frequently exhibits the opposite pattern, and NO_3^- concentrations that range from tens of micromolar [*Anschutz et al.*, 2009; *Kuwae*, 2003; *Niencheski et al.*, 2007] to thousands of micromolar [*Andersen et al.*, 2007] have been reported in numerous studies. There are several possible sources of this NO_3^- that are not mutually exclusive, including agricultural inputs [*Andersen et al.*, 2007], sewage [*Ueda et al.*, 2003], and nitrification [*Santos et al.*, 2008] of NH_4^+ from these sources or from mineralization of marine or terrestrial organic matter [*Bourke et al.*, 2014]. Cabretta Island is relatively pristine, so agriculture and sewage were unlikely to be the source of the observed NO_3^-. The Altamaha River carries a substantial NO_3^- load and discharges ~10 km South of the study site. However, beach porewater was still highly enriched in NO_3^- relative to surface ocean waters making it unlikely that beach NO_3^- was derived from the river. The range of maximum NO_3^- concentrations found in profiles across Cabretta Island (55-2950 μM) overlaps with the concentration range reported for several other beaches [*Boehm et al.*, 2004; *Sáenz et al.*, 2012; *Santoro*, 2010], and the distribution pattern with maximum NO_3^- concentrations observed near the top of the water table on the upper beach matches the distribution on a Florida beach closely [*Santos et al.*, 2008], indicating that similar processes may drive NO_3^- accumulation in beach porewater at different locations.

Dissolved oxygen concentrations in the porewater of intertidal permeable sediments can approach atmospheric saturation [*Brotas et al.*, 1990; *Charbonnier et al.*, 2013; *de Beer et al.*, 2005], or exceed it where benthic photosynthesis is important

[*Jansen et al.*, 2009; *Werner et al.*, 2006]. The depth of oxygen penetration is controlled by tidal patterns of exposure and inundation. In the Wadden Sea, oxygen was transported into the sediment by tide and wave driven porewater advection, with maximum oxygen penetration of up to 8 cm occurring when sediment was inundated [*de Beer et al.*, 2005; *Jansen et al.*, 2009; *Werner et al.*, 2006]. In contrast, oxygen penetration was highest when sediment from Ria Formosa was exposed, suggesting exchange of air with the permeable sediment [*Brotas et al.*, 1990]. Oxygen penetration into the upper beach on Cabretta Island displayed a fundamentally different pattern, with no relationship between oxygen penetration and tide or inundation. The oxygen signal was strongly correlated with photosynthetically available radiation, indicating that the balance between oxygen production by benthic photosynthesis and microbial consumption controlled oxygen penetration into the sediment. Infrequent inundation of the upper beach coupled with rapid drainage of beach sand yielded unsaturated sand to depths of tens of centimeters, facilitating deep penetration of oxygen produced by phototrophs near the sediment surface [*Neale et al.*, 2000].

Nitrification is likely to be active in oxygenated permeable coastal sediments, and has been inferred from NO_3^- profiles [*Huettel et al.*, 1998] or as a NO_3^- source for a measured denitrification rate [*Rao et al.*, 2008]. The few existing nitrification rates reported in the literature were measured in subtidal sands and range across two orders of magnitude. A rate of 0.0-0.2 mmol NO_3^- m^{-2} day^{-1} was reported in the estuary of the River Weser [*Ehrenhauss and Huettel*, 2004], 0-2.07 mmol NO_3^- m^{-2} day^{-1} in Florida [*Gihring et al.*, 2010], 0-6.78 mmol NO_3^- m^{-2} day^{-1} in the North Sea [*Braeckman et al.*,

2014], and 1.19-2.29 mmol NO_3^- m^{-2} day^{-1} in continental shelf sediment from the South Atlantic Bight [*Laursen and Seitzinger*, 2002].

The volumetric net NO_x production rate observed in Cabretta Island beach sands was 7.7 ± 1.5 mmol m^{-3} day^{-1}. Integrating over the 10 cm at the top of the observed depth profiles where NO_3^- concentrations were highest (Fig. 3.4) yields a net nitrification rate of 0.77 ± 0.15 mmol m^{-2} day^{-1}. The gross nitrification rate was higher than this, however, because NO_x accumulation would have driven consumption, as evidenced by the observed 7.8 ± 4.9 mmol m^{-3} day^{-1} of NO_x loss in NO_3^- amended sand under oxic conditions. The possible pathways for this NO_x loss were aerobic denitrification [*Gao et al.*, 2010] and microbial assimilation [*Porubsky*, 2008]. The depth range over which NO_3^- was enriched in situ to the same levels as those used to generate these estimates was at least 10 cm (Fig. 3.4), yielding a NO_3^- consumption rate of 0.78 ± 0.49 mmol m^{-2} day^{-1}. Assuming that nitrification supplied all of the NO_3^- that was lost, the gross nitrification rate was 1.6 ± 0.51 mmol m^{-2} day^{-1}. However, sand was only oxygenated during the day, implying that the in situ rate of nitrification, when averaged across seasons, would be approximately half of the daily rate reported above, or 0.78 ± 0.26 mmol m^{-2} day^{-1}, which falls within the range of nitrification rates reported in other permeable coastal sediments, described above. This yields a volumetric gross nitrification rate of 7.8 ± 2.6 mmol m^{-3} day^{-1} in the top 10 of the aquifer. Assuming that two moles of O_2 were consumed for every mole of NH_4^+ that was oxidized to NO_3^- by nitrifying microorganisms [*Konhauser*, 2007], this rate of nitrification would result in oxygen consumption at a rate of 16 ± 5.2 mmol m^{-3} day^{-1}. The net rate of oxygen consumption at this location and depth was 161 ± 65 mmol m^{-3} day^{-1} based on the decrease in DO concentration from its daily peak to

nearly zero at night. Therefore, nitrification accounted for around 10% of oxygen consumption, which is a reasonable value for coastal sediments [*Laursen and Seitzinger*, 2002].

The NO_x reduction rate at the same location under anoxic conditions was 22 ± 16 mmol m^{-3} day^{-1} and could be the result of denitrification, anammox, dissimilatory nitrate reduction to ammonium (DNRA), or microbial assimilation. Assimilation and DNRA retain the nitrogen in a bioavailable form rather than converting it into a gas like the other two processes [*Joye and Anderson*, 2008]. The DNRA rate at this location was estimated as the rate of net NH_4^+ production under anoxic conditions (4.8 ± 1.2 mmol m^{-3} day^{-1}). Organic matter mineralization could also generate NH_4^+, but this production was likely small compared with DNRA due to low organic nitrogen content of the beach sand (<0.05%) and porewater (~4 μM) in these incubations. Subtracting the rate of NH_4^+ production from the rate of NO_x consumption yields a net NO_x removal rate of 17 ± 16 mmol m^{-3} day^{-1} under anoxic conditions. DNRA is an anaerobic process, so it is not subtracted from the NO_x reduction rate to generate the net NO_x removal rate of 7.8 ± 4.9 mmol m^{-3} day^{-1} under oxic conditions. Integrating over the top 10 cm of elevated NO_3^- concentrations in situ (Fig. 3.4), NO_x removal occurred at a rate of 0.78 ± 0.49 mmol m^{-2} day^{-1} under oxic conditions and 1.7 ± 1.6 mmol m^{-2} day^{-1} under anoxic conditions. Therefore, assuming that sand was oxygenated during the day, the daily NO_x loss rate when averaged across seasons would be 1.2 ± 1.7 mmol m^{-2} day^{-1}. This rate is higher than most denitrification rates reported for coastal sediments in general [*Joye and Anderson*, 2008], but falls within the range of denitrification rates found in high permeability coastal sediments [*Huettel et al.*, 2014]. This rate is lower than the 11 mmol m^{-2} day^{-1} measured

by a field-based method at the same location (see Chapter 2). This difference can be explained in part by the fact that the rates measured in the relatively static bottle incubations presented here are likely underestimates of in situ rates since they do not take porewater advection into account [*Gao et al.*, 2010].

The nitrification rate measured in beach sand from Cabretta Island was indistinguishable from the rate of NOx consumption. However, assuming that this NOx consumption rate was an underestimate of the in situ rate, the measured nitrification rate was insufficient to support this rate of NOx removal. Yet NO_3^- persisted at high concentrations in beach porewater, indicating a weak coupling between nitrification and NOx consumption processes (denitrification and anammox) and a NOx supply rate that exceeded microbial consumption. It is possible that the measured nitrification rate was also lower than the in situ rate due to the lack of porewater advection in sediment incubations. However, it is also possible that another supply of NO_x supported the observed NO_3^- concentrations and reduction rates. Potential sources include atmospheric deposition [*Paerl et al.*, 2002] and nitrogen fixation in shallower sand strata. It is possible that the same photosynthetic organisms that drove the observed oxygen dynamics were also fixing nitrogen [*Steppe and Paerl*, 2005]. This would have required subsequent mineralization of the fixed organic nitrogen followed by nitrification and percolation of the NO_3^- produced down to the top of the water table where it was measured. This nitrification could have occurred at a shallower depth that was not measured in the experiments described here. Indeed, the DIN concentration within the NO_3^- hotspot was among the highest on Cabretta Island (Table 3.1). Some of this DIN may have been derived from groundwater flow from the dunes and island center, but DIN concentrations

there were insufficient to produce the greater than 1 mM NO_3^- concentrations observed beneath the upper beach. Combined with the exceptionally high DIN:DIP observed in beach porewater, this suggests that nitrogen fixation by benthic microorganisms may have played an important role in generating the high DIN concentrations observed at this site.

Nitrogen fixation can only be inferred based on these results, and future work should focus on measuring rates of this process in intertidal sands. High nitrogen fixation rates on beaches could be an important source of new nitrogen to the surf zone. This nitrogen source could be balanced by an active coupling between nitrification and denitrification stimulated by photosynthetic microorganisms, however [*An and Joye*, 2001]. It is possible that in situ nitrogen fixation supports a community of denitrifying microorganisms that are primed to remove nitrogen derived from external sources as a result, allowing beaches to act as a nitrogen filter. The low DIN:DIP observed in beach porewater may be maintained by this process. Submarine groundwater discharge is an important source of nitrogen and phosphorus to surface waters, and can be the dominant source in some regions [*Slomp and Van Cappellen*, 2004], including the South Atlantic Bight [*Moore et al.*, 2002]. Sand is the dominant sediment type on most beaches and around 70% of continental shelves globally [*Boudreau et al.*, 2001], meaning that most shallow groundwater must flow through sand prior to discharge. High rates of NO_3^- loss make these sands an important sink for nitrogen that contributes to the nitrogen limitation of seawater in the surf zone.

LITERATURE CITED

An, S., and S. Joye (2001), Enhancement of coupled nitrification-denitrification by benthic photosynthesis in shallow estuarine sediments, *Limnology and Oceanography*, *46*(1), 62-74.

Andersen, M. S., L. Baron, J. Gudbjerg, J. Gregersen, D. Chapellier, R. Jakobsen, and D. Postma (2007), Discharge of nitrate-containing groundwater into a coastal marine environment, *Journal of Hydrology*, *336*(1-2), 98-114.

Anderson, J. L. (2011), Field and numerical observations of groundwater dynamics within Cabretta Island, a barrier island off the coast of Georgia, edited, pp. 1-62, University of South Carolina.

Anschutz, P., T. Smith, A. Mouret, D. J., S. Bujan, D. Poirer, and P. Lecroart (2009), Tidal sands as biogeochemical reactors, *Estuarine, Coastal and Shelf Science*, *84*, 84-90.

Bendschneider, K., and R. J. Robinson (1952), A new spectrophotometric method for the determination of nitrite in sea water, *Journal of Marine Research*, *11*(1), 87-96.

Boehm, A. B., G. G. Shellenbarger, and A. Paytan (2004), Groundwater discharge: potential association with fecal indicator bacteria in the surf zone, *Environmental science & technology*, *38*(13), 3558-3566.

Boudreau, B. P., M. Huettel, S. Forster, R. A. Jahnke, A. McLachlan, J. J. Middelburg, P. Nielsen, F. Sansone, G. Taghon, and W. Van (2001), Permeable marine sediments: overturning an old paradigm, *EOS, Transactions American Geophysical Union*, *82*(11), 133-140.

Bourke, M. F., A. J. Kessler, and P. L. M. Cook (2014), Influence of buried Ulva lactuca on denitrification in permeable sediments, *Marine Ecology Progress Series*, *498*, 85-U420.

Braeckman, U., M. Y. Foshtomi, D. Van Gansbeke, F. Meysman, K. Soetaert, M. Vincx, and J. Vanaverbeke (2014), Variable importance of macrofaunal functional biodiversity for biogeochemical cycling in temperate coastal sediments, *Ecosystems*, *17*(4), 720-737.

Brotas, V., A. Amorim-Ferreira, C. Vale, and F. Catarino (1990), Oxygen profiles in intertidal sediments of Ria Formosa (S. Portugal), *Hydrobiologia*, *207*(1), 123-130.

Brown, A. C. (2001), Biology of sandy beaches, *Encyclopedia of Ocean Sciences*, *5*, 2496-2504.

Charbonnier, C., P. Anschutz, D. Poirier, S. Bujan, and P. Lecroart (2013), Aerobic respiration in a high-energy sandy beach, *Marine Chemistry*, *155*, 10-21.

Cline, J. D. (1969), Spectrophotometric determination of hydrogen sulfide in natural waters, *Limnology and Oceanography*, *14*(3), 454-458.

de Beer, D., F. Wenzhöfer, T. G. Ferdelman, S. E. Boehme, M. Huettel, J. E. E. van Beusekom, M. E. Böttcher, N. Musat, and N. Dubilier (2005), Transport and mineralization rates in north sea sandy intertidal sediments, Sylt-Rømø basin, Wadden sea, *Limnology and Oceanography*, *50*(1), 113-127.

Ehrenhauss, S., and M. Huettel (2004), Advective transport and decomposition of chain-forming planktonic diatoms in permeable sediments, *Journal of Sea Research*, *52*(3), 179-197.

Galloway, J. N., et al. (2004), Nitrogen cycles: past, present, and future, *Biogeochemistry*, *70*(2), 153-226.

Gao, H., F. Schreiber, G. Collins, M. M. Jensen, J. E. Kostka, G. Lavik, D. de Beer, H.-Y. Zhou, and M. M. Kuypers (2010), Aerobic denitrification in permeable Wadden Sea sediments, *The ISME Journal*, *4*, 417-426.

Gihring, T. M., A. Canion, A. Riggs, M. Huettel, and J. E. Kostka (2010), Denitrification in shallow, sublittoral Gulf of Mexico permeable sediments, *Limnology and Oceanography*, *55*(1), 43-54.

Hoagland, P., and S. Scatasta (2006), The economic effects of harmful algal blooms, in *Ecology of harmful algae*, edited, pp. 391-402, Springer.

Houston, J. R. (2008), The economic value of beaches—a 2008 update, *Shore & Beach*, *76*(3), 22-26.

Howarth, R. W. (1988), Nutrient limitation of net primary production in marine ecosystems, *Annual Review of Ecology and Systematics*, *19*, 89-110.

Huettel, M., P. Berg, and J. E. Kostka (2014), Benthic Exchange and Biogeochemical Cycling in Permeable Sediments, in *Annual Review of Marine Science, Vol 6*, edited by C. A. Carlson and S. J. Giovannoni, pp. 23-51.

Huettel, M., W. Ziebis, S. Forster, and G. W. Luther (1998), Advective transport affecting metal and nutrient distributions and interfacial fluxes in permeable sediments, *Geochimica et Cosmochimica Acta*, *62*(4), 613-631.

Jansen, S., E. Walpersdorf, U. Werner, M. Billerbeck, M. E. Bottcher, and D. de Beer (2009), Functioning of intertidal flats inferred from temporal and spatial dynamics of O_2, H_2S and pH in their surface sediment, *Ocean Dynamics*, *59*(2), 317-332.

Joye, S. B., and I. C. Anderson (2008), Nitrogen cycling in coastal sediments, in *Nitrogen in the Marine Environment, 2nd Edition*, edited by D. G. Capone, D. A. Bronk, M. R. Mulholland and E. J. Carpenter, pp. 686-902, Elsevier.

Konhauser, K. (2007), *Introduction to Geomicrobiology*, Blackwell Publishing, Malden, MA.

Kroeger, K. D., P. W. Swarzenski, W. J. Greenwood, and C. Reich (2007), Submarine groundwater discharge to Tampa Bay: nutrient fluxes and biogeochemistry of the coastal aquifer, *Marine Chemistry*, *104*(1), 85-97.

Kuwae, T. (2003), Effect of emersion and immersion on the porewater nutrient dynamics of an intertidal sandflat in Tokyo Bay, *Estuarine, Coastal and Shelf Science*, *57*(5-6), 929-940.

Lam, P., M. M. Jensen, G. Lavik, D. F. McGinnis, B. Muller, C. J. Schubert, R. Amann, B. Thamdrup, and M. M. M. Kuypers (2007), Linking crenarchaeal and bacterial nitrification to anammox in the Black Sea, *Proceedings of the National Academy of Sciences of the United States of America*, *104*(17), 7104-7109.

Laursen, A. E., and S. P. Seitzinger (2002), The role of denitrification in nitrogen removal and carbon mineralization in Mid-Atlantic Bight sediments, *Continental Shelf Research*, *22*(9), 1397-1416.

Moore, W. S. (1999), The subterranean estuary: a reaction zone of ground water and sea water, *Marine Chemistry*, *65*, 111-125.

Moore, W. S., J. M. Krest, G. Taylor, E. Roggenstein, S. B. Joye, and R. Lee (2002), Thermal evidence of water exchange through a coastal aquifer: Implications for nutrient fluxes, *Geophysical Research Letters*, *29*(14), 1704.

Neale, C. N., J. B. Hughes, and C. H. Ward (2000), Impacts of unsaturated zone properties on oxygen transport and aquifer reaeration, *Groundwater*, *38*(5), 784-794.

Niencheski, L., H. Windom, and W. S. Moore (2007), Submarine groundwater discharge of nutrients to the ocean along a coastal lagoon barrier, …, *Marine Chemistry*.

Nixon, S. W. (1995), Coastal marine eutrophication: a definition, social causes, and future concerns, *Ophelia*, *41*, 199-219.

Paerl, H. W. (1997), Coastal eutrophication and harmful algal blooms: Importance of atmospheric deposition and groundwater as" new" nitrogen and other nutrient sources, *Limnology and oceanography*, *42*(5), 1154-1165.

Paerl, H. W., R. L. Dennis, and D. R. Whitall (2002), Atmospheric deposition of nitrogen: implications for nutrient over-enrichment of coastal waters, *Estuaries*, *25*(4B), 677-693.

Porubsky, W. P. (2008), Nutrient-replete benthic microalgae as a source of dissolved organic carbon to coastal waters, *Estuaries and Coasts*, *31*(5), 860-876.

Rao, A. M. F., M. J. McCarthy, W. S. Gardner, and R. A. Jahnke (2007), Respiration and denitrification in permeable continental shelf deposits on the South Atlantic Bight: rates of carbon and nitrogen cycling from sediment column experiments, *Continental Shelf Research*, *27*(13), 1801-1819.

Rao, A. M. F., M. J. McCarthy, W. S. Gardner, and R. A. Jahnke (2008), Respiration and denitrification in permeable continental shelf deposits on the South Atlantic Bight: N-2 : Ar and isotope pairing measurements in sediment column experiments, *Continental Shelf Research*, *28*(4-5), 602-613.

Sáenz, J. P., E. C. Hopmans, D. Rogers, P. B. Henderson, M. A. Charette, S. Schouten, K. L. Casciotti, J. S. Sinninghe Damsté, and T. I. Eglinton (2012), Distribution of anaerobic ammonia-oxidizing bacteria in a subterranean estuary, *Marine Chemistry*, *136*, 7-13.

Santoro, A. E. (2010), Microbial nitrogen cycling at the salwater-freshwater interface, *Hydrogeology Journal*, *18*, 187-202.

Santos, I. R., W. C. Burnett, J. P. Chanton, and B. Mwashote (2008), Nutrient biogeochemistry in a Gulf of Mexico subterranean estuary and groundwater-derived fluxes to the coastal ocean, *Limnology and Oceanography*.

Slomp, C. P., and P. Van Cappellen (2004), Nutrient inputs to the coastal ocean through submarine groundwater discharge: controls and potential impact, *Journal of Hydrology*, *295*, 64-86.

Solorzano, L. (1969), Determination of ammonia in natural waters by the phenolhypochlorite method, *Limnology and Oceanography*, *14*(5), 799-801.

Steppe, T. F., and H. W. Paerl (2005), Nitrogenase activity and nifH expression in a marine intertidal microbial mat, *Microbial Ecology*, *49*(2), 315-324.

Strickland, J. D. H., and T. R. Parsons (1972), *A practical handbook of seawater analysis*, 2nd ed., Bulletin of the Fisheries Research Board of Canada.

Ueda, S., C.-S. U. Go, M. Suzumura, and E. Sumi (2003), Denitrification in a seashore sandy deposit influenced by groundwater discharge, *Biogeochemistry*, *63*(2), 187-205.

Werner, U., M. Billerbeck, L. Polerecky, U. Franke, M. Huettel, J. E. E. van Beusekom, and D. de Beer (2006), Spatial and temporal patterns of mineralization rates and

oxygen distribution in a permeable intertidal sand flat (Sylt, Germany), *Limnology and Oceanography*, *51*(6), 2549-2563.

Wilson, A. M., and L. R. Gardner (2006), Tidally driven groundwater flow and solute exchange in a marsh: numerical simulations, *Water Resources Research*, *42*(1).

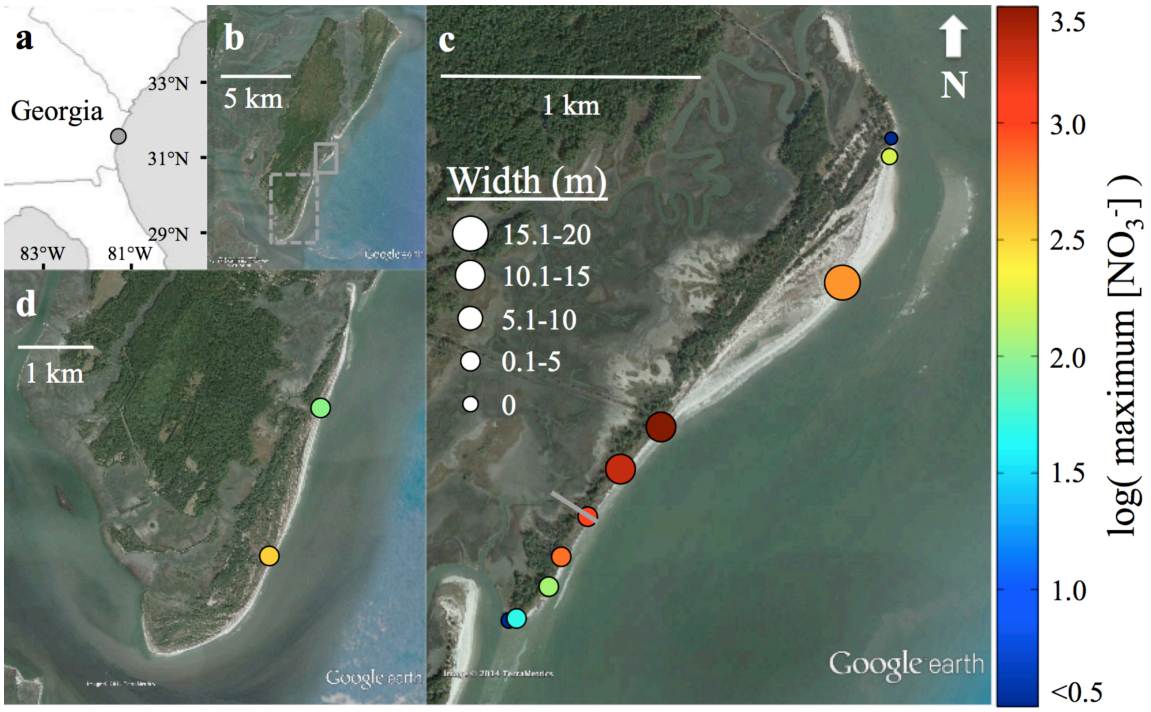

Figure 3.1. Sapelo Island (gray circle) is located on the coast of Georgia, USA (a). Satellite image of Sapelo Island (b). The dashed gray box shows the location of the image blown up in (c) while the solid gray box shows the location of the image blown up in (d). Satellite image of Cabretta Island (c) and the southern coast of Sapelo Island (d). The solid gray line on the South end of Cabretta Island shows the location of the groundwater monitoring well transect. The circles in (c) and (d) show the locations of sample collection for the nitrate survey conducted in October 2012. The size of the circle represents the width of the nitrate hotspot and the color of the circle represents the log-transformed nitrate concentration.

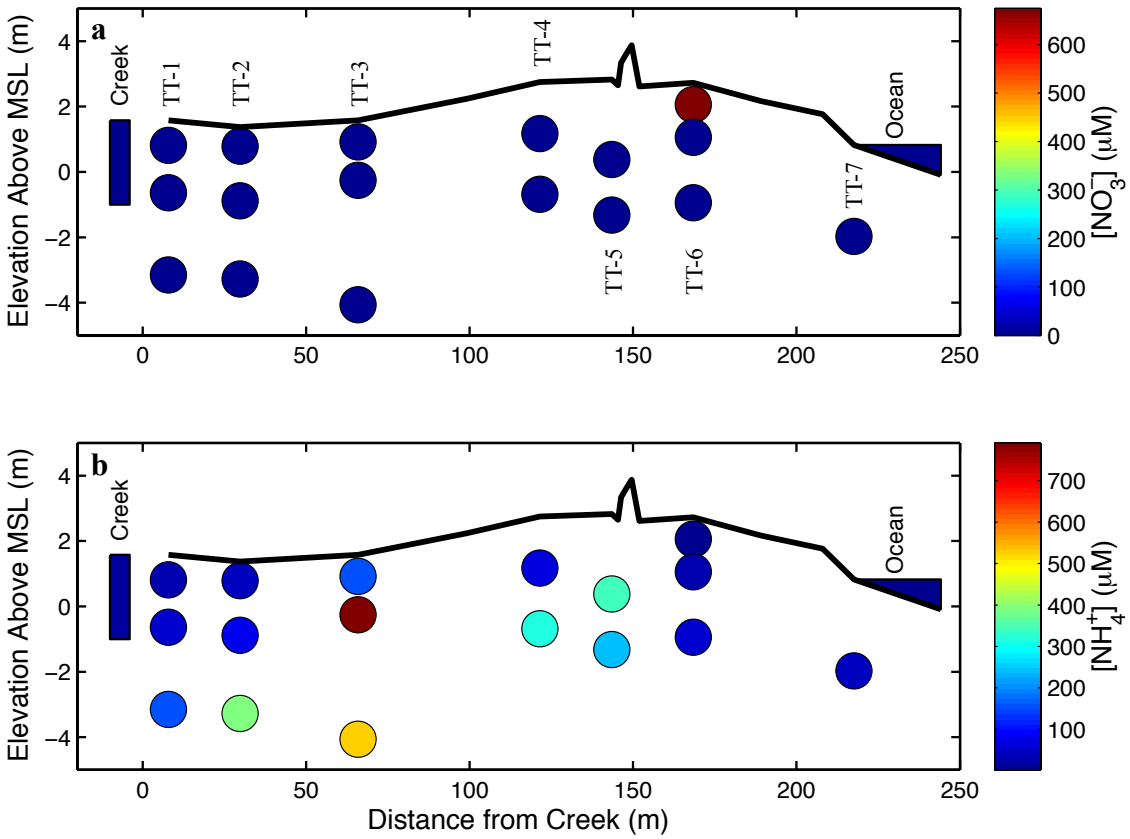

Figure 3.2. Cross sections of Cabretta Island (10:1 vertical exaggeration) showing the median concentrations of NO_3^- (a) and NH_4^+ (b) measured in groundwater monitoring wells sampled every other month from August 2008 to August 2010. Thirteen measurements were made at most wells with the exception of the shallowest well at TT-6, which washed away after only 3 measurements.

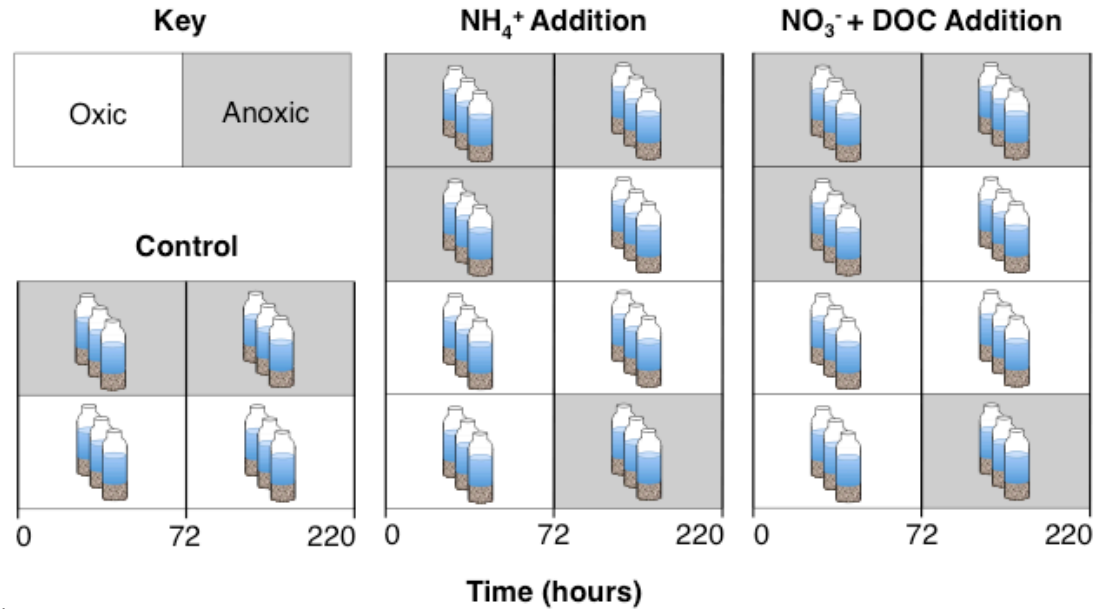

Figure 3.3. Schematic representation of the sand incubation procedure described in the methods section.

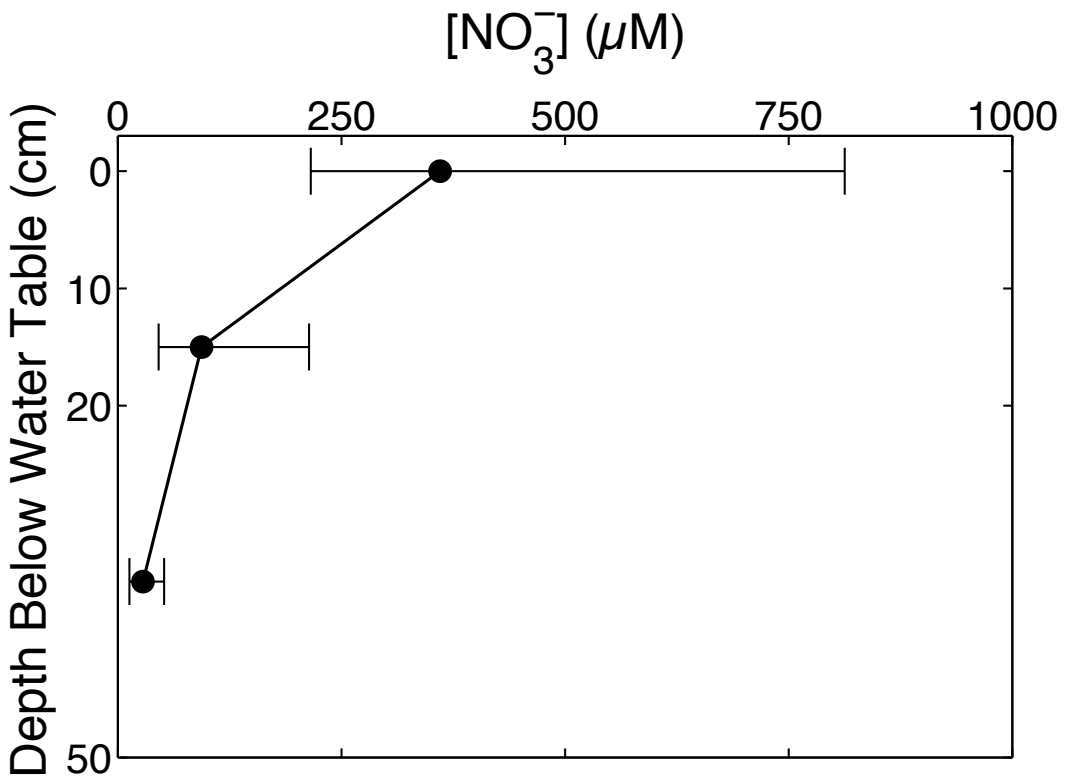

Figure 3.4. Nitrate concentrations from depth profiles measured during the October 2012 survey of the beach. This curve represents data aggregated from seven individual depth profiles collected on Cabretta and Sapelo Islands over the course of two days. The point at a depth of 0 cm is the median NO_3^- concentration measured at the top of each profile, near the top of the water table. The second point represents the median of all measurements made between 10 and 20 cm deep, and the final point represents the median of all values measured between 20 and 50 cm deep. The error bars show the interquartile range for each depth window.

Table 3.1. Median concentrations of organic carbon and nitrogen, inorganic carbon, nitrogen, and phosphorus, total iron, and sulfide in each well labeled in Figure 3.2 (n = 13 for most measurements except TT-6, 0.7 meters where the well washed away after only 3 measurements). All concentrations are expressed in units of μM. The range of values in parentheses represents the interquartile range.

Loc.	Depth	DOC	DON	DIC	DIN	DIP	Fe	H_2S
Creek	N/A	481 (332–550)	22 (15–34)	2360 (1920–2710)	24 (5.7–33)	2.7 (2–6.1)	0.2 (0–0.7)	0 (0–0)
TT-1	0.8	508 (325–615)	24 (17–43)	3240 (2770–4290)	33 (23–55)	1.3 (0.5–1.8)	10 (0.8–45)	0 (0–0.1)
TT-1	2.2	416 (395–488)	16 (9–23)	5860 (4880–6500)	62 (46–73)	47 (44–54)	173 (101–229)	0 (0–2.3)
TT-1	4.7	845 (721–960)	67 (37–82)	11000 (7750–12600)	162 (144–188)	108 (90–115)	1.4 (1.2–5.7)	2.8 (0–22)
TT-2	0.6	461 (404–611)	26 (20–36)	4200 (3550–5550)	40 (28–61)	4.7 (2.9–15)	34 (9.8–73)	0.1 (0–0.6)
TT-2	2.3	537 (477–554)	17 (3.4–32)	8950 (6540–10100)	92 (64–107)	86 (55–149)	124 (85–136)	0.2 (0–3.1)
TT-2	4.6	971 (864–1010)	18 (0–54)	12100 (9570–13000)	390 (352–417)	77 (72–82)	13 (10–14)	1.1 (0–5.3)
TT-3	0.7	936 (842–1020)	41 (15–57)	5630 (4600–6010)	169 (137–243)	9.2 (6–19)	12 (3.5–40)	0 (0–0)
TT-3	1.8	1540 (1420–1590)	68 (8.9–104)	13900 (11200–15600)	786 (695–818)	129 (125–135)	1.1 (0.8–1.4)	932 (198–1170)
TT-3	5.6	1060 (978–1130)	28 (0–110)	12900 (11100–13600)	528 (471–551)	56 (54–65)	23 (9.8–88)	3.1 (0–14)
TT-4	1.6	1100 (1040–1330)	46 (30–56)	2820 (2030–3620)	65 (48–117)	50 (40–55)	10 (8.3–17)	0.2 (0–4.1)
TT-4	3.4	2240 (1960–2860)	148 (101–174)	14100 (12500–17000)	321 (282–345)	154 (111–167)	1 (0.6–1.2)	305 (115–626)
TT-5	2.4	1420 (1230–1530)	156 (105–211)	8320 (4080–10600)	341 (294–482)	58 (42–67)	1.6 (0.8–2.3)	585 (137–2780)
TT-5	4.1	3340 (2490–3730)	167 (138–204)	10900 (8300–11600)	241 (200–274)	296 (248–393)	1.4 (1–2.6)	1820 (372–2660)
TT-6	0.7	1180 (916–1450)	0 (0–0)	1940 (1940–1940)	686 (159–1210)	5.4 (5.4–9.3)	0.5 (0.1–0.7)	0 (0–0)
TT-6	1.7	299 (238–401)	8.8 (7–16)	2260 (1670–2960)	30 (17–60)	11 (8.1–14)	14 (8–20)	0.2 (0–4.1)
TT-6	3.7	369 (258–595)	14 (2.2–20)	2700 (2150–3220)	60 (46–74)	22 (19–25)	5.1 (3.4–7.7)	5 (0–19)
TT-7	2.8	521 (368–662)	40 (20–62)	3550 (2900–3860)	66 (27–81)	17 (9.1–35)	3.4 (1–7.7)	0 (0–1.6)
Ocean	N/A	279 (235–293)	13 (10–19)	1920 (1770–2150)	3.4 (1.2–8.5)	1.1 (0.5–1.6)	0 (0–0.2)	0 (0–0.2)

Table 3.2. Median concentration ratios and results of calculations derived from the concentration data presented in Table 3.1 for each well labeled in Figure 3.2. All concentrations are expressed in units of μM. The range of values in parentheses represents the interquartile range.

Loc.	**Depth**	DOC:DON	DIC:DIN	DIN:DIP	DIC:DIP	Fe:DIP	H_2S:Fe
Creek	N/A	17 (15-23)	98 (73-404)	4.4 (2.6-9)	955 (484-1230)	0.1 (0-0.2)	0 (0-0.1)
TT-1	1	18 (11-24)	119 (106-173)	28 (23-56)	4120 (2670-7050)	8 (0.7-34)	0 (0-0)
TT-1	2.5	21 (17-29)	98 (74-126)	1.2 (0.9-1.5)	105 (92-150)	3.5 (2.3-4.3)	0 (0-0)
TT-1	5	13 (9.9-21)	71 (53-90)	1.7 (1.4-1.9)	113 (84-117)	0 (0-0.1)	1.7 (0-2.3)
TT-2	1	16 (12-23)	121 (67-227)	5.4 (2.8-8.9)	1190 (259-1540)	3.5 (2-6.7)	0 (0-0)
TT-2	2.5	26 (16-76)	101 (83-118)	1 (0.7-2.1)	73 (66-96)	1.2 (0.9-1.7)	0 (0-0)
TT-2	5	17 (13-40)	31 (17-33)	5.3 (4.7-6.4)	167 (123-182)	0.2 (0.1-0.2)	0.1 (0-0.4)
TT-3	1	21 (16-40)	34 (16-38)	13 (9.4-26)	471 (269-1170)	1.2 (0.5-4.2)	0 (0-0)
TT-3	2.5	17 (13-47)	18 (16-21)	6.2 (5.6-6.6)	114 (90-117)	0 (0-0)	409 (206-941)
TT-3	5	14 (5.4-19)	24 (22-28)	8.9 (8-9.7)	222 (183-244)	0.4 (0.1-1.6)	0.1 (0-1)
TT-4	2	24 (21-36)	41 (30-55)	1.4 (1.1-2.3)	56 (46-78)	0.2 (0.2-0.4)	0 (0-0.2)
TT-4	4	15 (13-21)	45 (36-52)	2.5 (2-2.7)	109 (82-128)	0 (0-0)	295 (148-622)
TT-5	2	9.5 (7.7-13)	22 (9.7-25)	6.2 (2.4-8.9)	126 (62-195)	0 (0-0)	257 (175-1750)
TT-5	3.7	16 (14-25)	47 (34-65)	0.8 (0.5-1.1)	32 (24-38)	0 (0-0)	578 (221-2440)
TT-6	1	ND	ND	128 (29-226)	183 (183-183)	0.1 (0-0.1)	0 (0-0)
TT-6	2	22 (19-46)	85 (50-116)	2.4 (1.6-4.6)	187 (153-300)	1.4 (0.7-1.9)	0 (0-0.2)
TT-6	4	21 (17-32)	55 (38-60)	2.6 (1.1-3)	108 (100-138)	0.3 (0.1-0.3)	0.6 (0-3.9)
TT-7	?	14 (11-22)	55 (40-77)	2.9 (2.1-3.5)	141 (109-244)	0.1 (0-0.4)	0 (0-0.2)
Ocean		18 (12-26)	668 (114-1380)	3.4 (1.3-13)	2050 (983-4380)	0 (0-0.5)	0 (0-0)

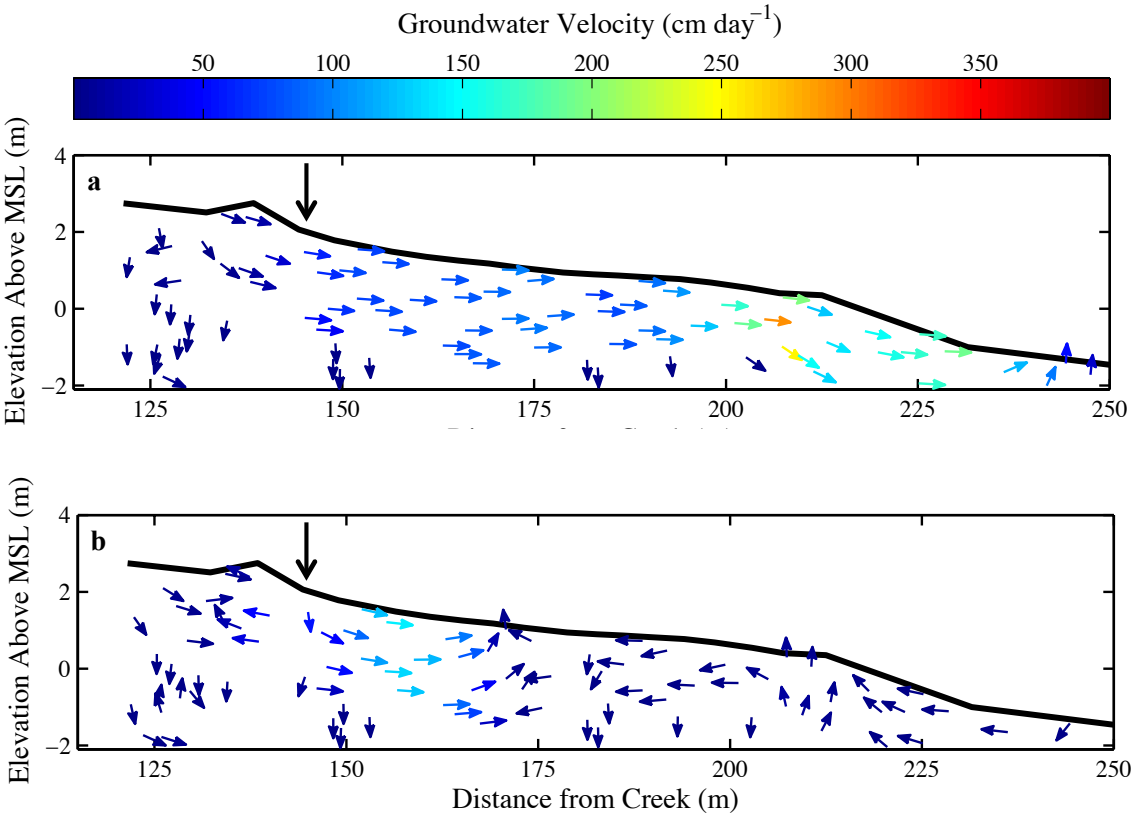

Figure 3.5. Cross section of the beach on Cabretta Island (5:1 vertical exaggeration) showing groundwater flow velocity on low tide (a) and high tide (b). The heavy black arrow indicates the position of the nitrate hotspot.

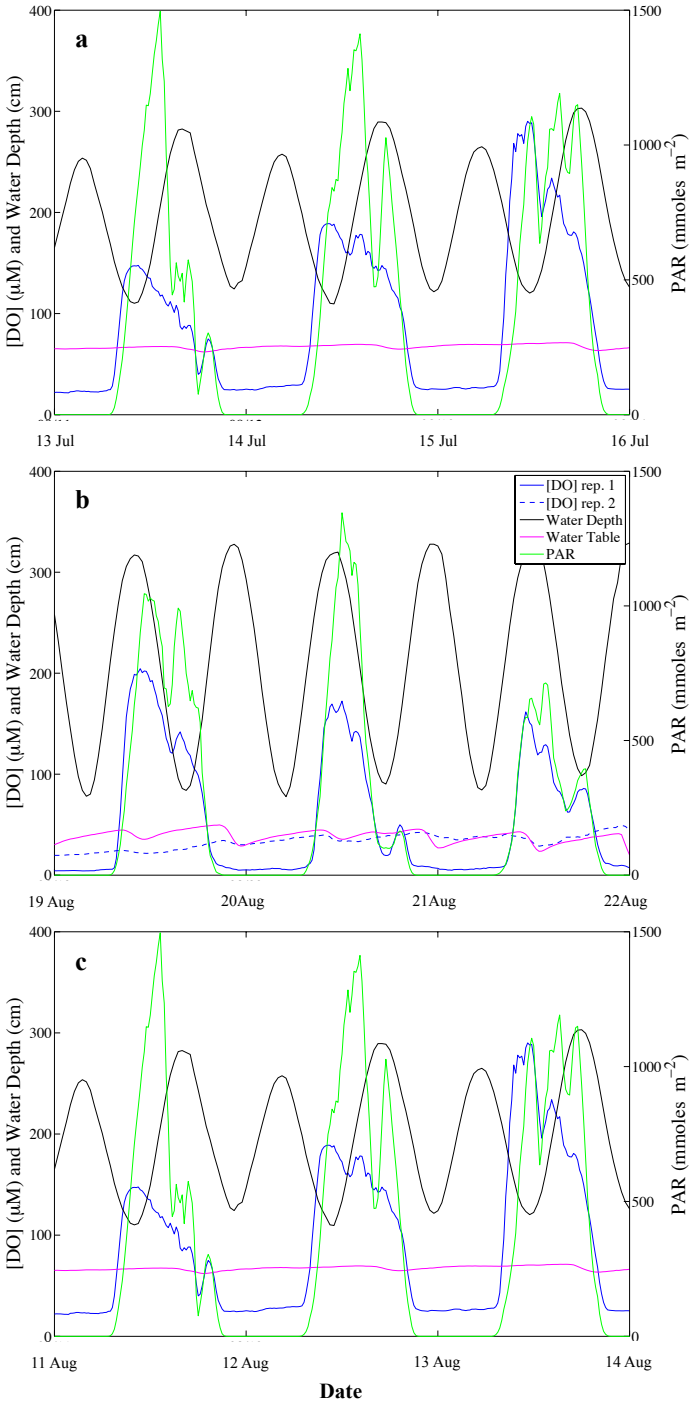

Figure 3.6. One-hour running averages of duplicate dissolved oxygen concentration time series, the depth of the water table beneath the sand surface, and total photosynthetically available radiation. The water depth in Doboy Sound is also plotted measured at 15-minute intervals. Each panel shows a 3-day snapshot from within one of the longer time series recorded during the summer of 2011 or 2012. These snapshots show a spring tide in 2011 (a), a spring tide in 2012 (b), and a neap tide in 2012 (c).

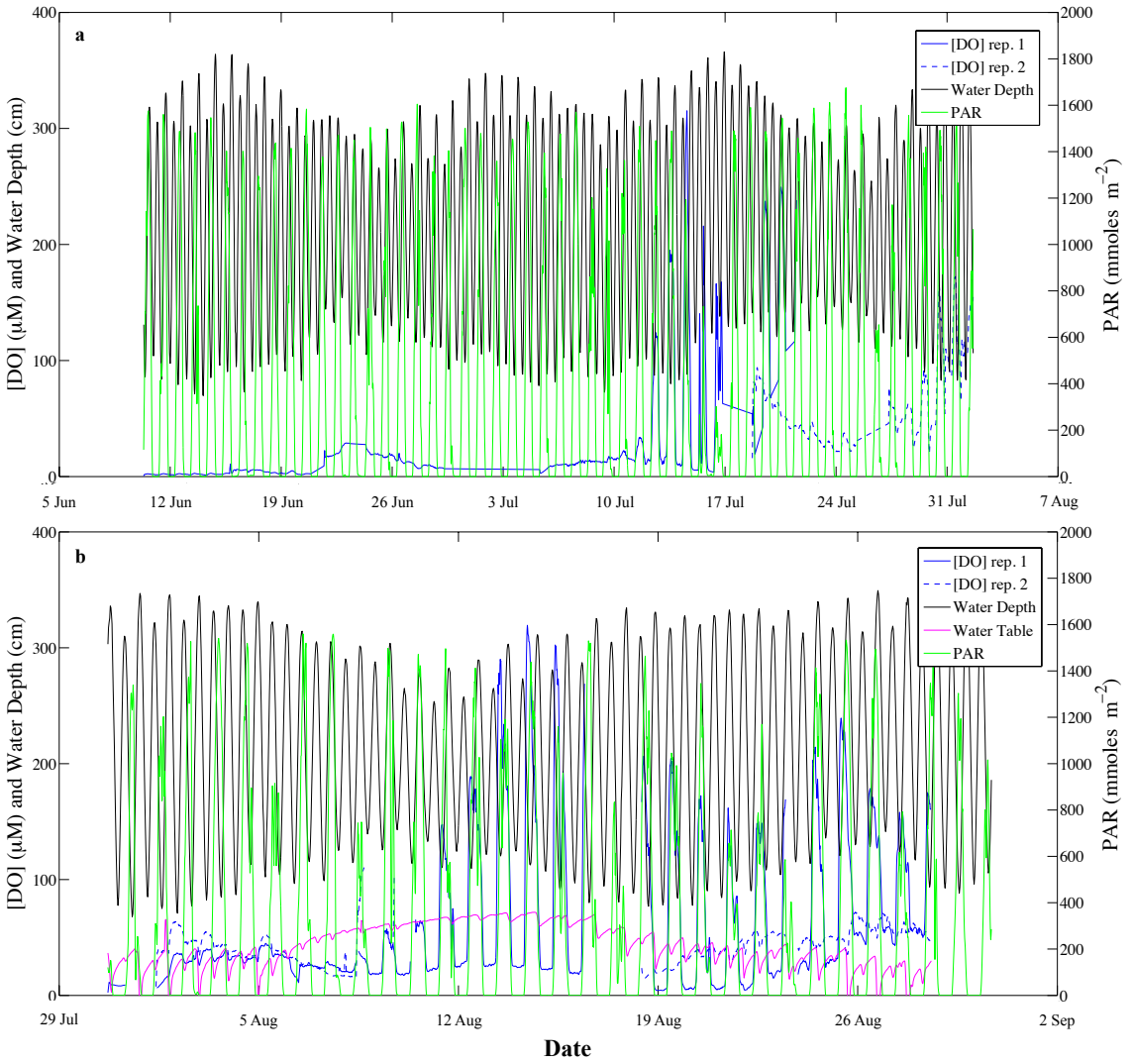

Figure 3.7. One-hour running average of complete dissolved oxygen time series from June and July of 2011 (a) and July and August of 2012 (b). Also included are the water depth in Doboy Sound recorded at 15-minute intervals, and one-hour running averages of total photosynthetically available radiation and the depth of the water table beneath the beach surface.

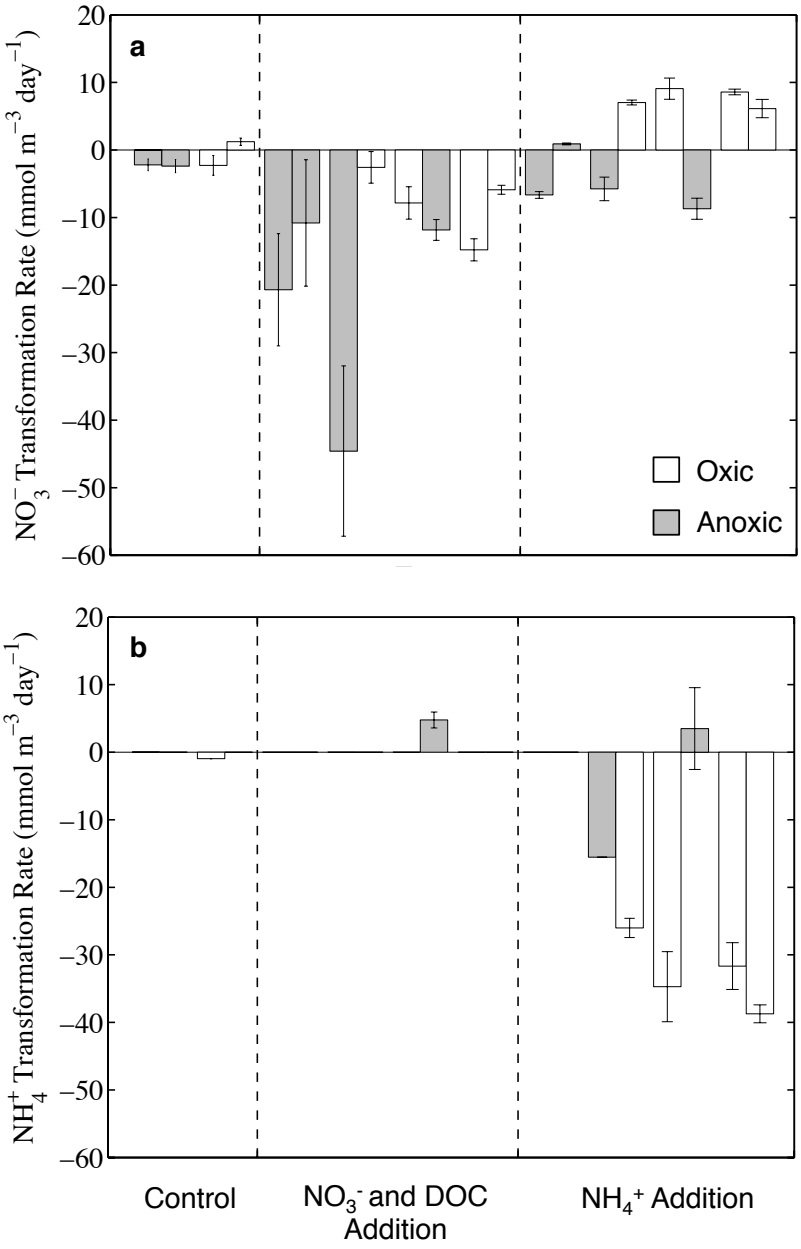

Figure 3.8. Nitrate (a) and ammonium (b) production (positive values) and consumption (negative values) rates in a slurry experiment with different nitrogen addition treatments under oxic and anoxic conditions. Paired bars represent the same set of bottles both before (left) and after (right) being reset in the middle of the experiment. The bars represent the mean of triplicate bottles and the error bars show the standard deviation. The data were too variable to calculate a rate where no bar is shown, and bars without error bars represent the rate measured from a single bottle.

CHAPTER 4

METHANOTROPHY CONTROLS GROUNDWATER METHANE EXPORT FROM A BARRIER ISLAND [3]

[3] Schutte, C.A., A.M. Wilson, T. Evans, W.S. Moore, and S.B. Joye. To be submitted to *Global Biogeochemical Cycles*.

ABSTRACT

Methane is the third most important greenhouse gas in Earth's atmosphere, and its concentration is increasing in response to human activities, such as agriculture and fossil fuel burning. Most of this methane is produced via microbial methanogenesis, a process that is substantial in fresh water habitats but is often overlooked in coastal environments. However, methane concentrations are high in coastal groundwater, resulting in methane export driven by submarine groundwater discharge. The magnitude of methane export from the coastal zone depends significantly on the rate of microbial methane consumption (methanotrophy) in coastal sediments and aquifers, a process that is not well studied. Here we describe a zone of methanogenesis within the freshwater lens of a barrier island aquifer and investigate the methane source/sink behavior of the barrier island system as a whole. The median concentration of methane dissolved in fresh groundwater beneath the center of the island was 597 μM, supported by high rates of potential methanogenesis (22 ± 11 mmol m^{-2} day^{-1}). However, rates of microbial methane consumption were also elevated in surrounding sediments (18 ± 2.1 mmol m^{-2} day^{-1}). Groundwater flowing from the zone of methanogenesis to the point of discharge into the ocean had a long residence time within methanotrophic sediments (~160 days) such that the majority of the methane produced within the barrier island aquifer was also consumed there.

INTRODUCTION

Methane (CH_4) accounts for 17% of the total radiative forcing of Earth's atmosphere, making it the third most important greenhouse gas behind water vapor and

carbon dioxide [*Myhre et al.*, 2013]. Since the industrial revolution, the atmospheric concentration of CH_4 has risen by 150% to 1.8 ppm. This increase was driven by human activities such as agriculture, energy production, and waste management [*Ciais et al.*, 2013]. The dominant sink for atmospheric CH_4 is chemical consumption by reaction with hydroxyl radicals [*Myhre et al.*, 2013]. Thus, CH_4 plays a critical role the global heat budget and is active in atmospheric chemistry. Understanding the atmospheric, terrestrial, aquatic, and marine sources and sinks of CH_4 is therefore highly relevant in the context of climate change.

Globally, the dominant CH_4 production mechanism is methanogenesis by autotrophic or heterotrophic microorganisms. In the terrestrial realm, these microorganisms are active primarily in anoxic, aquatic habitats [*Cicerone and Oremland*, 1988]. Therefore, the most important sites of CH_4 production are organic rich soils saturated with fresh water (e.g. marshes, rice paddies, landfills) [*Ciais et al.*, 2013]. Coastal environments are often overlooked in global CH_4 budgets because they are characterized by high salinity, which can inhibit methanogenesis. However, the coastal zone contributes substantially to the total marine CH_4 flux to the atmosphere [*Bange*, 2006], and the groundwater flowing through soils and sediments is the dominant source of this CH_4 to the coastal ocean [*Bugna et al.*, 1996; *Grunwald et al.*, 2009].

These interstitial fluids are enriched with dissolved CH_4 derived from methanogenesis in aquifers containing freshwater and sufficient organic carbon substrate [*Bugna et al.*, 1996]. Aquifers matching this description are not limited to inland environments. Coastal uplands develop a lens of fresh groundwater floating above a layer of denser, saline groundwater [*Collins and Easley*, 1999], thereby creating a zone with

the potential for CH_4 production. Barrier islands are globally important coastal landforms, occupying 15,100 km (6.5%) of open ocean shorelines [*Stutz and Pilkey*, 2001] and an additional 7,410 km of lower energy coastal environments [*Pilkey et al.*, 2009]. Therefore, barrier island methanogenesis could contribute substantially to coastal CH_4 budgets.

Methane in coastal surface waters is often associated with submarine groundwater discharge (SGD) and has been used as a tracer for SGD in numerous studies [*Cable et al.*, 1996; *Kim and Hwang*, 2002]. However, before reaching the ocean, groundwater traverses multiple zones of intense biogeochemical cycling within coastal aquifers. These zones, where freshwater mixes with seawater and rapid porewater advection is driven by wave and tidal action, are referred to as the subterranean estuary [*Moore*, 1999]. Around 97% of global SGD is brackish or saline [*Burnett et al.*, 2003], attesting to the widespread nature of this environment. The subterranean estuary is likely to host active CH_4 oxidation by both aerobic and anaerobic methanotrophic microorganisms. Therefore, the balance between CH_4 production, transport and consumption rates within the subterranean estuary will control the flux of CH_4 to the adjacent coastal ocean.

Barrier islands have the potential to export CH_4 efficiently because of the close proximity of methanogenic zones to discharge points; they are relatively small, with little elevation and they are located immediately adjacent to the ocean. Therefore, CH_4-laden groundwater from the freshwater lens has a short distance to flow before it can be discharged to the ocean. Additionally, the low elevation of most barrier islands places the water table near the ground surface, shortening the distance of unsaturated pore space that

CH_4 must diffuse through before reaching the atmosphere. These two unique characteristics of barrier islands may limit the exposure of CH_4 to sites of methanotrophy.

In this work, we tested the hypotheses that: 1) barrier island aquifers support zones of microbial CH_4 production, 2) a fraction of this CH_4 is exported to the atmosphere or ocean, and 3) the dominant fate for CH_4 is microbial consumption within the barrier island system. The ratio of CH_4 export from the barrier island aquifer to total CH_4 production within the aquifer is controlled by the CH_4 consumption rate in sediments along the groundwater flow path and the residence time of CH_4-bearing groundwater within those methanotrophic sediments. We investigated these processes on a barrier island in Georgia, USA by surveying groundwater CH_4 concentrations, CH_4 production and consumption rates, diffusive and advective CH_4 fluxes, and CH_4 efflux to the atmosphere across the island.

METHODS

Cabretta Island is a small barrier island (~200 m wide) located on the coast of Georgia, USA (Fig 4.1). It is a transgressive barrier island composed of alternating layers of mud and sand. Trees and shrubs grow on the upland of the island, which is flanked by a small tidal creek and salt marsh on one side and a dune and beach system on the other. It experiences semidiurnal tides with a tidal range of 2-3 meters. A transect of groundwater monitoring wells with 30 cm screened intervals was installed across the island in 2008. Wells were placed in 7 clusters with 2 or 3 wells per cluster. These clusters were distributed across the range of environments present on the barrier island, including salt marsh, wooded upland, dune, and beach. Within each cluster, wells

covered a range of depths from 1–5 meters below the sediment surface. A more detailed description of the site and wells is provided by Wilson et al. [2011].

An initial survey of the geochemistry of these wells was carried out with samples collected every other month from August 2008 – August 2010. Groundwater samples were collected by first purging stagnant groundwater from the well using a peristaltic pump. Freshly recharged groundwater was collected into a disposable syringe using tygon tubing. The sampling apparatus was rinsed with ~30 mL of groundwater prior to sample collection. The salinity of the sample was determined in the field using a handheld meter (YSI Model 30). Four subsamples were collected in the field, and all of them (with the exception of the gas sample) were filtered through a 0.2-μM Target filter. The first subsample was fixed with 20% (w/v) zinc acetate and stored at 4°C for subsequent colorimetric analysis of sulfide (H_2S) [*Cline*, 1969]. A second subsample of 10 mL was injected into a 20 mL headspace vial that was sealed with a butyl rubber septum and purged with helium. This sample was fixed with a sodium hydroxide pellet and stored upside down prior to analysis of CH_4 via gas chromatography (Shimadzu GC-2010 with flame ionization detector and Carbosphere column). The detection limit for this method was determined to be 0.5 μM from field blanks. The third subsample was stored frozen in an acid-washed Nalgene bottle until analysis for dissolved organic carbon (DOC) using a Shimadzu TOC-5000 analyzer, nitrate plus nitrite using an Antek 745 vanadium reduction assembly coupled with an Antek 7050 chemiluminescent nitric oxide detector, and ammonium using the phenol hypochlorite method [*Solorzano*, 1969]. The final 20 mL subsample was stored in an acid-washed glass scintillation vial and fixed with 50 μL of concentrated nitric acid. This sample was analyzed for chloride and sulfate

concentration via ion chromatography (Dionex ICS-2000), phosphate via standard spectrophotometric methods [*Strickland and Parsons*, 1972], and total iron via atomic adsorption spectroscopy.

A more detailed investigation of CH_4 cycling within the barrier island aquifer was conducted during the winter (February-March) and summer (July-August) of 2012. Equilibration chambers were used to measure CH_4 concentrations in the pore space of barrier island sediment (Fig. 4.2a). These watertight chambers were constructed from PVC and covered with a CH_4-permeable silicone rubber membrane (see Chapter 2). Chambers were connected to a photoacoustic field gas monitor (Innova 1412, LumaSense Technologies Inc., Santa Clara, CA) to measure the concentration of CH_4 within the chamber by recirculating the gas between the chamber and monitor in a closed loop. Silicone membranes were used in CH_4 sampling devices previously [*Grunwald et al.*, 2009]. CH_4 equilibration across the membranes of these chambers was tested in the laboratory by spiking five chambers with CH_4 to a final concentration of ~2000 ppm. The concentration of CH_4 within each chamber was tracked through time using the field gas monitor. CH_4 concentrations within the chamber returned to near atmospheric concentrations within two days (Fig. 4.2b). Four equilibration chambers were stacked inside a PVC housing (Fig. 4.2c) in order to measure a depth profile of CH_4 concentration. These profilers covered a 2-meter depth range, with individual chambers measuring average CH_4 concentrations over 0.5-meter intervals. These average concentrations and associated measurements are discussed and displayed as being located at the middle of the depth range covered by each chamber throughout this manuscript.

Based on observed CH_4 concentration distributions (Fig. 4.3), an intensive study of sediment CH_4 cycling was carried out at the center of Cabretta Island and near the spring high tide line on the beach. Three depth profilers were installed at each location spaced one meter apart in a line parallel to the shoreline of Cabretta Island. CH_4 concentration profiles were measured from the island center twice during the winter (February-March) and the summer (July-August) of 2012. On the beach, profiles were measured six times in the winter and twelve times in the summer. In October 2012, another four small equilibration chamber profiles (0-0.5 and 0.5-1.0 meter depth intervals) were installed in a transect down the beach at Cabretta Island, spaced approximately evenly from the high to the low tide line. CH_4 concentrations were only measured in these chambers once because profilers were rapidly destroyed by waves.

The vertical diffusive flux of CH_4, J_W (μmol m^{-2} day^{-1}), through saturated sediment was calculated using the following equation [*Deurer et al.*, 2008]:

$$J_W = a^{4/3} \cdot D_W \cdot \frac{\partial C}{\partial z} \qquad \text{Equation 4.1}$$

The sediment porosity, a (m^3 m^{-3}), was assumed to be 0.43, 0.43, and 0.45 at 0.75, 1.25, and 1.75 meters depth, respectively. The first two values are from the literature for fine sand and the third was measured for this site. The higher porosity at the deepest depth reflects a shift from sand to mud. The $a^{4/3}$ term includes a tortuosity correction. Different values were used for D_w, the diffusion coefficient of CH_4 in water (m^2 day^{-1}), in the winter and the summer: 0.0001512 (20°C) and 0.0009613 (30°C) [*Broecker and Peng*, 1974]. $\frac{\partial C}{\partial z}$ is the vertical concentration gradient of CH_4 measured between two equilibration chambers as described above (μmol m^{-4}).

Potential CH_4 production and consumption rates were measured in laboratory bottle incubations. During winter and summer 2012, sediment was collected from triplicate profiles at the island center and on the beach with individual samples taken from the midpoint of each 0.5 m depth interval represented by an equilibration chamber. These samples were returned to the lab and 120 cc of sediment was placed in 500 mL Schott bottles. Bottles were split into oxic and anoxic treatments and their headspaces were purged with air and nitrogen, respectively, and then spiked with CH_4 to approximate *in situ* concentrations. Each treatment was carried out in triplicate at all four depths at both locations. The experiment was scaled up following the winter field season, so more treatments were included in the summer experiment. After a 24-hour pre-incubation at *in situ* temperature (17°C winter, 27°C summer), the headspace of each bottle was reset by purging with air or nitrogen and spiking with CH_4. Headspace CH_4 concentrations were measured approximately 0, 3, 6, 12, 24, and 48 hours following the headspace reset using the field gas monitor. The linear rate of change in concentration was used to calculate the rate of CH_4 production or consumption in 120 cc of sediment. This rate was then scaled up to the 0.5 m^3 of sediment represented by a 0.5 m depth interval (the length of one equilibration chamber) in a sediment column with a cross-sectional area of 1 m^2. The volumetric rate was converted to an areal rate by dividing by the height of the sediment layer represented by the equilibration chamber (0.5 m) for ease of comparison with transport fluxes.

The flux of CH_4 from the sediment surface to the atmosphere was measured using triplicate flux chambers. These chambers were Plexiglass cylinders with a surface area of 0.047 m^{-2} and a volume of ~ 8 L. One chamber was placed next to each of the

equilibration chamber profilers immediately before or after concentration profiles were measured. Flux chambers were covered throughout the measurement period such that fluxes were quantified in the dark. Two pieces of gas impermeable tubing entered each chamber through a septum in the top and were connected to the field gas monitor such that gas was circulated between the chamber and detector during measurement. Triplicate CH_4 concentration measurements within each flux chamber were recorded every 20-30 minutes over a 1-2 hour period using the field gas monitor. The CH_4 flux was calculated as the linear increase or decrease in CH_4 concentration within the flux chamber over time. The flux was quantified by linear regression of this time series [*Samarkin et al.*, 2010]. The slope of each linear regression was tested to ensure that it was significantly different from zero ($p < 0.025$).

The groundwater flow velocity field across the upland and beach of Cabretta Island was estimated based on a SUTRA-based flow model. A detailed model description can be found elsewhere (see Chapter 2). This model took into account the stratigraphy of the island that was measured using electrical resistivity tomography surveys and coring during groundwater monitoring well installation. The beach consisted of fine-grained, isotropic sand with a permeability of $2x10^{-11}$ m^2 [*Anderson*, 2011]. This unconfined surface aquifer was underlain by a confining unit 1-2 meters below the surface that was composed of a relic marsh mud layer with a permeability of $5x10^{-15}$ m^2. Groundwater flow in this model occurred due to influx of fresh groundwater on the landward vertical boundary and an idealized semi-diurnal tide with a period of 12 hours and amplitude of 1.85 meters.

Data were gathered for several variables that potentially control the concentration of CH_4 in surface waters adjacent to Cabretta Island. Tidal data for the National Oceanic and Atmospheric Administration's station at Fort Pulaski, GA (http://co-ops.nos.noaa.gov/waterlevels.html?id=8670870) was used to calculate the mean water level and tidal amplitude at the time of each CH_4 measurement. Mean water level was calculated as a 30-day running average of the water level data, and the tidal range was calculated as the difference in water level between consecutive low and high tides that bracketed CH_4 sample collection. Wind speed and wave height data from the National Data Buoy Center's buoy located at Gray's Reef (http://www.ndbc.noaa.gov/station_history.php?station=41008) were used for these analyses.

RESULTS

The initial survey of groundwater geochemistry across the barrier island aquifer (2008–2010) showed that the median concentration of CH_4 dissolved in groundwater underlying the marsh and beach of Cabretta Island was 6 µM with an interquartile range (IQR) of 2.3–15 µM (n=159). This concentration is around 3300 times higher than expected (1.8 nM) based on equilibration of seawater (35 PSU, 25°C) with the atmosphere [*Yamamoto et al.*, 1976]. Groundwater CH_4 concentrations beneath the island upland exceeded the background concentration observed elsewhere by two orders of magnitude. The well with the highest median CH_4 concentration, 726 µM (IQR 566–1730 µM), was located near the center of Cabretta Island at 3.4 meters depth (Fig. 4.3), and had a maximum concentration of 2780 µM. CH_4 concentrations were elevated beneath

the upland and dunes, covering at least a 1.7 meter depth range and extending across at least 22 m of the island cross section.

This CH_4 hotspot was located within the freshwater lens, a feature created by rainwater infiltration into the barrier island soil. The soil profile at this location consisted of a confining silt/mud layer between a surficial and a deep sand layer [*Wilson et al.*, 2011]. The pore water within the lens was characterized by low salinity, low sulfate and dissolved oxygen concentrations, and high concentrations of dissolved organic carbon (Table 4.1), which provided ideal conditions for methanogenesis [*Cicerone and Oremland*, 1988]. The high sulfide concentrations observed at this location indicate active sulfate reduction that may compete with methanogenesis for organic carbon substrate. However, sulfide may be sequestered in the sediment through the formation of Fe-S minerals during organic matter degradation [*Schippers and Jørgensen*, 2002]. Therefore, the low iron concentrations observed in groundwater at this location could prevent the formation of Fe-S minerals, allowing sulfide build up even with low rates of sulfate reduction. Elsewhere on the island, saline pore water replete with sulfate allowed sulfate reduction to take precedence over methanogenesis. While methanogenesis fueled by noncompetitive substrates could occur contemporaneously with sulfate reduction [*Oremland and Polcin*, 1982], we observed no evidence for net CH_4 production outside the freshwater lens.

Methane cycling was investigated in greater detail in the top two meters of sediment within the zone of high CH_4 concentrations observed at the center of Cabretta Island during the winter (February–March) and summer (July–August) of 2012. The median groundwater CH_4 concentration in the monitoring well within this shallower

depth range was 326 μM (IQR = 278-787 μM, n=13), around half the concentration observed in the deeper well. However, the geochemistry at the bottom of this two meter depth profile was similar to that observed in the deeper well and elsewhere within the freshwater lens. Therefore, the processes taking place within this shallower zone (0–2 meters) of intensive study were likely representative of the processes taking place throughout the freshwater lens.

Within the two-meter depth profile, the highest CH_4 concentrations were observed at 1.75 meters depth (Fig. 4.4a). The median summer concentration of 151 μM (IQR = 143–158, n=9) was significantly lower (2-sample t-test, $p << 0.01$) than the median winter concentration of 189 μM (IQR = 182–195, n=6). Median CH_4 concentrations at 1.25 meters were significantly higher (2-sample t-test, $p < 0.025$) in the summer (45 μM, IQR = 2–161) than the winter (12 μM, IQR = 7.5–60). The CH_4 concentration in the top meter of sediment was 0.02 μM (IQR = 0.02–0.06), much lower than the 6 μM median groundwater concentration observed in saline porewater elsewhere on the island.

This steep concentration gradient drove diffusion of CH_4 toward the sediment surface regardless of depth or season (Fig. 4.4b). The maximum concentration gradient was observed at the bottom of the profile, resulting in the highest upward CH_4 flux from 1.75 meters to 1.25 meters depth. This flux was 18 μmol CH_4 m^{-2} day^{-1} (IQR = 13–19) in the winter and 15 μmol CH_4 m^{-2} day^{-1} (IQR = -0.9–17) in the summer. The upward diffusive flux decreased closer to the sediment surface and reached a minimum at 0.25 meters. The CH_4 concentration in this zone was still elevated relative to the atmosphere, driving an upward diffusive flux of 0.04 μmol CH_4 m^{-2} day^{-1} (IQR = 0.003–0.12) in the winter and 0.003 μmol CH_4 m^{-2} day^{-1} (IQR = 0.002–0.003) in the summer. Seasonal

differences in diffusive flux were not statistically significant at any depth (2-sample t-test, $p>0.025$). The diffusive fluxes calculated here are likely underestimates of the *in situ* flux as the large spatial scale over which the concentration gradient was measured has the potential to artificially decrease the gradient.

High CH_4 concentrations at 1.75 meters were supported by 22 ± 11 mmol m^{-2} day^{-1} of net potential CH_4 production. There was no statistically significant difference between summer and winter rates (2-sample t-test, $p>0.025$), so the 5 replicates represented in Fig. 4.4c were averaged to generate this value. At 1.25 meters, the potential CH_4 consumption rate was significantly lower (2-sample t-test, $p<0.01$) during the winter (9.4 ± 1.1 mmol m^{-2} day^{-1}, n=3) than in the summer (18 ± 2.1 mmol m^{-2} day^{-1}, n=3). Maximum rates of potential CH_4 consumption were observed at 0.75 meters: 98 ± 18 mmol m^{-2} day^{-1} (n=3) under oxic conditions in the summer, 40 ± 20 mmol m^{-2} day^{-1} (n=3) under anoxic conditions in the summer, and 15 ± 8.7 mmol m^{-2} day^{-1} (n=3) under anoxic conditions in the winter. These data indicate that microorganisms carrying out both aerobic and anaerobic CH_4 oxidation were active within the same depth horizon, albeit under different environmental conditions. In the top meter of sediment, very low CH_4 concentrations coupled with consumption rates that far exceeded the supply rate from diffusion indicated quantitative consumption of the CH_4 diffusing into this horizon from the deeper production zone.

Elevated CH_4 concentrations (10 ± 5.2 μM in the winter and 40 ± 21 μM in the summer) were also observed at 1.75 meters at the spring high tide line on the beach (Fig. 4.4d). This concentration was much lower than the concentration at the same depth in the island center because no net CH_4 production took place at any depth beneath the beach

(Fig. 4.4f). The potential CH_4 consumption rate in beach sands did not vary significantly with depth or season, and the median rate across all measurements was 10 mmol CH_4 m^{-2} day^{-1} (IQR = 7.8–18 mmol m^{-2} day^{-1}, n = 17). The concentration gradient observed at this location drove diffusion of CH_4 upward through the sediment column (Fig. 4.4e), where it was rapidly consumed.

Data from the equilibration chamber transect down the beach (installed in October 2012 and washed away after a single measurement) showed that elevated CH_4 relative to the atmosphere persisted in the pore space down to the low tide line (Fig 4.5a). The degree of CH_4 supersaturation in the pore space depended on the sediment layer, however. The median CH_4 concentration in the top meter of beach sand from the entire study period was 0.11 μM (IQR = 0.03–0.25 μM, n = 105). In contrast, the median CH_4 concentration in the mud layer underlying the beach over the same time period was 22 μM (IQR = 8–51 μM, n = 47).

Atmospheric CH_4 was consumed at a rate of -247 μmol m^{-2} day^{-1} (IQR = -222 to -278 μmol m^{-2} day^{-1}, n = 6) in surface soils overlying the freshwater lens at the center of Cabretta Island (Fig. 4.5b). In contrast, the median efflux of CH_4 from the upper beach was 0 μmol m^{-2} day^{-1} (IQR = -116–228 μmol m^{-2} day^{-1}, n = 84). This high range in CH_4 efflux values was also observed in the middle of the beach (median = 42 μmol m^{-2} day^{-1}, IQR = 0–128 μmol m^{-2} day^{-1}, n = 6) and near the low tide line on the beach (median = -58 μmol m^{-2} day^{-1}, IQR = -242–64 μmol m^{-2} day^{-1}, n = 12). Low tide efflux measurements were made on or around a mud outcrop (Fig. 4.6). These features were ephemeral, being periodically covered and uncovered as sand was transported to and from different locations on the beach by waves and currents. Though mud outcrops only

covered a small fraction of the beach at any given time, they suggest that the mud layer was not far beneath the sediment surface across much of the low tide line of the beach. The most likely source of the CH_4 exported during the observed positive CH_4 efflux events was the shallow mud layer given the higher CH_4 concentrations found there relative to the surficial sand layer. This export was possible when the beach face was not inundated, allowing rapid CH_4 diffusion through unsaturated sand. However, the approximately equal division between positive and negative efflux values across all measurements on the beach shows that net export of CH_4 from the beach face to the atmosphere was unlikely.

The groundwater flow model revealed a location near the low tide line on the beach with high potential for groundwater discharge to the ocean (arrows crossing the sediment/water interface in Fig. 4.5c). The mean tidally-averaged groundwater flow rate in this zone was estimated to be 0.64 ± 0.19 m day^{-1}. The CH_4 concentration in the porewater of the beach sand measured in the equilibration chamber nearest this location was 0.9 μM (equivalent to 0.9 mmol m^{-3}). The advective flux of CH_4 was calculated by multiplying the concentration by the porosity (0.43) and the groundwater flow rate (0.64 m day^{-1}), yielding a flux of 0.25 mmol m^{-2} day^{-1}. The median areal CH_4 consumption rate in beach sand was 10 mmol m^{-2} day^{-1} (integrated over a 0.5 meter depth interval), which is equivalent to a volumetric rate of 20 mmol m^{-3} day^{-1}. Dividing the advective CH_4 flux by the volumetric consumption rate results in a distance of 1.2 cm. Dissolved CH_4 will be quantitatively consumed if groundwater must traverse a greater distance than this before discharging into the ocean. In other words, groundwater with the observed CH_4 concentration must be located less than 1.2 cm from the sediment-water interface in order

to generate a positive flux of CH_4 to the ocean. Even a vey high groundwater flow rate of 2.5 m day^{-1} only increases this distance to 4.8 cm, so faster groundwater flow at different phases of the tidal cycle is unlikely to generate pulses of CH_4 export from shallow beach sands.

A contiguous mud layer extended from methanogenesis zone at the center of Cabretta Island to the low tide groundwater discharge point on beach, and CH_4 concentrations within this layer were elevated relative to the overlying sand (Fig. 4.5a). There was no lateral groundwater flow through this layer that could transport CH_4 from the zone of methanogenesis to the mud layer beneath the beach (Fig. 4.5c). Furthermore, there was no detectable net CH_4 production or consumption in the portion of the mud layer beneath the beach that contained saline porewater (Fig. 4.4f). The most likely mechanism for CH_4 transport was downward advection of CH_4-rich groundwater from the zone of methanogenesis beneath the island center followed by mixing with groundwater in the confined, sandy aquifer beneath the mud layer. This CH_4 was then carried towards the ocean by groundwater flow and some was mixed back into the mud layer beneath the beach via transverse dispersion. No CH_4 concentration or rate data was collected from this deeper aquifer, making it impossible to estimate the total CH_4 flux from the barrier island.

While CH_4 concentrations in the surf zone of the Atlantic Ocean and Cabretta Creek, the surface water bodies adjacent to Cabretta Island, tended to be below the detection limit (~0.5 μM), they exceeded 3 μM on four occasions during the study period (Fig. 4.7). These high CH_4 concentrations indicate supersaturation of surface waters with respect to the atmosphere. The most likely source of this excess CH_4 was groundwater

discharge, indicating occasional pulses of groundwater-derived CH_4. However, there was no correlation between CH_4 concentration and mean water level (Fig. 4.7a) or tidal range (Fig. 4.7b), which control groundwater discharge, or between CH_4 concentration and wind speed (Fig. 4.7c) or wave height (Fig. 4.7d), which control exchange of CH_4 between surface waters and the atmosphere.

DISCUSSION

The dissolved CH_4 concentration observed in fresh groundwater on Cabretta Island (median = 597 μM, IQR = 326–1055 μM, maximum = 2780 μM) is among the highest ever reported in coastal groundwater systems. They rival concentrations found in a Texas aquifer (350–1733 μM) [*Grossman et al.*, 1989], and exceed concentrations observed in coastal groundwater in Denmark (400–600 μM) [*Jakobsen and Postma*, 1999] and Florida (40–271 μM) [*Bugna et al.*, 1996]. The lower CH_4 concentrations observed in saline groundwater on Cabretta Island (6 μM) were comparable with concentrations in intertidal wells in Florida [*Santos et al.*, 2009a]. The CH_4 concentrations observed in the shallow pore space on the beach at Cabretta Island in both the sand (0.11 μM) and mud (22 μM) layers were much lower than the porewater concentrations reported for shallow, organic-rich intertidal sediments such as fresh (up to 2400 μM) and salt marshes (up to 1100 μM) in Georgia [*Segarra et al.*, 2013], and a tidal creek bed (500 μM) in the UK [*Parkes et al.*, 2012]. Concentrations of CH_4 were even higher in porewater from organic-rich, subtidal sediment (1000–8000 μM) [*Heyer and Berger*, 2000; *Jorgensen and Parkes*, 2010; *Martens et al.*, 1998; *Thang et al.*, 2013].

Incubation-based potential CH_4 production rates in the freshwater lens on Cabretta Island (22 ± 11 mmol m^{-2} day^{-1}) were of the same order of magnitude as in the organic-rich sediments of Cape Lookout Bight, North Carolina, USA [*Martens et al.*, 1998] and exceeded those measured in a variety of other coastal sediments [*Deborde et al.*, 2010; *Jakobsen and Postma*, 1999; *Jorgensen and Parkes*, 2010; *Parkes et al.*, 2012]. Over the long term, methanogenesis must be supported by an equivalent flux of organic carbon into the sediment at this location. The most probable source of organic carbon to the methanogenesis zone is soil organic carbon storage by island vegetation. While this parameter was not measured in this study, the island upland was inhabited by pine trees and Post and Kwon [2000] report an average soil organic carbon storage rate of 2.6 ± 3.5 mmol C m^{-2} day^{-1} in warm temperate moist pine forest, an order of magnitude lower than the measured methanogenesis rate.

The observed methanogenesis rate of 22 ± 11 mmol m^{-2} day^{-1} was measured in a 0.5 meter thick layer of sediment in the freshwater lens beneath the center of the barrier island. It is possible to calculate the total organic carbon pool within this layer in order to estimate the amount of organic carbon available to methanogenic microorganisms. Assuming the median DOC concentration of 1532 μM in upland groundwater (Table 4.1) and porosity of 0.45, the DOC pool was 1300 mmol m^{-2}. Similarly, the mean particulate organic carbon (POC) concentration in the mud layer was 0.64% and the mean sediment density was 1.32 g cm^{-3}, yielding a POC pool of 352,000 mmol m^{-2} and a total organic carbon pool (DOC + POC) of 353,000 mmol m^{-2}. Not all of this organic carbon was available to methanogens, however, as there would be competition from microorganisms capable of using other terminal electron acceptors such as dissolved oxygen, nitrate,

oxidized metals, or sulfate. No dissolved oxygen or nitrate was detected at this depth however (data not shown), and the low sulfate and high sulfide concentrations (Table 4.1) suggest sulfate reduction activity, making metal reduction unlikely. Assuming the median sulfate concentration in upland groundwater (0.1 mM, Table 4.1), the total sulfate pool was 22 mmol m^{-2}. Further assuming a sulfate reduction stoichiometry of 2 carbon atoms oxidized for every one sulfur atom reduced [*Konhauser*, 2007], complete consumption of the sulfate pool would have a negligible impact on the amount of organic carbon available to methanogens. Assuming that all of this organic carbon was in a form that methanogens are capable of using, this is sufficient carbon substrate to support the observed rate of methanogenesis for more than 40 years.

Salt marshes are buried by overwashing sand on retrograding barrier islands such as Cabretta, and this is likely the source of the observed mud layer. Thus, the particulate carbon consumed by methanogens at the island center was stored earlier in the island's history through high rates of primary production and sedimentation by a living marsh. St. Catherine's Island, just north of Cabretta, retreated at a rate of several meters per year between 1945 and 1990 [*Goodfriend and Rollins*, 1998]. For a small island like Cabretta that is only ~200 meters wide, this means that marsh buried on the landward side of the island will be exhumed on the seaward side in less than a century. Indeed, buried marshes on the seaward side of St. Catherine's were less than a century old [*Goodfriend and Rollins*, 1998]. Retrograding barrier islands act as conveyer belts that, through the constant burial of salt marsh sediment, maintain a supply of sedimentary organic carbon within the freshwater lens that is capable of supporting high rates of methanogenesis.

The CH_4 oxidation rates on Cabretta Island (9.4 ± 1.1 mmol m^{-2} day^{-1} during winter and 18 ± 2.1 mmol m^{-2} day^{-1} during summer in the mud layer, and 10 mmol m^{-2} day^{-1} (IQR = 7.8–18 mmol m^{-2} day^{-1}) in beach sands) fall within the range reported by Deborde et al. [2010] (0.3–199 mmol m^{-2} day^{-1}) and are comparable to rates reported in other intertidal and subtidal coastal sediments [*Carini et al.*, 2003; *Jorgensen and Parkes*, 2010; *Segarra et al.*, 2013; *Treude and Ziebis*, 2010]. Groundwater flow patterns show that it is unlikely that CH_4 was transported into the shallow barrier island aquifer from a deeper or more distant groundwater source, suggesting that the only source of CH_4 to Cabretta Island was methanogenesis within the freshwater lens. Therefore, the rate of methanotrophy in shallow sediments across the island was likely to be limited by the rate of methane transport from the freshwater lens.

This methanotrophy was likely responsible for the soil overlying the freshwater lens acting as a sink for atmospheric CH_4, with a median consumption rate of -247 μmol m^{-2} day^{-1} (IQR = -222 to -278 μmol m^{-2} day^{-1}). Assuming that this rate was constant across the 11.5-meter freshwater lens (half the distance between the TT-4 well cluster that sampled fresh groundwater at the island center and the TT-5 well cluster that sampled brackish water in the dunes), the integrated rate of atmospheric CH_4 consumption per meter of barrier island shoreline was -2.8 mmol CH_4 m^{-1} day^{-1} (IQR = -2.6 to -3.2 mmol CH_4 m^{-1} day^{-1}). These rates of atmospheric CH_4 consumption are at the high end of the range observed across a variety of forest, grassland, and tundra environments [*King*, 1997]. Atmospheric CH_4 consumption was not consistently observed in sediments and soils elsewhere on Cabretta Island, however. This is likely because the methanogenic community in the freshwater lens sustained the population of

methanotrophs that occupied shallower strata, facilitating their consumption of atmospheric CH_4 [*Le Mer and Roger*, 2001].

Occasional supersaturated CH_4 concentrations in the surf zone of the ocean show that dissolved CH_4 was exported from the barrier island aquifer at least some of the time. The lack of supersaturation at other times could indicate that either there was little CH_4 export at those times, or that CH_4 export was overwhelmed by loss processes in surface waters. The concentration of CH_4 in the coastal ocean is a function of loss to the atmosphere and inputs from groundwater and riverine discharge [*Bugna et al.*, 1996; *Santos et al.*, 2009b]. The rate of atmospheric loss is controlled by the extent of wave and wind driven mixing [*Grunwald et al.*, 2009] and should be higher with larger waves and higher winds. Rates of groundwater discharge are highest in the late winter when mean water level is at a minimum and on spring tides when the tidal range is maximized (A. M. Wilson, T. Evans, W. S. Moore, C. A. Schutte, and S. B. Joye, What time scales are important for monitoring submarine groundwater discharge? Insights from a salt marsh, submitted to Water Resources Research, 2014). However, elevated CH_4 concentrations in the surface ocean adjacent to Cabretta had no relationship with mean water level, tidal range, wind speed, or wave height (Fig. 4.7). This implies that a different process controls CH_4 concentrations in these waters. Methanotrophy within coastal aquifers may be an important control process that prevents CH_4 export much of the time in spite of high rates of CH_4 production elsewhere in the aquifer.

The residence time of groundwater within the aquifer as it transits the distance between the loci of CH_4 production and CH_4 discharge determines the exposure of groundwater CH_4 to methanotrophy. Beach sand is highly permeable, resulting in

relatively fast groundwater flow of 0.64 ± 0.19 m day^{-1} in the unconfined aquifer above the mud layer when averaged across tidal cycles. However, CH_4 production occurred around 100 meters from the point of discharge to the ocean on Cabretta. The resulting residence time for groundwater following this average flow path was around 160 days, providing ample opportunity for methanotrophs to consume the 0.11 μM CH_4 observed there (Fig. 4.8). Therefore, microbial consumption can act as an efficient CH_4 sink in surficial sandy aquifers. The more probable pathway for CH_4 export was downward advection through the mud layer at the island center, mixing with groundwater in the confined sandy aquifer beneath the mud, and lateral advection to the low tide discharge point. This downward mixing of CH_4 drove high concentrations (726 μM, IQR = 566–1730 μM) in the confined, sandy aquifer. Low groundwater flow rates (0.025 ± 0.011 m day^{-1}) resulted in a very long residence time (>10 years), however. Given this long residence time, rates of methanotrophy must have been near zero in order for groundwater discharge from the confined aquifer to support the pulses of CH_4 observed in surface waters near Cabretta (Fig. 4.8). This >10 year residence time assumes steady state conditions, however, and barrier island aquifers can be flushed out over time scales of days to weeks by storm surges [*Wilson et al.*, 2011]. Event-scale processes have the potential to influence CH_4 export from barrier islands strongly.

Methane has been used as a tracer for submarine groundwater discharge in a number of studies [*Cable et al.*, 1996; *Kim and Hwang*, 2002]. However, CH_4 is only an effective tracer if its transport via groundwater flow is faster than rates of methanotrophy within the aquifer. The tight correlation between CH_4 concentration in surface water and the rate of groundwater discharge in these studies demonstrates that this is a safe

assumption in cases where groundwater discharge is rapid and concentrated at point sources, such as near springs [*Cable et al.*, 1996]. However, groundwater discharge is slower and more evenly distributed in aquifers composed of silt, mud, and sand that are typical of many coastlines. It is clear that under most conditions, methanotrophy will have a significant impact on the groundwater-derived flux of CH_4 to surface waters. Under these circumstances, it is possible to use CH_4 as an indicator or qualitative tracer of groundwater discharge [*Dulaiova et al.*, 2010]. Even this should be done with caution, however, as a lack of CH_4 in surface waters does not necessarily preclude the presence of discharging groundwater.

The geologic history and fate of barrier islands is likely to play an important role in determining its CH_4 source/sink behavior. Retrograding barrier islands, such as Cabretta Island, have layers of mud and sand, creating overlap between organic-rich muds and the freshwater lens. As the island continues to retrograde, or break apart and be inundated by rising sea levels, the freshwater lens will shrink along with the zone of methanogenesis. Therefore, this type of barrier island may become a stronger CH_4 sink in the future. On the other hand, rates of methanotrophy were higher in sands overlying the methanogenic zone at the center of Cabretta Island than in beach sand, indicating that methanogenesis within the freshwater lens may prime methanotrophy in adjacent barrier island sediment layers. If this were the case, the disappearance of the methanogenic zone would result in a slowing of rates of methanotrophy. Mechanisms that determine the heterogeneity of methanogenesis and methanotrophy in coastal sediments are an important topic for future research.

LITERATURE CITED

Anderson, J. L. (2011), Field and numerical observations of groundwater dynamics within Cabretta Island, a barrier island off the coast of Georgia, edited, pp. 1-62, University of South Carolina.

Bange, H. W. (2006), Nitrous oxide and methane in European coastal waters, *Estuarine Coastal and Shelf Science*, *70*(3), 361-374.

Broecker, W. S., and T. H. Peng (1974), Gas-exchange rates between air and sea, *Tellus*, *26*(1-2), 21-35.

Bugna, G. C., J. P. Chanton, J. E. Cable, W. C. Burnett, and P. H. Cable (1996), The importance of groundwater discharge to the methane budgets of nearshore and continental shelf waters of the northeastern Gulf of Mexico, *Geochimica et Cosmochimica Acta*, *60*(23), 4735-4746.

Burnett, W. C., H. Bokuniewicz, M. Huettel, W. S. Moore, and M. Taniguchi (2003), Groundwater and pore water inputs to the coastal zone, *Biogeochemistry*, *66*(1-2), 3-33.

Cable, J. E., G. C. Bugna, W. C. Burnett, and J. P. Chanton (1996), Application of 222Rn and CH4 for assessment of groundwater discharge to the coastal ocean, *Limnological Oceanography*, *41*(6), 1347-1353.

Carini, S. A., B. N. Orcutt, and S. B. Joye (2003), Interactions between methane oxidation and nitrification in coastal sediments, *Geomicrobiology Journal*, *20*(4), 355-374.

Ciais, P., et al. (2013), Carbon and other biogeochemical cycles, in *Climate Change 2013: The Physical Science Basis. Contribution of Working Group I to the Fifth*

Assessment Report of the Intergovernmental Panel on Climate Change, edited by T. F. Stocker, D. Qin, G.-K. Plattner, M. Tignor, S. K. Allen, J. Boschung, A. Nauels, Y. Xia, V. Bex and P. M. Midgley, Cambridge University Press, Cambridge, United Kingdom and New York, NY, USA.

Cicerone, R. J., and R. S. Oremland (1988), Biogeochemical aspects of atmospheric methane, *Global Biogeochemical Cycles*, *2*(4), 299-327.

Cline, J. D. (1969), Spectrophotometric determination of hydrogen sulfide in natural waters, *Limnology and Oceanography*, *14*(3), 454-458.

Collins, W. H., and D. H. Easley (1999), Fresh-water lens formation in an unconfined barrier-island aquifer, *Journal of the American Water Resources Association*, *35*(1), 1-21.

Deborde, J., P. Anschutz, F. Guerin, D. Poirier, D. Marty, G. Boucher, G. Thouzeau, M. Canton, and G. Abril (2010), Methane sources, sinks and fluxes in a temperate tidal Lagoon: the Arcachon lagoon (SW France), *Estuarine Coastal and Shelf Science*, *89*(4), 256-266.

Deurer, M., C. von der Heide, J. Böttcher, W. H. M. Duijnisveld, D. Weymann, and R. Well (2008), The dynamics of N_2O near the groundwater table and the transfer of N_2O into the unsaturated zone: a case study from a sandy aquifer in Germany, *Catena*, *72*(3), 362-373.

Dulaiova, H., R. Camilli, P. B. Henderson, and M. A. Charette (2010), Coupled radon, methane and nitrate sensors for large-scale assessment of groundwater discharge and non-point source pollution to coastal waters, *Journal of Environmental Radioactivity*, *101*, 553-563.

Goodfriend, G. A., and H. B. Rollins (1998), Recent barrier beach retreat in Georgia: dating exhumed salt marshes by aspartic acid racemization and post-bomb radiocarbon, *Journal of Coastal Research*, *14*(3), 960-969.

Grossman, E. L., B. K. Coffman, S. J. Fritz, and H. Wada (1989), Bacterial production of methane and its influence on groundwater chemistry in east-central Texas aquifers, *Geology*, *17*(6), 495-499.

Grunwald, M., O. Dellwig, M. Beck, J. W. Dippner, J. A. Freund, C. Kohlmeier, B. Schnetger, and H. Brumsack (2009), Methane in the southern North Sea: sources, spatial distribution and budgets, *Estuarine Coastal and Shelf Science*, *81*(4), 445-456.

Heyer, J., and U. Berger (2000), Methane emission from the coastal area in the southern Baltic Sea, *Estuarine Coastal and Shelf Science*, *51*(1), 13-30.

Jakobsen, R., and D. Postma (1999), Redox zoning, rates of sulfate reduction and interactions with Fe-reduction and methanogenesis in a shallow sandy aquifer, Romo, Denmark, *Geochimica Et Cosmochimica Acta*, *63*(1), 137-151.

Jorgensen, B. B., and R. J. Parkes (2010), Role of sulfate reduction and methane production by organic carbon degradation in eutrophic fjord sediments (Limfjorden, Denmark), *Limnology and Oceanography*, *55*(3), 1338-1352.

Kim, G., and D. W. Hwang (2002), Tidal pumping of groundwater into the coastal ocean revealed from submarine ^{222}Rn and CH_4 monitoring, *Geophysical Research Letters*, *29*(14), 1678.

King, G. M. (1997), Responses of atmospheric methane consumption by soils to global climate change, *Global Change Biology*, *3*(4), 351-362.

Konhauser, K. (2007), *Introduction to Geomicrobiology*, Blackwell Publishing, Malden, MA.

Le Mer, J., and P. Roger (2001), Production, oxidation, emission and consumption of methane by soils: a review, *European Journal of Soil Biology*, *37*(1), 25-50.

Martens, C. S., D. B. Albert, and M. J. Alperin (1998), Biogeochemical processes controlling methane in gassy coastal sediments - Part 1. A model coupling organic matter flux to gas production, oxidation and transport, *Continental Shelf Research*, *18*(14-15), 1741-1770.

Moore, W. S. (1999), The subterranean estuary: a reaction zone of ground water and sea water, *Marine Chemistry*, *65*, 111-125.

Myhre, G., et al. (2013), Anthropogenic and natural radiative forcing, in *Climate Change 2013: The Physical Science Basis. Contribution of Working Group I to the Fifth Assessment Report of the Intergovernmental Panel on Climate Change*, edited by T. F. Stocker, D. Qin, G.-K. Plattner, M. Tignor, S. K. Allen, J. Boschung, A. Nauels, Y. Xia, V. Bex and P. M. Midgley, Cambridge University Press, Cambridge, United Kingdom and New York, NY, USA.

Oremland, R. S., and S. Polcin (1982), Methanogenesis and sulfate reduction - competitive and noncompetitive substrates in estuarine sediments, *Applied and Environmental Microbiology*, *44*(6), 1270-1276.

Parkes, R. J., F. Brock, N. Banning, E. R. C. Hornibrook, E. G. Roussel, A. J. Weightman, and J. C. Fry (2012), Changes in methanogenic substrate utilization and communities with depth in a salt-marsh, creek sediment in southern England, *Estuarine Coastal and Shelf Science*, *96*, 170-178.

Pilkey, O. H., J. A. G. Cooper, and D. A. Lewis (2009), Global distribution and geomorphology of fetch-limited barrier islands, *Journal of Coastal Research*, *25*(4), 819-837.

Post, W. M., and K. C. Kwon (2000), Soil carbon sequestration and land‐use change: processes and potential, *Global change biology*, *6*(3), 317-327.

Samarkin, V. A., M. T. Madigan, M. W. Bowles, K. L. Casciotti, J. C. Priscu, C. P. Mckay, and S. B. Joye (2010), Abiotic nitrous oxide emission from the hypersaline Don Juan Pond in Antarctica, *Nature Geoscience*, *3*(5), 341-344.

Santos, I. R., W. C. Burnett, T. Dittmar, I. G. N. A. Suryaputra, and J. P. Chanton (2009a), Tidal pumping drives nutrient and dissolved organic matter dynamics in a Gulf of Mexico subterranean estuary, *Geochimica et Cosmochimica Acta*, *73*(5), 1325-1339.

Santos, I. R., N. Dimova, R. N. Peterson, B. Mwashote, J. P. Chanton, and W. C. Burnett (2009b), Extended time series measurements of submarine groundwater discharge tracers (^{222}Rn and CH_4) at a coastal site in Florida, *Marine Chemistry*, *113*(1), 137-147.

Schippers, A., and B. B. Jørgensen (2002), Biogeochemistry of pyrite and iron sulfide oxidation in marine sediments, *Geochimica et Cosmochimica Acta*, *66*(1), 85-92.

Segarra, K. E. A., C. Comerford, J. Slaughter, and S. B. Joye (2013), Impact of electron acceptor availability on the anaerobic oxidation of methane in coastal freshwater and brackish wetland sediments, *Geochimica Et Cosmochimica Acta*, *115*, 15-30.

Solorzano, L. (1969), Determination of ammonia in natural waters by the phenolhypochlorite method, *Limnology and Oceanography*, *14*(5), 799-801.

Strickland, J. D. H., and T. R. Parsons (1972), *A practical handbook of seawater analysis*, 2nd ed., Bulletin of the Fisheries Research Board of Canada.

Stutz, M. L., and O. H. Pilkey (2001), A review of global barrier island distribution, *Journal of Coastal Research*(Special Issue 34), 15-22.

Thang, N. M., V. Bruchert, M. Formolo, G. Wegener, L. Ginters, B. B. Jorgensen, and T. G. Ferdelman (2013), The Impact of Sediment and Carbon Fluxes on the Biogeochemistry of Methane and Sulfur in Littoral Baltic Sea Sediments (Himmerfjarden, Sweden), *Estuaries and Coasts*, *36*(1), 98-115.

Treude, T., and W. Ziebis (2010), Methane oxidation in permeable sediments at hydrocarbon seeps in the Santa Barbara Channel, California, *Biogeosciences*, *7*(10), 3095-3108.

Wilson, A. M., W. S. Moore, S. B. Joye, J. L. Anderson, and C. A. Schutte (2011), Storm-driven groundwater flow in a salt marsh, *Water Resources Research*, *47*(2), W02535.

Yamamoto, S., J. B. Alcauskas, and T. E. Crozier (1976), Solubility of methane in distilled water and seawater, *Journal of Chemical and Engineering Data*, *21*(1), 78-80.

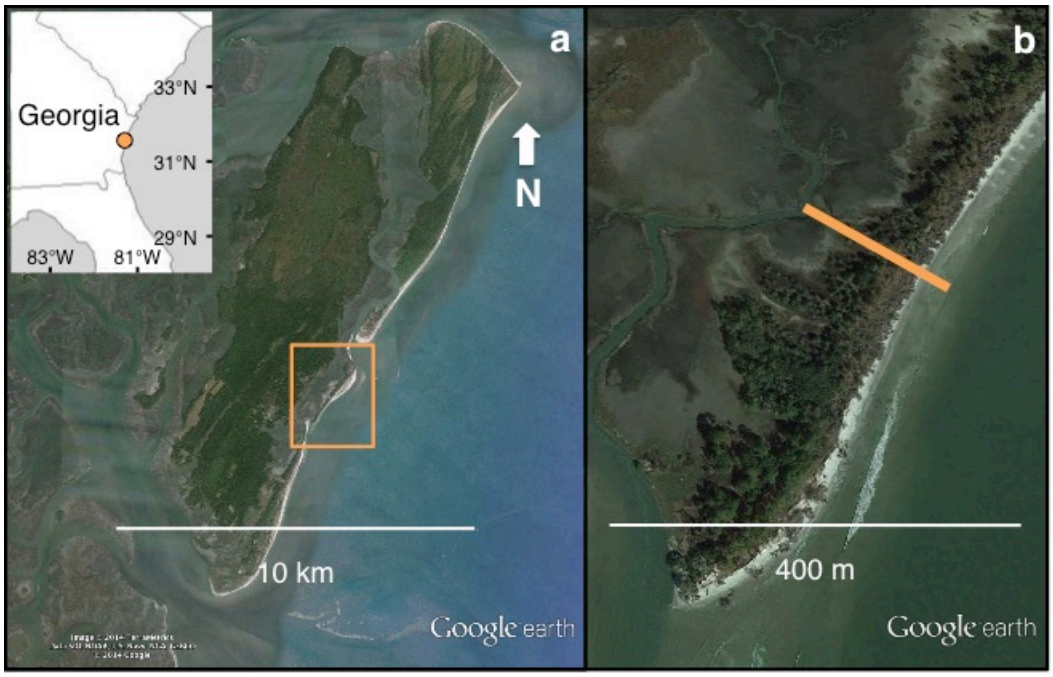

Figure 4.1. The location of the study site (orange dot on inset), Cabretta Island (orange box), on the coast of Georgia, USA (a). The southern tip of Cabretta Island with the transect of groundwater monitoring wells denoted by the orange line (b).

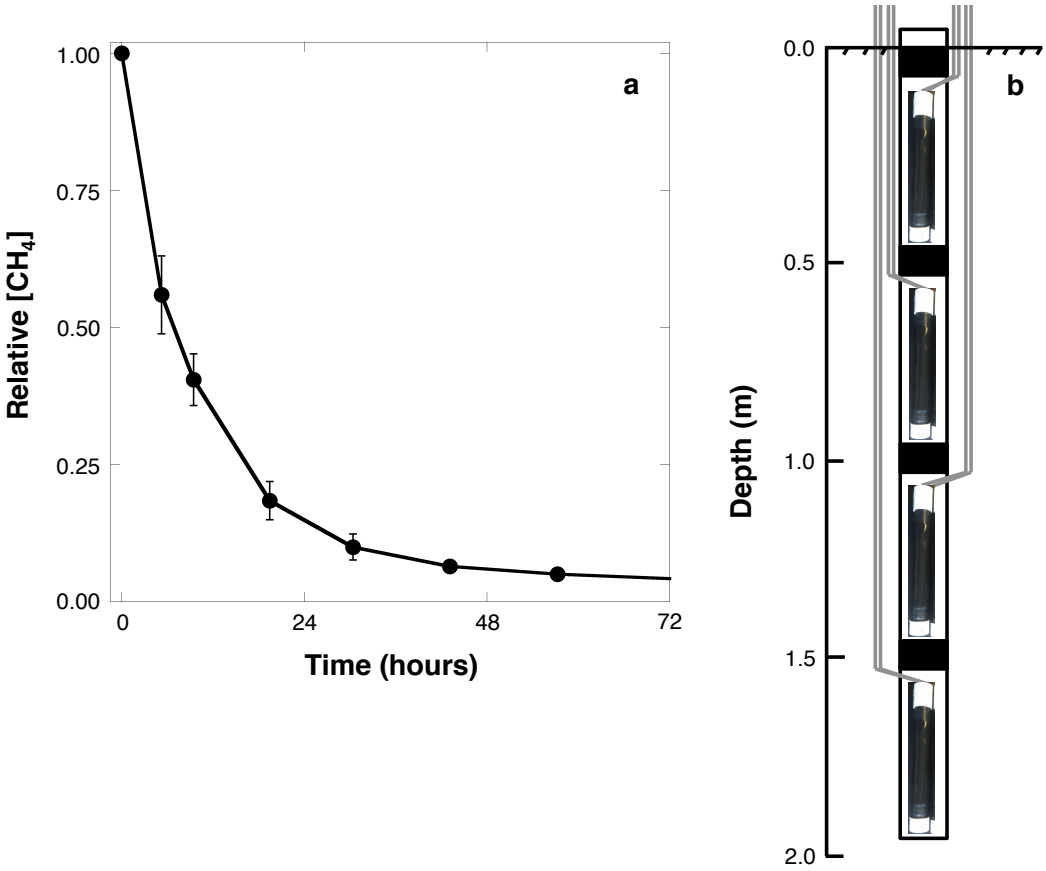

Figure 4.2. Time required for the CH_4 concentration within an equilibration chamber to equilibrate with the atmosphere following CH_4 addition (a). Diagram showing the arrangement of individual equilibration chambers within a PVC housing following installation at Cabretta Island (b).

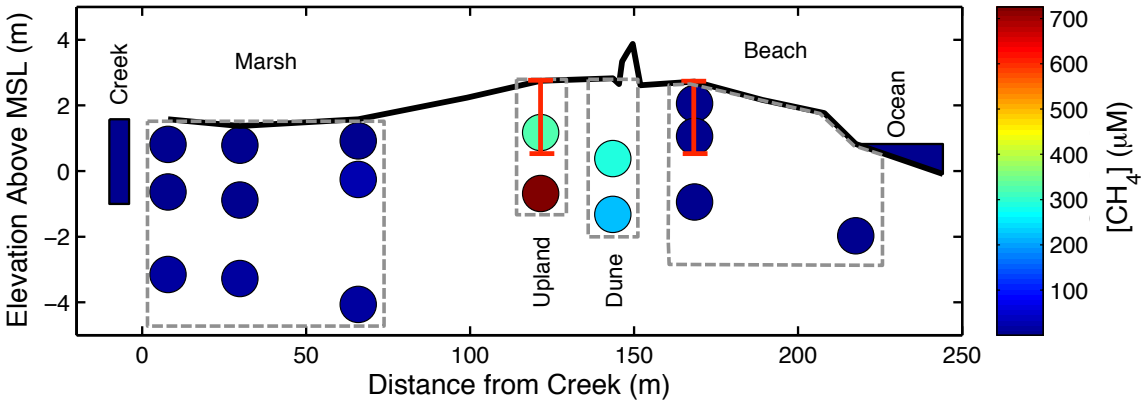

Figure 4.3. A cross section of Cabretta Island with the black line representing the island surface (10:1 vertical exaggeration). Each circle indicates a groundwater monitoring well that was sampled every other month from August 2008 – August 2010 (n=13). The color represents the median CH_4 concentration dissolved in the groundwater (circles) or surface water (rectangle or triangle). The dashed gray lines show how individual wells were clustered into environment type for subsequent analyses. The two red lines show the locations where equilibration chamber profilers were installed for intensive study of CH_4.

Table 4.1. Geochemical parameters of groundwater monitoring wells and adjacent surface water bodies from Cabretta Island clustered by environment type (see graphic representation of well clusters in Fig. 4.1). The central tendency of each data set is displayed as either the mean (for normally distributed data, standard font) or the median (for skewed data distributions, *italic font*). The variability of the data is displayed as either the standard deviation (for normally distributed data, standard font) or the interquartile range (for skewed data distributions, *italic font*).

Site	CH_4 (μM)	DOC (μM)	Salinity (ppt)	Cl^- (mM)	SO_4^{2-} (mM)	H_2S (μM)	Fe (μM)	HPO_4^{2-} (μM)	DIN (μM)
Creek (n=13)	*0.8*	*481*	31.9	485	25	*0.0*	*0.2*	*2.7*	*24*
Variability	*0.4–1*	*332–550*	4.3	64	3.4	*0–0*	*0.03–0.7*	*2.0–6.1*	*5.7–33*
Marsh (n=117)	*7.3*	*836*	35.8	563	27	95	*14*	*56*	*153*
Variability	*2.6–19*	*510–1046*	7.6	115	5.6	295	*2.3–91*	*14–91*	*53–400*
Upland (n=26)	*597*	*1532*	*2.8*	*37*	*0.1*	222	*3.5*	94	*199*
Variability	*326–1045*	*1103–2240*	*1.0–4.1*	*10–77*	*0.1–0.3*	370	*1–10*	53	*65–321*
Dune (n=25)	*232*	*1838*	*4.4*	*58*	*0.8*	*1333*	*1.5*	*227*	*274*
Variability	*153–400*	*1478–3363*	*4.1–4.9*	*51–56*	*0.2–1*	*202–2747*	*0.9–2.4*	*60–351*	*220–338*
Beach (n=39)	*4.3*	*398*	21.9	342	*18*	*0.2*	*5.8*	*17*	*54*
Variability	*1.7–9.7*	*250–564*	7.3	286–437	*15–23*	*0–5*	*3.3–9.7*	*11–25*	*23–74*
Ocean (n=13)	*0.4*	*279*	32.5	528	*27*	*0.0*	0.7	*1.1*	*3.4*
Variability	*0.4–1.9*	*235–293*	2.9	491–537	*25–28*	*0–0.2*	1.6	*0.5–1.6*	*1.2–8.5*

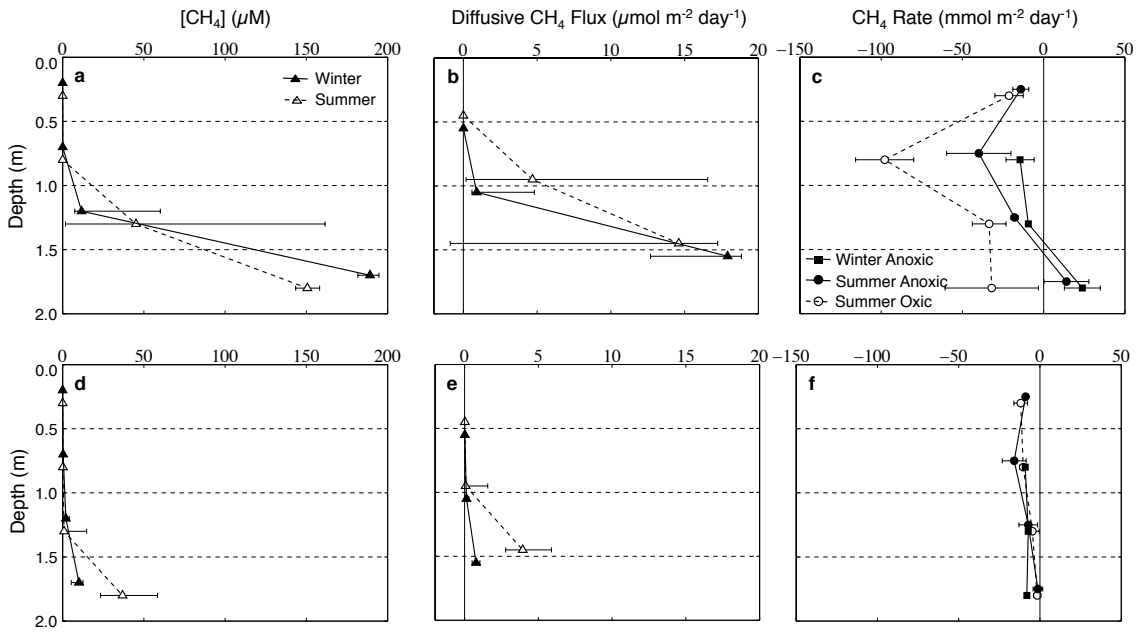

Figure 4.4. Panels a–c show data from the center of Cabretta Island. Panels d–f show data from the upper beach. Median CH_4 concentration in the pore space (a, d). Median diffusive flux of CH_4 from zone represented to the zone above it (b, e) where positive values indicate upward flux. Error bars for these four plots show the interquartile range. The mean rate of methane production (positive) and consumption (negative) under anoxic conditions in winter and summer 2012 and oxic conditions during summer 2012 (c, f), with error bars showing the standard deviation.

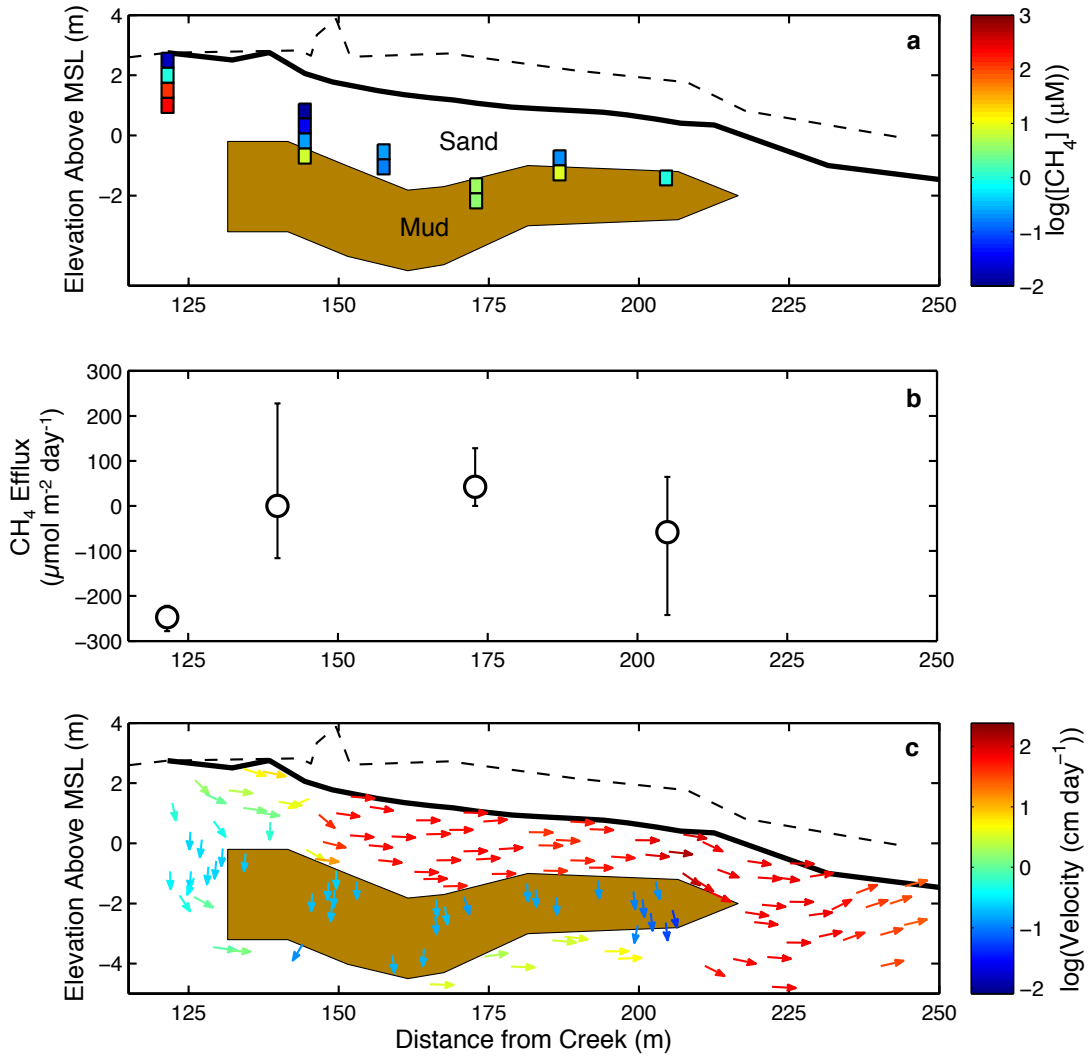

Figure 4.5. Methane concentrations on the beach at Cabretta Island (a, 5:1 vertical exaggeration). The dashed black line represents the surface of Cabretta Island from 2008-2010 (as shown in Figure 4.1). The heavy black line represents the island surface in 2012. Stacked rectangles represent gas equilibration chambers installed from the island center to the low tide line on the beach. The color of these boxes display the log-transformed CH_4 concentration. Methane efflux from the sediment surface to the atmosphere (b). Negative values represent consumption of atmospheric methane in surficial sediment. Model-based groundwater velocity estimates (c, 5:1 vertical exaggeration). The arrows show the direction of groundwater flow across the island and the arrow color shows the log-transformed speed of that flow.

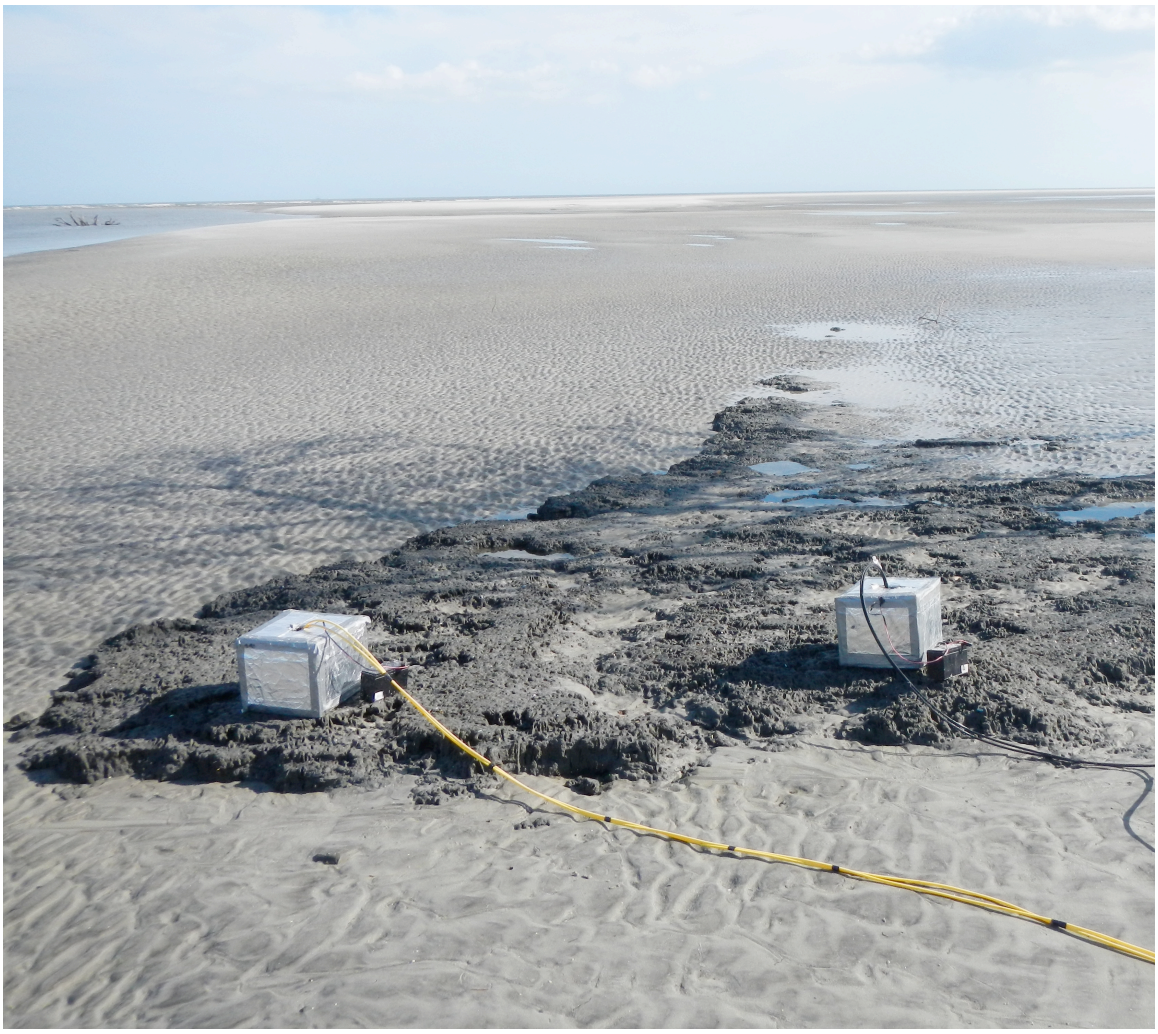

Figure 4.6. Mud outcrop near the low tide line on Cabretta Island.

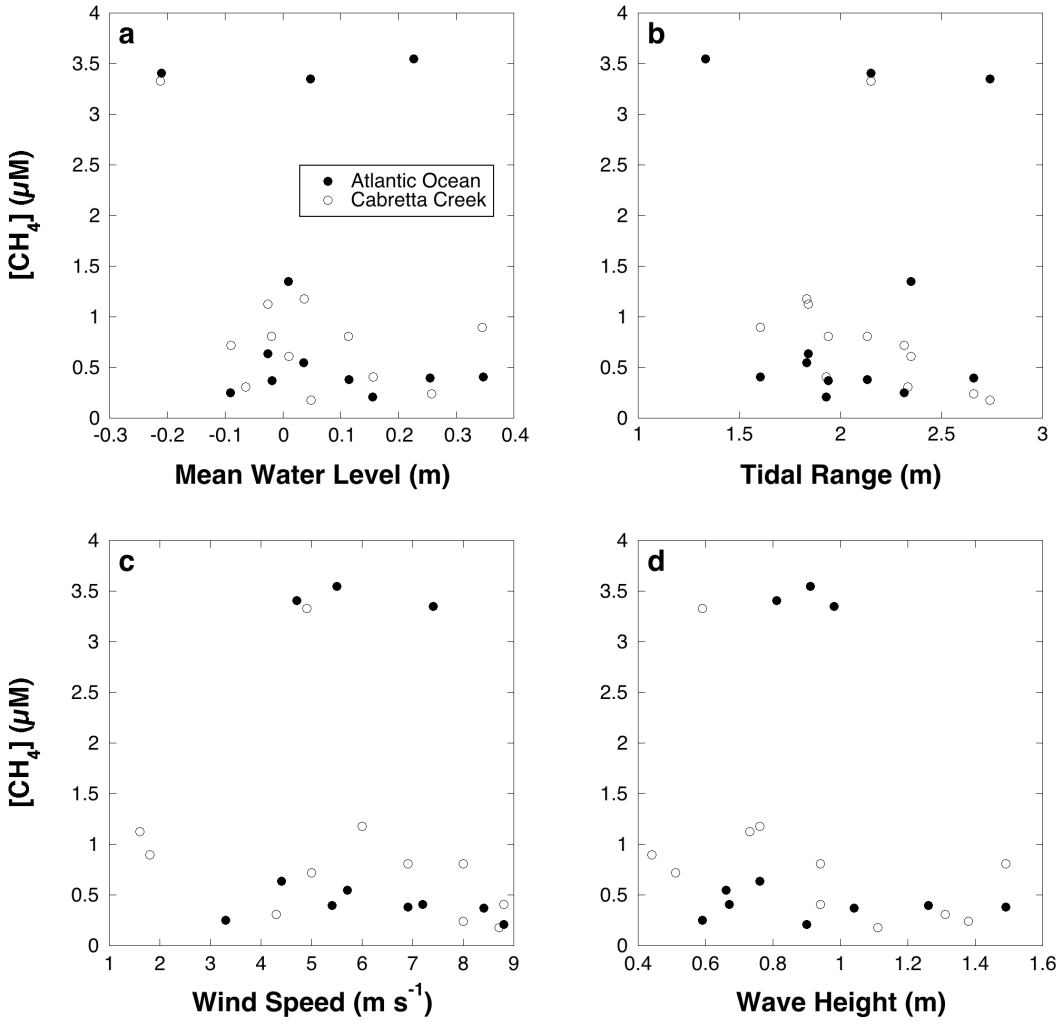

Figure 4.7. Relationship between CH_4 concentration in surface waters adjacent to Cabretta Island (Cabretta Creek and the surf zone of the Atlantic Ocean) and mean water level (a), tidal range (b), wind speed (c), and wave height (d) during the 2008-2010 survey.

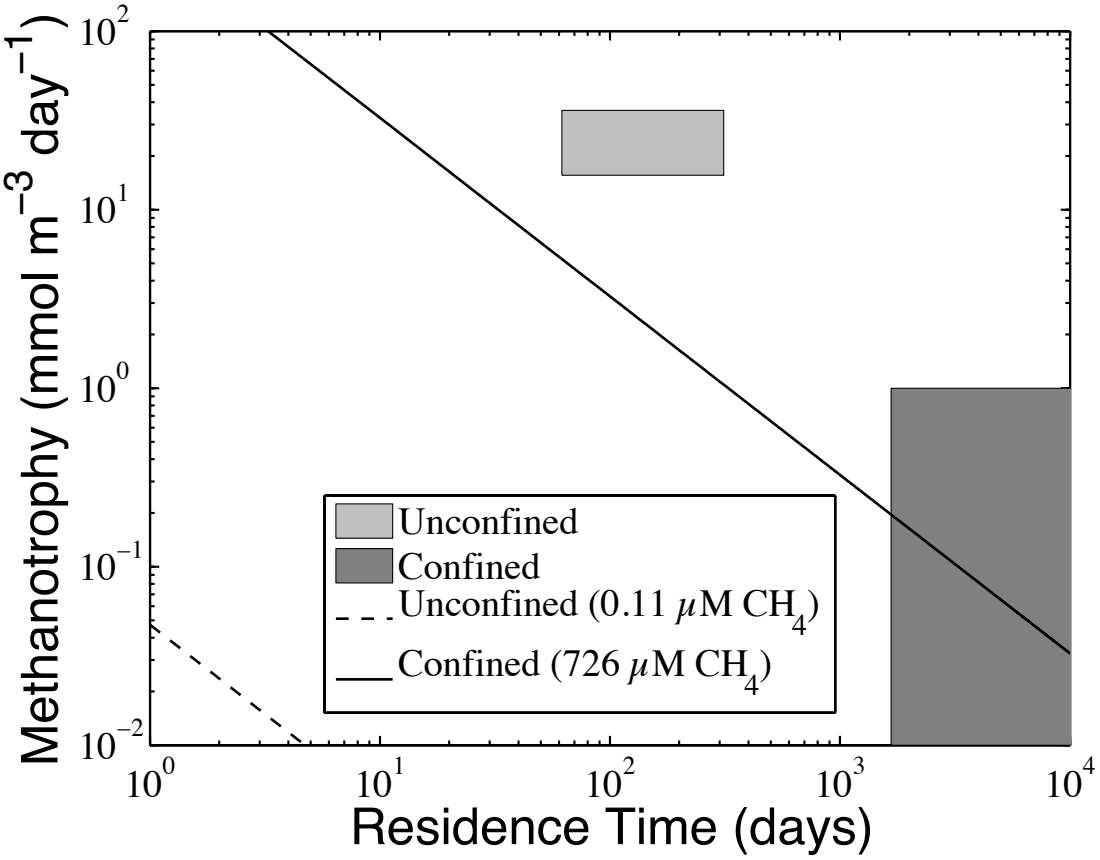

Figure 4.8. The rate of methanotrophy within the aquifer versus the residence time of groundwater within the aquifer. The dashed line represents the CH_4 concentration in the unconfined beach aquifer, derived from October 2012 equilibration chamber measurements, while the solid line represents the median CH_4 concentration in the confined aquifer, derived from the deepest well at the island center during the 2008-2010 survey. If the rate of methanotrophy and the residence time for an aquifer plot below the line representing the CH_4 concentration within that aquifer, then not all of the CH_4 in the groundwater will be consumed and the potential for a positive flux of CH_4 to adjacent surface waters exist. If the aquifer plots above this line, then no groundwater-derived CH_4 flux should be expected. The range of residence times and the interquartile range of the rate of methanotrophy are displayed for the unconfined aquifer. Methanotrophy rates for the confined aquifer were not measured; these values are displayed to show the highest possible rates that could still generate a positive CH_4 flux to the ocean.

CHAPTER 5

SUBMARINE GROUNDWATER DISCHARGE DERIVED FLUXES OF DIC, CH_4, AND N_2O FROM SALT MARSHES TO THE COASTAL OCEAN [4]

[4] Schutte, C.A., W. S. Moore, A.M. Wilson, and S.B. Joye. To be submitted to *Nature Geoscience*.

ABSTRACT

Climate change is one of the greatest threats facing Earth's ecosystems, and it is caused in large part by excess greenhouse gases such as carbon dioxide, methane, and nitrous oxide in the atmosphere. Salt marsh grasses capture carbon dioxide from the atmosphere, transform it into organic matter, and store it in the soil. Therefore, marsh soils are a potential carbon sink that could help to mitigate anthropogenic carbon dioxide loading to the atmosphere. However, microbial processes in marsh soil also produce carbon dioxide, methane, and nitrous oxide, some fraction of which is exported via soil-atmosphere exchange, counteracting some of the benefit of the "blue carbon" that is captured and stored within salt marshes. Another pathway for greenhouse gas export from marshes is submarine groundwater discharge; this pathway has been largely overlooked to date. Marsh groundwater is enriched in dissolved greenhouse gases, and they can therefore be exported to adjacent surface waters via submarine groundwater discharge. Here, we show substantial fluxes of dissolved inorganic carbon and methane from four salt marsh aquifers on the coast of Georgia, USA. Combined with fluxes reported from other salt marshes, the average flux was 0.90 ± 1.4 mol m^{-2} day^{-1} for DIC, 0.41 ± 0.84 mmol m^{-2} day^{-1} for methane, and 4.7 μmol m^{-2} day^{-1} for nitrous oxide. These fluxes are of the same order of magnitude as the average carbon dioxide (0.23 ± 0.21 mol m^{-2} day^{-1}), methane (0.6 ± 2.8 mmol m^{-2} day^{-1}), and nitrous oxide (-5.2 ± 68 mmol m^{-2} day^{-1}). Therefore, submarine groundwater discharge is a major pathway for the export these greenhouse gases from salt marshes.

INTRODUCTION

The concentrations of carbon dioxide (CO_2), methane (CH_4), and nitrous oxide (N_2O) in Earth's atmosphere have increased substantially in response to human activity since the industrial revolution [*Myhre et al.*, 2013]. These three greenhouse gases (GHGs) account for the majority of Earth's anthropogenic radiative forcing [*Myhre et al.*, 2013], which drives the climate change that disrupts ecosystems across the globe [*Walther et al.*, 2002]. Coastal salt marshes have received a great deal of attention for their ability to store "blue carbon" in their soils [*Chmura et al.*, 2003; *McLeod et al.*, 2011]. Salt marshes capture this carbon through two mechanisms: high rates of primary production fix atmospheric CO_2 into organic carbon and sedimentation of suspended solids that are rich in organic carbon from inundating tidal waters. Therefore, salt marshes provide an ecosystem service by storing this carbon and preventing it from entering the atmosphere as CO_2 where it would contribute to climate change. However, salt marshes may also export CO_2, CH_4, and N_2O to the atmosphere through soil-atmosphere exchange [*Chmura et al.*, 2011]. Methane and nitrous oxide are more potent GHGs than carbon dioxide on a per molecule basis by factors of 28 and 265, respectively [*Myhre et al.*, 2013]. Therefore, even small releases of these two GHGs could reduce the benefit of sequestering large quantities of fixed CO_2 in salt marsh soils. A careful accounting of these GHG budgets within salt marsh systems is necessary to fully understand their potential impacts on climate change.

Beneath salt marshes lie coastal aquifers, zones of intense biogeochemical activity called the subterranean estuary [*Moore*, 1999]. Subterranean estuaries occur in any coastal aquifer where waves and tides drive mixing of reduced, fresh or brackish

groundwater and oxidized, salty seawater. Microorganisms use the steep chemical gradients created by this mixing to power a broad suite of metabolisms. Carbon dioxide, methane, and nitrous oxide are all byproducts of microbial processes within aquifers and their associated soils and sediments. Carbon dioxide is produced by the heterotrophic degradation of organic matter and can take place in both oxic and anoxic environments. Methane is produced by methanogenic microorganisms that are largely obligate anaerobes. Nitrous oxide is produced as a byproduct of ammonia oxidation in oxic environments (nitrification) and nitrate reduction in anoxic environments (denitrification and dissimilatory nitrate reduction to ammonium). These microbial processes can produce high concentrations of reduced chemicals such as these GHGs, ammonium, phosphate, sulfide, reduced metals, dissolved organic carbon, and protons in coastal groundwater relative to surface water [*Porubsky et al.*, 2014; *Weston et al.*, 2006].

A variety of dissolved materials are released from coastal aquifers to adjacent surface water bodies via submarine groundwater discharge (SGD) [*Charette and Buesseler*, 2004; *Krest et al.*, 2000; *Santos et al.*, 2008]. Though SGD accounts for only a small amount of the total flux of fresh water to the ocean, brackish water exchange between surface waters and coastal sediments is very large [*Burnett et al.*, 2003]. This exchange drives inorganic nitrogen and phosphorus inputs from aquifers to coastal surface waters that rival those from rivers in many regions [*Slomp and Van Cappellen*, 2004]. While the SGD-derived flux of inorganic nutrients is well established, few studies have explored this mechanism of GHG export to coastal waters [*Atkins et al.*, 2013; *Cai et al.*, 2003; *Moore et al.*, 2006; *Porubsky et al.*, 2014]. Estuaries are known to be important contributors of CO_2 [*Cai et al.*, 2003], CH_4 [*Bange*, 2006], and N_2O [*Bange*,

2006; *Middelburg et al.*, 1995], to the atmosphere. Some of this gas flux is supported by riverine discharge and microbial production within estuarine waters, but a potentially significant fraction may be derived from SGD.

Here we report SGD-derived fluxes of dissolved inorganic carbon (DIC, a component of which is CO_2), CH_4, and N_2O from four salt marsh aquifers on the coast of Georgia, USA and compile other SGD-derived GHG fluxes from the literature. In order to calculate GHG fluxes, the volumetric flux of groundwater into the tidal creek per tidal cycle at each site was estimated by developing a radium mass balance for the tidal creek. Radium isotope ratios were used to identify specific groundwater monitoring wells that sampled the portion of the aquifer actively discharging groundwater into the tidal creek. Finally the volumetric groundwater flux was multiplied by the concentration of DIC, CH_4, and N_2O in marsh groundwater to estimate the flux of these gases from the aquifer to the adjacent tidal creek. Fluxes were normalized to the salt marsh-dominated, intertidal portion of each tidal creek estuary in order to compare SGD-derived GHG fluxes between sites and with direct measurements of GHG efflux from the marsh surface to the atmosphere as reported in the literature.

METHODS

Sapelo Island is a large barrier island (~67 km^2) on the coast of Georgia, USA (Fig. 5.1a). It experiences semidiurnal tides with a range of ~2-3 meters, making it a mesotidal system. Sapelo's seaward coastline is fronted by sandy beaches and dunes while its landward coastline is composed of salt marshes dominated by *Spartina alterniflora*. Most of Sapelo Island is owned and managed by the state of Georgia, and

the island has less than 200 residents, making Sapelo a relatively pristine area that is ideal for studying the natural processes taking place on a barrier island.

Four groundwater monitoring sites were established on and around Sapelo Island between 2002 and 2008. At each site, PVC wells were installed in transects across a salt marsh from the banks of an adjacent tidal creek to the edge of a nearby upland area. The first site was located near a back barrier island designated HN_i_1 (HN) behind the western edge of Blackbeard Island, itself located just North of Sapelo Island (Fig. 5.1b). The second study site was located on Cabretta Island (CI), a small barrier island separated from the eastern edge of Sapelo Island by a small tidal creek and a narrow salt marsh (Fig. 5.1c). Wells at this site were installed in clusters with each cluster containing wells at approximately 1, 2.5, and 5 meters depth [*Wilson et al.*, 2011]. The third site was Moses Hammock (MH), a large back barrier island on the western edge of Sapelo Island [*Porubsky et al.*, 2010; *Schultz and Ruppel*, 2002] within the watershed of the Duplin River (Fig. 5.1d) [*Schutte et al.*, 2013].The final site was situated at another back barrier island, PC_i_29 (PC), just off the southern end of Sapelo Island (Fig. 5.1e).

Each well at HN and PC was sampled every other month from 2008-2009, MH wells were sampled quarterly over the same time periods, and CI wells were sampled with every other month from 2008-2010. Prior to sample collection, stagnant groundwater was pumped out of each well using a peristaltic pump. Radium samples were then collected as described by Moore et al. [2006]. Briefly, freshly recharged groundwater was pumped into a 4 L cubitainer, which was rinsed three times with sample before being filled. For surface water, a 26 L sample was collected into a large plastic drum. Each sample was then gravity-filtered through 15-20 g of Mn-saturated acrylic

fibers in order to trap the dissolved radium. The activities of ^{226}Ra and ^{228}Ra were later determined using a gamma ray spectrometer following their HCl-extraction from the Mn fiber. Activities were corrected for the radioactive decay that took place between sample collection and analysis.

Following radium sampling, a second groundwater sample was collected using tygon tubing connected to a disposable syringe. Both were rinsed with ~30 mL of fresh groundwater prior to sample collection. Ten mL of unfiltered groundwater were collected into a He-purged, 20-mL headspace vial that contained a sodium hydroxide pellet to fix the sample. Samples were later acidified with 0.5 mL of concentrated HCl to convert DIC to CO_2. Each sample was vigorously shaken to equilibrate gases between the headspace and dissolved phase, and a headspace sample was injected into a Shimadzu GC-2014 gas chromatograph with Carbosphere column, methanizer, and flame ionization detector to measure DIC and CH_4 simultaneously. A second injection was made into a Shimadzu GC-8A gas chromatograph with electron capture detector and Hayesep DB column to quantify N_2O. Detection limits for these methods, defined as 3 times the standard deviation of the concentrations measured in field blanks (n =41), were 0.87 mM for DIC, 0.45 μM for CH_4, and 31 nM for N_2O.

In order to calculate the groundwater flux from each site, it was first necessary to estimate the return flow into each tidal creek. The return flow (b) is defined as the fraction of the water that leaves the estuary on ebb tide that returns to the estuary on the following flood tide. Return flow was estimated using a three-endmember mixing model with riverine (Altamaha River), nearshore ocean, and groundwater endmembers mixing to produce the observed creek water [*Moore et al.*, 2006]. Water, salt, and radium mass

balance equations were written for this mixing model and solved for the fraction of nearshore ocean water in creek water. This ocean fraction was assumed to be equal to the return flow according to the equation:

$$b = \frac{\frac{A_C - A_R}{A_{GW} - A_R} - \frac{S_C - S_R}{S_{GW} - S_R}}{\frac{A_O - A_R}{A_{GW} - A_R} - \frac{S_O - S_R}{S_{GW} - S_R}} \qquad \text{Equation 5.1}$$

Where b is return flow, A_C, A_R, A_{GW}, and A_O are the radium activities of the tidal creek, river, groundwater, and nearshore ocean, respectively (dpm L^{-1}), and S_C, S_R, S_{GW}, and S_O are the salinities of the same water bodies. This method of calculating the return flow produced a similar result to a momentum balance approach in a South Carolina estuary [*Moore*, 2006]. S_O was assumed to be 35 and S_R 0. Values of 0.21 and 0.34 dpm L^{-1} were used for ^{226}Ra and ^{228}Ra activities for nearshore ocean water (A_O) [*Moore*, 2007]. The dissolved radium activity of the Altamaha River was 0.039 and 0.038 dpm L^{-1} for ^{226}Ra and ^{228}Ra respectively [*Moore and Shaw*, 2008]. The median concentration of suspended solids in the Altamaha from 2001 to 2009 measured at GCE7, a freshwater site monitored by the Georgia Coastal Ecosystems Long Term Ecological Research (GCE-LTER) program, was 83.8 mg L^{-1} (https://gce-lter.marsci.uga.edu/public/app/dataset_details.asp?accession=NUT-GCEM-0909a). Assuming that each gram of suspended material in the river desorbed 2 dpm of ^{226}Ra and ^{228}Ra [*Moore and Shaw*, 2008], the desorbable activity in the Altamaha River was 0.168 dpm L^{-1} for both radium isotopes. Summing the dissolved and desorbable radium activities yielded a total radium activity (A_R) for the Altamaha River of 0.207 and 0.206 for ^{226}Ra and ^{228}Ra respectively.

The volumetric flux of groundwater into the tidal creeks at each of the four study sites was estimated using a radium mass balance approach according to Equation 5.2 adapted from Porubsky et al. [2014]:

$$J_{GW}\ A_{GW} = \frac{P}{T}[A_C - A_O + b(A_O - A_C)] \qquad \text{Equation 5.2}$$

Where J_{GW} is the volumetric groundwater flux (m^3 day^{-1}), P is the tidal prism of the creek (m^3), and T is the tidal period (0.517 days). This equation assumes that the sole source of radium to the creek was groundwater discharge and that the only radium sink was mixing of ebb tide creek water with nearshore ocean water. While the Altamaha River did export radium to the estuary, radium activity in river water was similar to its activity in nearshore ocean water such that riverine radium could not support the excess radium observed in the tidal creeks that drove the radium export calculated in this equation. Therefore, this excess radium must have been derived from groundwater. This mass balance ignores radioactive decay and should only be used with the long-lived radium isotopes, ^{226}Ra (half live = 1600 years) and ^{228}Ra (half life = 5.7 years) whose loss through mixing far exceeds loss due to radioactive decay.

The tidal prism is defined as the volume of water leaving the tidal creek on ebb tide. The tidal prism was estimated for the Duplin River (adjacent to MH) by comparing the elevations of the ground surface within the watershed to the elevation of the tide across the entire range of tidal elevations observed in the creek. This comparison was made using a digital elevation model of the Duplin watershed with 1 m^2 resolution and elevations referenced to NADV88 (http:// gce-lter.marsci.uga.edu/public/app/data-set_details.asp?accession=GIS-GCED-1104) was generated using LIDAR [*Hladik and Alber*, 2012] coupled with bathymetric mapping. Water depth in Doboy Sound, just south

of Sapelo Island, was monitored at a hydrographic station (Fig. 5.1a) maintained by the Georgia Coastal Ecosystems Long Term Ecological Research program (https://gce-lter.marsci.uga.edu/portal/gce_hydro.htm). Water levels were corrected for the absolute elevation (relative to NADV88) of the sensor to calculate the tidal elevation, and the minimum and maximum tidal elevation and average low and high tide elevations were calculated over the entire study period (2008-2010).

A hypsometric curve was generated by calculating the area of the Duplin River estuary with an elevation less than the tidal elevation with tidal elevation starting at the minimum observed value and stepping up to the maximum value at 1 cm intervals. The inundated area was then normalized to the total subtidal and intertidal area of the estuary (Fig. 5.2a). In order to determine the volume of water within the estuary at a given tidal elevation, the depth of the water overlying each inundated 1 m^2 DEM element was calculated and these volumes were summed over the entire estuary (Fig. 5.2b). The estuary volume was then normalized to the total area of the estuary, which was estimated using the DEM.

The total estuary area of the other three tidal creeks was determined using satellite imagery from Google Earth. The area of marsh surrounding the tidal creek at each site and bordered by adjacent tidal creeks or forested upland areas was estimated by visual inspection using the ImageJ software package (Fig. 5.1b-e). For comparison, the Duplin estuary area estimated using this method was ~22% lower than the estimate based on the more precise DEM. The tidal prism for each sampling campaign at all four study sites was estimated based on the response of the area-normalized Duplin watershed volume to tidal elevation. First, the tidal elevations at the low and high tides that bracketed each

sampling campaign were determined for all study sites. The area-normalized Duplin estuary volume at each tidal elevation was multiplied by the total estuary area for the site where sample collection took place to estimate the volume of water within the watershed at low and high tide. The tidal prism was then calculated by subtracting the low tide estuary volume from the high tide estuary volume. This calculation assumes that all marshes within the study domain experienced similar tides, were at the same elevation relative to the tide, and experienced similar patterns of inundation. The close proximity of these sites to one another, coupled with their similar vegetation patterns with much of the intertidal estuary area dominated by *Spartina alterniflora* suggests that these assumptions were reasonable.

The dissolved greenhouse gas flux was calculated by multiplying the volumetric groundwater flux (calculated using Equation 5.2) by the concentration of dissolved greenhouse gases in groundwater according to Equation 5.3:

$$J_{GHG} = J_{GW} \times C_{GW} \qquad \text{Equation 5.3}$$

Where J_{GHG} is the GHG flux (mol day^{-1}), J_{GW} is the volumetric groundwater flux (m^3 day^{-1}), and C_{GW} is the groundwater GHG concentration (mol m^{-3}). The GHG fluxes were normalized to the area of salt marsh within each estuary, approximated as the intertidal estuarine area, to facilitate cross-site comparisons. The intertidal estuarine area was calculated by subtracting the subtidal estuarine area (estimated from Google Earth satellite imagery as described above), from the total estuarine area. The fraction of the total estuarine area defined as intertidal ranged between 83% and 95% for these sites, similar to the 90% estimated by a different method for the Okatee River estuary in South Carolina, USA [*Moore et al.*, 2006].

RESULTS

The tidal creeks at the four study sites shared similar mean ^{226}Ra (0.44-0.55 dpm L^{-1}) and ^{228}Ra (1.25-1.69 dpm L^{-1}) activities (Table 5.1). There was more variability in groundwater radium activity across sites, with the highest activity ($^{226}Ra = 5.23 \pm 1.41$ dpm L^{-1}, $^{228}Ra = 8.33 \pm 2.08$ dpm L^{-1}) observed at MH and the lowest activity ($^{226}Ra = 0.52 \pm 0.26$ dpm L^{-1}, $^{228}Ra = 2.82 \pm 1.46$ dpm L^{-1}) at PC, though the ^{228}Ra activity was similarly low at HN. At CI, groundwater was enriched in both ^{226}Ra and ^{228}Ra by a factor of approximately nine relative to creek water (Table 5.1). At HN and PC, groundwater was more enriched in ^{228}Ra than ^{226}Ra relative to tidal creek water, and groundwater was more enriched in ^{226}Ra at MH. Since the more enriched isotope acts as a better tracer for groundwater flux, ^{228}Ra activity was used for CI, HN, and PC while ^{226}Ra activity was used for MH in subsequent calculations. While groundwater radium activities tended to be higher than radium activities in adjacent tidal creeks, creek water radium activities were higher than those found in nearshore ocean surface water ($^{226}Ra = 0.21$ dpm L^{-1}, $^{228}Ra = 0.34$ dpm L^{-1}) [*Moore*, 2007]. The intermediate radium activities of the tidal creeks likely resulted from mixing between nearshore ocean water and groundwater, indicating that groundwater discharge influenced the chemistry of these tidal creeks.

Linear relationships between ^{228}Ra and ^{226}Ra activity in each creek that fell along lines between marine and groundwater endmembers (Fig. 5.3a-d) suggest that creek radium activities were driven by two endmember mixing of these water masses. These radium mixing curves contain groundwater radium activities from only one or two wells at each site. The other wells had different slopes from these mixing lines, indicating that they sampled aquifers with different sediment geology. ^{226}Ra and ^{228}Ra are derived from

^{230}Th and ^{232}Th found in minerals within the sediment such that different ^{228}Ra:^{226}Ra in groundwater indicates different ^{230}Th:^{232}Th in the sediment, likely driven by variations in mineral composition of the sediment. Groundwater radium activities from the wells in Figure 5.3 fall along a mixing line with the tidal creek and nearshore ocean meaning that these wells sampled aquifers that were actively discharging into the tidal creek. Therefore, radium activities and GHG concentrations from these wells were used in all subsequent analyses. At PC, two wells had similar slopes to the mixing line between the tidal creek and ocean without matching it perfectly. In this case, data from these two wells was averaged to estimate the discharging groundwater composition. At CI, two wells fell along the mixing line in Figure 5.3. The well with the highest radium activity (Groundwater-Ra) was used as the groundwater endmember in volumetric groundwater flux calculations (Equation 5.2). However, the second well (Groundwater-GHG) represents a mixture of water from Groundwater-Ra and the creek, indicating that it was hydrologically closer to the point of groundwater discharge. GHG data from this well was used in GHG flux calculations in order to minimize the potential error associated with GHG concentrations being altered by processes taking place within the aquifer prior to discharge.

Marsh groundwater DIC concentrations were highest at CI (12.3 ± 3.0 mM) and lowest at MH (2.0 ± 1.2 mM; Table 5.2). Groundwater CH_4 concentrations were also highest at CI (17.4 ± 6.2 μM), with the next highest concentrations observed at HN (2.9 ± 5.7 μM), and the lowest concentrations at MH (0.13 ± 0.11 μM). Groundwater and tidal creek water N_2O concentrations were below the detection limit at these sites. Marsh groundwater was enriched in DIC and CH_4 relative to the adjacent tidal creek at all four

study sites by factors of 2-5 and 2-60, respectively (Table 5.2). Dissolved inorganic carbon concentrations in creek water ranged between 1 and 3 mM at all sites, with average concentrations at CI, HN, and PC being slightly higher than the expected concentration of 2 mM in surface seawater [*Millero*, 2006]. Methane concentrations in creek water were more variable, ranging from near zero to nearly 8 μM, with higher concentrations at HN and PC than at CI and MH. Creek water tended to be enriched in CH_4 relative to the concentration expected (1.8 nM) based on equilibration of seawater (35 PSU, 25°C) with the atmosphere [*Yamamoto et al.*, 1976]. These data indicate that the higher than expected DIC and CH_4 concentrations in creek water could be supplied by groundwater that is enriched in these GHGs.

To estimate the groundwater flux, it was first necessary to estimate the volume of the tidal prism at each location using the hypsometric curve of the Duplin River. The initial, relatively flat portion of the hypsometric curve (Fig. 5.2a) shows the Duplin River channel filling in response to an incoming tide, resulting in little additional marsh inundation. Once the tide overtopped the creek bank, the marsh flooded rapidly in response to only small increases in tidal elevation, as indicated by the steep upward slope in the hypsometric curve. The flattening of the hypsometric curve at very high tides reflects that most of the marsh was already flooded and creek water approached nearby upland areas, resulting in little additional inundation. The volume of water within the Duplin estuary increased rapidly in response to the rising tide (Fig. 5.2b). Of the tidal creeks flowing past the four study sites, the Duplin River estuary had the largest total area (1.5×10^7 m^2, Table 5.3). The other three sites were located within estuaries that were two orders of magnitude smaller than the Duplin estuary. The intertidal portions of these

estuaries had total areas of $1.8x10^5 – 4.9x10^5$ m^2 (Table 5.3). These differences in area resulted in a similar cross-site difference in the volume of the tidal prism, with the mean tidal prism of the Duplin ($8.3x10^6$ m^3) being an order of magnitude larger than the other three sites ($1.1x10^5 – 2.3x10^5$ m^3, Table 5.4). The Duplin tidal prism volumes reported here were similar to those reported by Ragotzkie and Bryson [1955]. The mean return flow factor for these sites varied between 0.43 at PC and 0.78 at CI (Table 5.4).

The volumetric groundwater flux calculated for each sampling campaign at each study site based on Equation 5.2 and the data in Tables 5.1 and 5.2. The Duplin watershed (MH) had the highest groundwater flux ($2.0x10^5 \pm 0.95x10^5$ m^3 day^{-1}) and CI the lowest ($4.3x10^3 \pm 3.1x10^3$ m^3 day^{-1}, Table 5.4). The groundwater-derived DIC flux normalized to marsh area ranged from 0.04 ± 0.03 mol m^{-2} day^{-1} at MH to 2.2 ± 2.4 mol m^{-2} day^{-1} at PC. In spite of higher groundwater DIC concentrations at CI, the higher volumetric groundwater flux from HN and PC drove higher DIC fluxes. The groundwater-derived CH_4 flux was highest at CI, however (0.48 ± 0.44 mmol m^{-2} day^{-1}), driven by much higher groundwater CH_4 concentrations. The lowest CH_4 flux was observed at MH (0.003 ± 0.003 mmol m^{-2} day^{-1}). It was not possible to calculate a groundwater-derived N_2O flux at these sites since groundwater N_2O concentrations were below the detection limit of 31 nM. But it is possible to set an upper limit on this flux by multiplying the minimum detectable groundwater N_2O concentration by the volumetric groundwater flux at each site and normalizing to marsh area. This upper limit was around 0.5-12.5 μmol m^{-2} day^{-1} across the four study sites.

DISCUSSION

The SGD-derived fluxes of DIC from the four salt marshes reported here ranged from 0.04-1.53 mol m^{-2} day^{-1}. These fluxes are similar to the 0.17 mol m^{-2} day^{-1} [*Cai et al.*, 2003] and 1.2 mol m^{-2} day^{-1} [*Porubsky et al.*, 2014] reported from other salt marshes in South Carolina, USA and mostly fall within the range in SGD-derived DIC fluxes reported from other coastal wetlands (0.25-1.62 mol m^{-2} day^{-1}) [*Atkins et al.*, 2013; *Maher et al.*, 2013]. There is only one report of SGD-derived CH_4 flux from a salt marsh (0.94 mmol m^{-2} day^{-1}) in the literature [*Porubsky et al.*, 2014], which is higher than the range of 0.003-0.48 mmol m^{-2} day^{-1} reported here. LaMontagne et al. [2003] demonstrated a substantial SGD contribution (0.6 mol day^{-1}) of N_2O to a northeastern United States estuary, but insufficient data was provided to calculate an areal flux for comparison. Porubsky et al. [2014] also reported a SGD-derived N_2O flux of 4.7 μmol m^{-2} day^{-1} from a salt marsh. This flux would have been at or below the detection limit for the method presented here, so it is possible that because of this high detection limit, a substantial N_2O flux from the salt marshes around Sapelo Island was missed in this study.

In spite of the paucity of SGD-derived greenhouse gas fluxes in the literature, a great deal of evidence suggests that these fluxes are globally relevant. Salt marsh groundwater DIC concentrations range from 2-16 mM [*Cai et al.*, 2003; *Porubsky et al.*, 2014] and from 2-60 mM for surficial porewater [*Segarra et al.*, 2013; *Weston et al.*, 2006]. Groundwater methane concentrations range between 10 and 40 μM [*Porubsky et al.*, 2014] and between 0.2 and 3 mM in porewater [*Segarra et al.*, 2013; *Weston et al.*, 2006]. These groundwater DIC and CH_4 concentrations closely match the range of values observed at the four sites described here, though the CH_4 concentrations at PC and MH

were as low as 0.37 μM. Finally, salt marsh groundwater averaged 0.2 μM N_2O [*Porubsky et al.*, 2014] and ranged from 1 to 12.5 μM in a nitrogen-contaminated aquifer [*LaMontagne et al.*, 2003]. These concentrations are generally much higher than concentrations observed in coastal marine surface waters [*Bange*, 2006]. This enrichment of GHGs in groundwater combined with evidence for extensive and substantial fluxes of groundwater from salt marsh aquifers into adjacent surface waters [*Charette et al.*, 2003; *Krest et al.*, 2000; *Moore et al.*, 2006] indicates that SGD may be a critical source of these dissolved GHGs to the coastal ocean. While these dissolved gases can be consumed by microbial processes as they transit aquifers and creek banks, high GHG concentrations and groundwater fluxes suggest that SGD-derived loading of GHGs to coastal surface waters is likely to be a widespread phenomenon in salt marsh ecosystems.

Another potential pathway for GHG export is direct efflux from the sediment surface to the atmosphere. Mean CO_2 fluxes reported for salt marshes range from 0.059-0.370 mol m^{-2} day^{-1} [*Chmura et al.*, 2011; *Magenheimer et al.*, 1996; *Moseman-Valtierra et al.*, 2011], similar to the SGD-derived fluxes described above. Direct fluxes to the atmosphere are more variable for CH_4, covering a range from 0.028-2.7 mmol m^{-2} day^{-1} [*Chmura et al.*, 2011; *King and Wiebe*, 1978; *Lipschultz*, 1981; *Magenheimer et al.*, 1996; *Moseman-Valtierra et al.*, 2011] that encompasses the values of SGD-derived CH_4 fluxes available in the literature. The mean N_2O flux to the atmosphere is between -32 and 7.2 μmol m^{-2} day^{-1} [*Chmura et al.*, 2011; *Moseman-Valtierra et al.*, 2011; *Smith et al.*, 1983], which also encompasses the range of SGD-derived N_2O fluxes reported in the literature. Averaged across all studies, the SGD-derived inorganic carbon flux from salt marshes was 0.9 ± 1.4 mol m^{-2} day^{-1} compared with 0.23 ± 0.21 mol m^{-2} day^{-1} of CO_2 that

was exported directly to the atmosphere (Table 5.5). The SGD-derived CH_4 flux averaged across all sites was 0.41 ± 0.84 mmol m^{-2} day^{-1} compared with an average efflux to the atmosphere of 0.6 ± 2.8 mmol m^{-2} day^{-1}. Much less data exists regarding N_2O export making it impossible to determine which export pathway is dominant. Nonetheless, SGD is an important pathway for greenhouse gas export from salt marsh ecosystems that has been overlooked in the past. This is a particularly important finding in light of the increased interest in salt marshes as net carbon sinks [*Chmura et al.*, 2003] that could mitigate anthropogenic climate change. SGD-derived greenhouse gas fluxes should be considered in future studies of the "blue carbon" [*McLeod et al.*, 2011] sequestered by salt marshes and other coastal wetlands.

Salt marshes cover approximately 22,000 km^2 of North America, Europe, and parts of Africa [*Chmura et al.*, 2003]. This is a substantial underestimate of the true global extent of salt marshes because it does not include South America, Asia, or Australia. Scaling the average areal SGD-derived fluxes of DIC, CH_4, and N_2O up to 22,000 km^2 yields total fluxes of $7.2x10^{12}$, $3.3x10^9$, and $3.8x10^7$ mol $year^{-1}$ respectively, which equate to 0.09 Pg C $year^{-1}$, 0.05 Tg CH_4 $year^{-1}$, and 0.001 Tg N_2O-N $year^{-1}$. To put these fluxes in the perspective of global budgets, the riverine flux of carbon to the ocean is estimated to be 0.9 Pg $year^{-1}$, the CH_4 flux from methane hydrates to the atmosphere is 2-9 Tg $year^{-1}$, and 0.1-2.9 Tg of nitrogen in the form of N_2O enters the atmosphere each year from rivers, estuaries, and coastal zones [*Ciais et al.*, 2013]. Furthermore, estuarine systems make substantial contributions of CO_2 to the atmosphere [*Cai et al.*, 2003] and coastal surface waters are a net source of CH_4 and N_2O to the atmosphere [*Bange*, 2006].

This work demonstrates that these observed fluxes are supported, in part, by delivery of DIC, CH_4, and N_2O to the coastal surface waters via SGD.

LITERATURE CITED

Atkins, M. L., I. R. Santos, S. Ruiz-Halpern, and D. T. Maher (2013), Carbon dioxide dynamics driven by groundwater discharge in a coastal floodplain creek, *Journal of Hydrology*, *493*, 30-42.

Bange, H. W. (2006), Nitrous oxide and methane in European coastal waters, *Estuarine Coastal and Shelf Science*, *70*(3), 361-374.

Burnett, W. C., H. Bokuniewicz, M. Huettel, W. S. Moore, and M. Taniguchi (2003), Groundwater and pore water inputs to the coastal zone, *Biogeochemistry*, *66*(1-2), 3-33.

Cai, W. J., Y. C. Wang, J. Krest, and W. S. Moore (2003), The geochemistry of dissolved inorganic carbon in a surficial groundwater aquifer in North Inlet, South Carolina, and the carbon fluxes to the coastal ocean, *Geochimica Et Cosmochimica Acta*, *67*(4), 631-639.

Charette, M., R. Splivallo, and C. Herbold (2003), Salt marsh submarine groundwater discharge as traced by radium isotopes, *Marine Chemistry*.

Charette, M. A., and K. O. Buesseler (2004), Submarine groundwater discharge of nutrients and copper to an urban subestuary of Chesapeake Bay (Elizabeth River), *Limnology and Oceanography*, *49*(2), 376-385.

Chmura, G. L., L. Kellman, and G. R. Guntenspergen (2011), The greenhouse gas flux and potential global warming feedbacks of a northern macrotidal and microtidal salt marsh, *Environmental Research Letters*, *6*(4).

Chmura, G. L., S. C. Anisfeld, D. R. Cahoon, and J. C. Lynch (2003), Global carbon sequestration in tidal, saline wetland soils, *Global Biogeochemical Cycles*, *17*(4).

Ciais, P., et al. (2013), Carbon and other biogeochemical cycles, in *Climate Change 2013: The Physical Science Basis. Contribution of Working Group I to the Fifth Assessment Report of the Intergovernmental Panel on Climate Change*, edited by T. F. Stocker, D. Qin, G.-K. Plattner, M. Tignor, S. K. Allen, J. Boschung, A. Nauels, Y. Xia, V. Bex and P. M. Midgley, Cambridge University Press, Cambridge, United Kingdom and New York, NY, USA.

Hladik, C., and M. Alber (2012), Accuracy assessment and correction of a LIDAR-derived salt marsh digital elevation model, *Remote Sensing of Environment*, *121*, 224-235.

King, G. M., and W. J. Wiebe (1978), Methane release from soils of a Georgia salt marsh, *Geochimica Et Cosmochimica Acta*, *42*(4), 343-348.

Krest, J. M., W. S. Moore, L. R. Gardner, and J. T. Morris (2000), Marsh nutrient export supplied by groundwater discharge: evidence from radium measurements, *Global Biogeochemical Cycles*, *14*(1), 167-176.

LaMontagne, M. G., R. Duran, and I. Valiela (2003), Nitrous oxide sources and sinks in coastal aquifers and coupled estuarine receiving waters, *The Science of the Total Environment*, *309*, 139-149.

Lipschultz, F. (1981), Methane release from a brackish intertidal salt-marsh embayment of Chesapeake Bay, Maryland, *Estuaries*, *4*(2), 143-145.

Magenheimer, J. F., T. R. Moore, G. L. Chmura, and R. J. Daoust (1996), Methane and carbon dioxide flux from a macrotidal salt marsh, Bay of Fundy, New Brunswick, *Estuaries*, *19*(1), 139-145.

Maher, D. T., I. R. Santos, L. Golsby-Smith, J. Gleeson, and B. D. Eyre (2013), Groundwater-derived dissolved inorganic and organic carbon exports from a mangrove tidal creek: The missing mangrove carbon sink?, *Limnology and Oceanography*, *58*(2), 475-488.

McLeod, E., G. L. Chmura, S. Bouillon, R. Salm, M. Bjork, C. M. Duarte, C. E. Lovelock, W. H. Schlesinger, and B. R. Silliman (2011), A blueprint for blue carbon: toward an improved understanding of the role of vegetated coastal habitats in sequestering CO2, *Frontiers in Ecology and the Environment*, *9*(10), 552-560.

Middelburg, J. J., G. Klaver, J. Nieuwenhuize, R. M. Markusse, T. Vlug, and F. J. W. A. van der Nat (1995), Nitrous oxide emissions from estuarine intertidal sediments, *Hydrobiologia*, *311*, 43-55.

Millero, F. J. (2006), *Chemical Oceanography*, Third ed., CRC Press, Taylor & Francis Group, Boca Raton.

Moore, W. S. (1999), The subterranean estuary: a reaction zone of ground water and sea water, *Marine Chemistry*, *65*, 111-125.

Moore, W. S. (2007), Seasonal distribution and flux of radium isotopes on the southeastern U.S. continental shelf, *Journal of Geophysical Research*, *112*(C10), 1-16.

Moore, W. S., and T. J. Shaw (2008), Fluxes and behavior of radium isotopes, barium, and uranium in seven Southeastern US rivers and estuaries, *Marine Chemistry*, *108*(3), 236-254.

Moore, W. S., J. O. Blanton, and S. B. Joye (2006), Estimates of flushing times, submarine groundwater discharge, and nutrient fluxes to Okatee Estuary, South Carolina, *Journal of Geophysical Research*, *111*, C09006.

Moseman-Valtierra, S., R. Gonzalez, K. D. Kroeger, J. W. Tang, W. C. Chao, J. Crusius, J. Bratton, A. Green, and J. Shelton (2011), Short-term nitrogen additions can shift a coastal wetland from a sink to a source of N2O, *Atmospheric Environment*, *45*(26), 4390-4397.

Myhre, G., et al. (2013), Anthropogenic and natural radiative forcing, in *Climate Change 2013: The Physical Science Basis. Contribution of Working Group I to the Fifth Assessment Report of the Intergovernmental Panel on Climate Change*, edited by T. F. Stocker, D. Qin, G.-K. Plattner, M. Tignor, S. K. Allen, J. Boschung, A. Nauels, Y. Xia, V. Bex and P. M. Midgley, Cambridge University Press, Cambridge, United Kingdom and New York, NY, USA.

Porubsky, W. P., S. B. Joye, W. S. Moore, K. Tuncay, and C. Meile (2010), Field measurements and modeling of groundwater flow and biogeochemistry at Moses Hammock, a backbarrier island on the Georgia coast, *Biogeochemistry*, *104*, 69-70.

Porubsky, W. P., N. B. Weston, W. S. Moore, C. Ruppel, and S. B. Joye (2014), Dynamics of submarine groundwater discharge and associated fluxes of dissolved nutrients, carbon, and trace gases to the coastal zone (Okatee River estuary, South Carolina), *Geochimica et Cosmochimica Acta*, *131*, 81-97.

Ragotzkie, R. A., and R. A. Bryson (1955), Hydrography of the Duplin River, Sapelo Island, Georgia, *Bulletin of Marine Science of the Gulf and Caribbean*, *5*(4), 297-314.

Santos, I. R., W. C. Burnett, J. P. Chanton, and B. Mwashote (2008), Nutrient biogeochemistry in a Gulf of Mexico subterranean estuary and groundwater-derived fluxes to the coastal ocean, *Limnology and Oceanography*.

Schultz, G., and C. Ruppel (2002), Constraints on hydraulic parameters and implications for groundwater flux across the upland-estuary interface, *Journal of Hydrology*, *260*, 255-269.

Schutte, C. A., K. Hunter, P. McKay, D. Di Iorio, S. B. Joye, and C. Meile (2013), Patterns and controls of nutrient concentrations in a southeastern United States tidal creek, *Oceanography*, *26*(3), 132-139.

Segarra, K. E. A., C. Comerford, J. Slaughter, and S. B. Joye (2013), Impact of electron acceptor availability on the anaerobic oxidation of methane in coastal freshwater and brackish wetland sediments, *Geochimica Et Cosmochimica Acta*, *115*, 15-30.

Slomp, C. P., and P. Van Cappellen (2004), Nutrient inputs to the coastal ocean through submarine groundwater discharge: controls and potential impact, *Journal of Hydrology*, *295*, 64-86.

Smith, C. J., R. D. Delaune, and W. H. Patrick (1983), Nitrous oxide emission from Gulf Coast wetlands, *Geochimica Et Cosmochimica Acta*, *47*(10), 1805-1814.

Walther, G.-R., E. Post, P. Convey, A. Menzel, C. Parmesan, T. J. C. Beebee, J.-M. Fromentin, O. Hoegh-Guldberg, and F. Bairlein (2002), Ecological responses to recent climate change, *Nature*, *416*(6879), 389-395.

Weston, N. B., W. P. Porubsky, V. A. Samarkin, M. Erickson, S. E. Macavoy, and S. B. Joye (2006), Porewater stoichiometry of terminal metabolic products, sulfate, and dissolved organic carbon and nitrogen in estuarine intertidal creek-bank sediments, *Biogeochemistry*, *77*(3), 375-408.

Wilson, A. M., W. S. Moore, S. B. Joye, J. L. Anderson, and C. A. Schutte (2011), Storm-driven groundwater flow in a salt marsh, *Water Resources Research*, *47*(2), W02535.

Yamamoto, S., J. B. Alcauskas, and T. E. Crozier (1976), Solubility of methane in distilled water and seawater, *Journal of Chemical and Engineering Data*, *21*(1), 78-80.

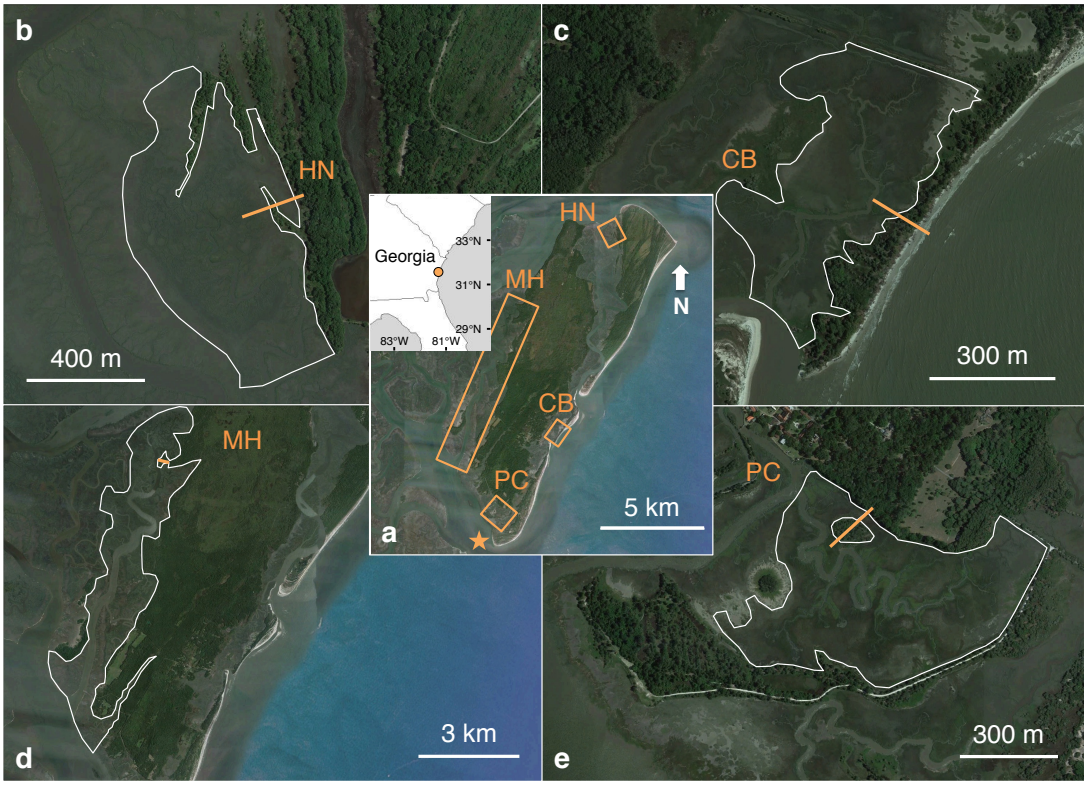

Figure 5.1. Satellite images of Sapelo Island on the coast of Georgia, USA with the four study sites highlighted by orange boxes (a). Images were acquired from Google Maps on July 26, 2014. The orange star shows the location where tide data was collected. The four study sites include: (b) HN_i_1 (HN), (c) Cabretta Island (CB), (d) Moses Hammock (MH), and (d) PC_i_29 (PC). For each site, the white polygon represents the area of the tidal creek watershed and the orange line shows the location of the groundwater monitoring well transect.

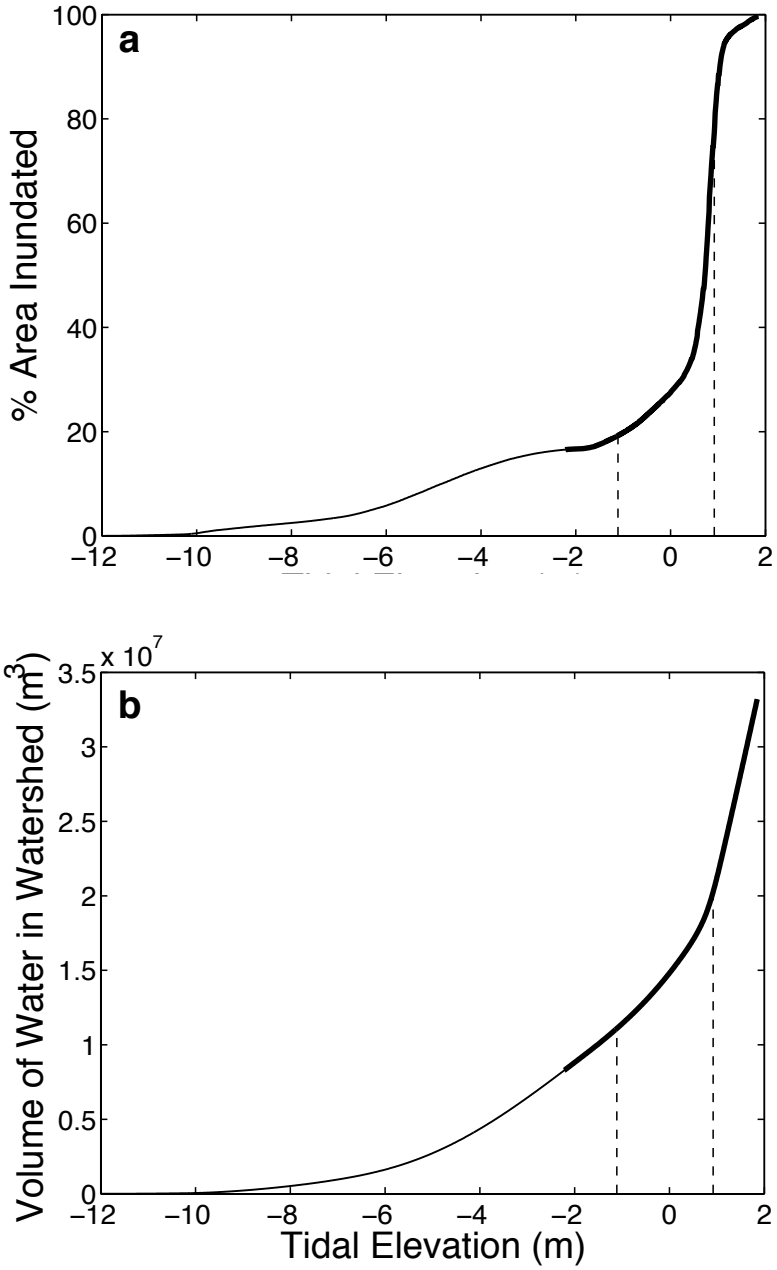

Figure 5.2. A hypsometric curve for the Duplin River (a) showing the percentage of the total marsh area flooded within the tidal creek watershed as a function of the elevation of the water in the creek relative to NADV88. The volume of water within the Duplin River watershed as a function of tidal elevation (b). The mean low and high tides from 2008-2010 in Doboy Sound just South of Sapelo Island are displayed as dashed lines in both plots. The bold portion of the curve represents the range in tidal elevation observed over the study period.

Table 5.1. The activity of ^{226}Ra and ^{228}Ra in tidal creek water and groundwater from each sampling campaign at all four study sites. Activities are in units of dpm L^{-1}. The ratio of groundwater to tidal creek water activity was calculated for both radium isotopes (right two columns). The mean radium activity and standard deviation for each site are displayed in italics.

	Tidal Creek		Groundwater		Groundwater:Creek	
Date	^{226}Ra	^{228}Ra	^{226}Ra	^{228}Ra	^{226}Ra	^{228}Ra
CI						
08/23/08	0.89	1.28	2.10	4.60	2.36	3.58
09/08/08	0.80	1.99	3.60	8.78	4.53	4.42
03/26/09	0.30	0.71	4.36	10.48	14.70	14.70
05/23/09	0.40	1.20	3.20	8.93	7.96	7.47
09/30/09	0.60	1.52	3.55	9.01	5.88	5.92
12/03/09	0.35	0.79	3.56	8.91	10.21	11.26
01/26/10	0.43	1.04	3.98	9.41	9.21	9.02
03/30/10	0.28	0.57	4.82	10.44	17.14	18.45
05/20/10	0.58	1.34	5.46	12.78	9.44	9.56
08/01/10	0.90	2.02	4.66	10.58	5.20	5.23
Mean	*0.55*	*1.25*	*3.93*	*9.39*	*8.66*	*8.96*
Std. Dev.	*0.24*	*0.50*	*0.95*	*2.09*	*4.58*	*4.76*
HN						
08/14/08	0.46	1.48	0.65	3.71	1.42	2.51
09/09/08	0.77	2.68	1.00	3.25	1.30	1.21
10/22/08	0.85	1.69	1.11	3.69	1.31	2.19
03/27/09	0.54	1.82	0.82	2.67	1.53	1.47
05/24/09	0.36	1.16	0.55	2.02	1.53	1.74
12/01/09	0.46	1.31	0.44	1.50	0.95	1.14
Mean	*0.57*	*1.69*	*0.76*	*2.81*	*1.34*	*1.71*
Std. Dev.	*0.19*	*0.54*	*0.26*	*0.91*	*0.22*	*0.55*
PC						
08/14/08	0.51	1.61	0.71	4.70	1.41	2.91
09/07/08	0.59	2.03	0.92	4.64	1.56	2.28
01/26/09	0.30	0.66	0.67	3.67	2.26	5.56
03/28/09	0.45	1.42	0.46	1.43	1.02	1.01
05/25/09	0.42	1.30	0.42	1.85	0.99	1.42
10/01/09	0.44	1.18	0.23	1.78	0.52	1.52
12/02/09	0.38	1.00	0.25	1.66	0.67	1.67
Mean	*0.44*	*1.31*	*0.52*	*2.82*	*1.20*	*2.34*
Std. Dev.	*0.09*	*0.44*	*0.26*	*1.46*	*0.59*	*1.55*

	Tidal Creek		Groundwater		Groundwater:Creek	
Date	^{226}Ra	^{228}Ra	^{226}Ra	^{228}Ra	^{226}Ra	^{228}Ra
MH						
07/12/08	0.71	1.88	4.51	6.95	6.35	3.70
10/12/08	0.57	1.91	7.33	11.32	12.77	5.93
01/23/09	0.45	1.21	4.31	6.90	9.64	5.71
04/18/09	0.25	0.75	4.76	8.14	18.98	10.86
Mean	*0.50*	*1.44*	*5.23*	*8.33*	*11.94*	*6.55*
Std. Dev.	*0.20*	*0.56*	*1.41*	*2.08*	*5.38*	*3.04*

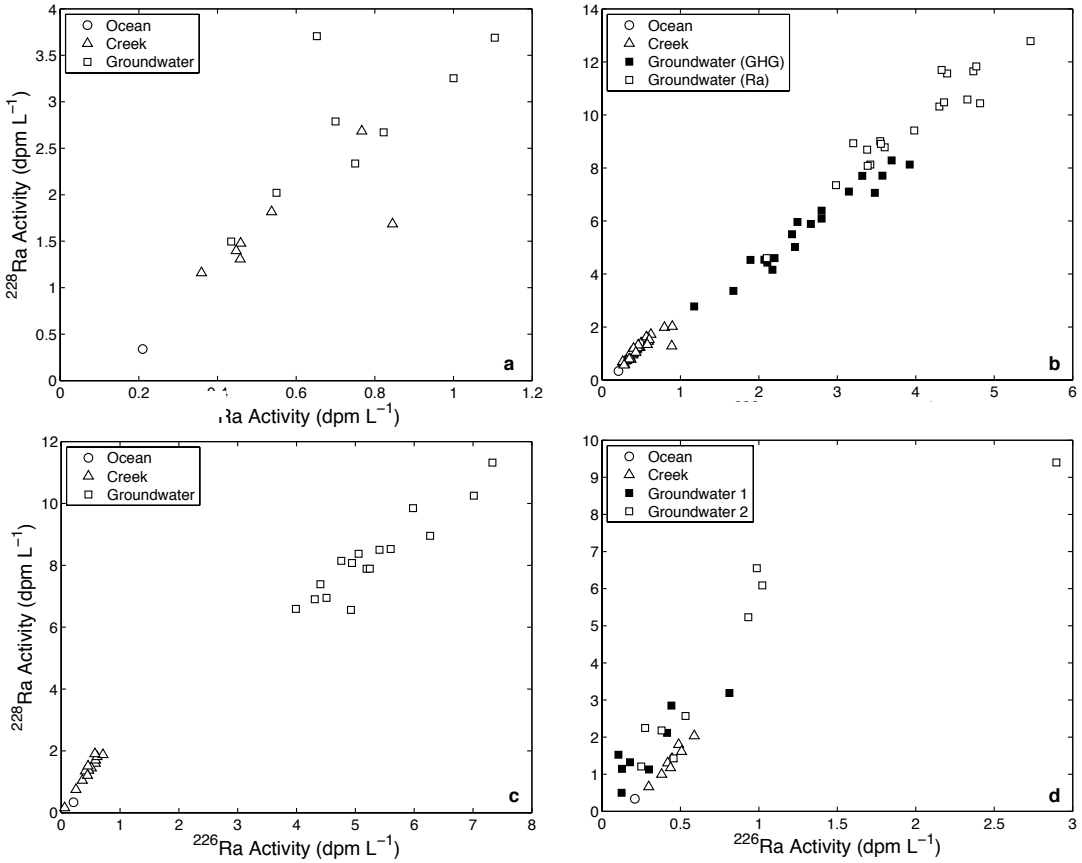

Figure 5.3. Plots of ^{228}Ra activity versus ^{226}Ra activity that show that tidal creek radium activities fall along a conservative mixing line between seawater and groundwater endmembers at HN (a), CI (b), MH (c), and PC (d). Each set of groundwater points represents data from a single monitoring well. Note that most wells are not displayed here as they did not fall on a mixing line with the tidal creek and ocean. At CI (b), two wells fell on the mixing line. The well labeled Groundwater (Ra) was used as the groundwater endmember for all Ra-based calculations while the Groundwater (GHG) well was used in the GHG flux calculation. At PC (d), two wells fell on the mixing line, but were indistinguishable from one another. For this reason all calculations at this site are based on the average Ra activities and GHG concentrations in these two wells at each time point.

Table 5.2. Salinity and the concentrations of DIC, CH_4, and N_2O in tidal creek water and groundwater during each sampling campaign at each of the four study sites. The mean concentration and the standard deviation for each site is displayed in italics. n.d. = no data, b.d. = below detection limit where the detection limit was 0.87 mM for DIC, 0.45 μM for CH_4, and 31 nM for N_2O.

	Tidal Creek				Groundwater			
Date	Salinity	DIC (mM)	CH_4 (μM)	N_2O (nM)	Salinity	DIC (mM)	CH_4 (μM)	N_2O (nM)
CI								
08/23/08	36.0	n.d.	0.36	9.61	43.0	n.d.	23.00	b.d.
09/08/08	40.0	n.d.	0.50	b.d.	42.0	7.3	11.04	b.d.
03/26/09	32.4	2.5	b.d.	b.d.	39.7	12.9	12.55	b.d.
05/23/09	26.8	2.6	0.16	b.d.	40.0	13.1	13.14	b.d.
09/30/09	33.0	2.8	0.45	b.d.	37.1	10.8	14.10	b.d.
12/03/09	29.0	1.9	b.d.	b.d.	35.6	12.1	18.74	b.d.
01/26/10	23.3	2.2	0.36	b.d.	41.8	13.2	26.10	b.d.
03/30/10	30.4	1.8	b.d.	b.d.	41.6	14.7	28.07	b.d.
05/20/10	30.6	3.0	0.27	4.56	40.4	17.3	12.41	b.d.
08/01/10	36.2	1.9	0.68	b.d.	40.9	9.0	15.11	b.d.
Mean	*31.8*	*2.3*	*0.28*	*1.42*	*40.2*	*12.3*	*17.43*	b.d.
Std. Dev.	*4.9*	*0.5*	*0.24*	*3.22*	*2.3*	*3.0*	*6.20*	b.d.
HN								
08/14/08	34.0	2.5	5.64	0.00	24.0	3.4	14.35	n.d.
09/09/08	41.0	3.2	0.69	0.00	26.0	4.4	0.17	b.d.
10/22/08	33.5	2.0	b.d.	33.53	31.5	4.6	0.48	b.d.
03/27/09	32.4	2.2	0.67	0.00	29.5	5.6	0.25	b.d.
05/24/09	21.8	2.1	6.13	0.00	20.7	4.5	1.89	b.d.
12/01/09	26.7	4.0	0.41	0.00	19.1	3.2	b.d.	b.d.
Mean	*31.6*	*2.7*	*2.26*	*5.59*	*25.1*	*4.3*	*2.86*	b.d.
Std. Dev.	*6.6*	*0.8*	*2.83*	*13.69*	*4.9*	*0.9*	*5.67*	b.d.
PC								
08/14/08	28.0	2.2	7.71	NaN	31.3	2.7	3.58	b.d.
09/07/08	30.0	2.9	0.63	15.68	34.0	4.8	0.72	b.d.
01/26/09	29.4	1.7	b.d.	b.d.	32.9	6.9	0.36	b.d.
03/28/09	28.0	1.6	b.d.	b.d.	32.5	5.0	0.39	b.d.
05/25/09	24.2	1.9	3.83	b.d.	30.3	4.9	0.51	b.d.
10/01/09	27.8	3.2	2.49	b.d.	23.4	4.8	0.54	b.d.
12/02/09	23.3	2.0	b.d.	b.d.	26.5	7.6	0.81	3.24
Mean	*27.2*	*2.2*	*2.09*	*2.61*	*30.1*	*5.2*	*0.99*	*0.46*
Std. Dev.	*2.5*	*0.6*	*2.89*	*6.40*	*3.8*	*1.6*	*1.16*	*1.22*

Date	Tidal Creek Salinity	DIC (mM)	CH_4 (µM)	N_2O (nM)	Groundwater Salinity	DIC (mM)	CH_4 (µM)	N_2O (nM)
MH								
07/12/08	31.0	2.0	0.35	44.08	25.0	2.8	0.29	71.75
10/12/08	29.0	b.d.	b.d.	b.d.	25.0	3.0	0.12	28.79
01/23/09	28.0	1.8	0.04	b.d.	30.0	0.4	0.06	6.62
04/18/09	15.4	0.8	b.d.	b.d.	25.1	1.7	0.05	35.36
Mean	*25.9*	*1.2*	*0.10*	*11.02*	*26.3*	*2.0*	*0.13*	*35.63*
Std. Dev.	*7.1*	*0.9*	*0.17*	*22.04*	*2.5*	*1.2*	*0.11*	*27.04*

Table 5.3. The total estuary area, the area of the subtidal portion of the estuary, and the area of the intertidal portion of the estuary that is dominated by salt marsh grasses.

Site	Estuary Area (m^2)	Subtidal Area (m^2)	Intertidal Area (m^2)
CI	$1.8x10^5$	$1.1x10^4$	$1.6x10^5$
HN	$4.9x10^5$	$2.7x10^4$	$4.6x10^5$
PC	$3.2x10^5$	$2.7x10^4$	$3.0x10^5$
MH	$1.5x10^7$	$1.9x10^6$	$1.2x10^7$

Table 5.4. The tidal prism (derived from hypsometric curves), return flow factor (calculated from equation 5.1), volumetric groundwater flux (equation 5.2), total DIC and CH_4 flux (equation 5.3), and the flux of DIC and CH_4 normalized to marsh area. These values were calculated for each sampling campaign at each of the four study sites. The average and standard deviation for each study site are presented in italics.

Date	Tidal Prism (m^3)	Return Flow b	GW Flux (m^3 day^{-1})	DIC Flux (mol day^{-1})	CH_4 Flux (mmol day^{-1})	DIC Flux (mol m^{-2} day^{-1})	CH_4 Flux (mmol m^{-2} day^{-1})
CI							
08/23/08	$1.2x10^5$	0.76	$1.1x10^4$	n.d.	$2.6x10^5$	n.d.	1.56
09/08/08	$6.1x10^4$	0.91	$2.0x10^3$	$1.4x10^4$	$2.2x10^4$	0.09	0.13
03/26/09	$1.5x10^5$	0.88	$1.2x10^3$	$1.5x10^4$	$1.5x10^4$	0.09	0.09
05/23/09	$1.1x10^5$	0.65	$7.4x10^3$	$9.7x10^4$	$9.8x10^4$	0.59	0.59
09/30/09	$8.1x10^4$	0.80	$4.2x10^3$	$4.5x10^4$	$5.9x10^4$	0.28	0.36
12/03/09	$1.7x10^5$	0.77	$3.8x10^3$	$4.6x10^4$	$7.1x10^4$	0.28	0.43
01/26/10	$7.9x10^4$	0.57	$4.9x10^3$	$6.5x10^4$	$1.3x10^5$	0.40	0.79
03/30/10	$1.4x10^5$	0.84	$9.1x10^2$	$1.3x10^4$	$2.6x10^4$	0.08	0.16
05/20/10	$1.2x10^5$	0.78	$3.8x10^3$	$6.6x10^4$	$4.7x10^4$	0.40	0.29
08/01/10	$8.0x10^4$	0.84	$3.9x10^3$	$3.5x10^4$	$5.9x10^4$	0.21	0.36
Mean	*$1.1x10^5$*	*0.78*	*$4.3x10^3$*	*$4.4x10^4$*	*$7.8x10^4$*	*0.27*	*0.48*
Std. Dev.	*$3.4x10^4$*	*0.10*	*$3.1x10^3$*	*$2.8x10^4$*	*$7.2x10^4$*	*0.17*	*0.44*
HN							
08/14/08	$2.3x10^5$	0.74	$3.6x10^4$	$1.2x10^5$	$5.1x10^5$	0.27	1.12
09/09/08	$1.6x10^5$	0.59	$9.4x10^4$	$4.2x10^5$	$1.6x10^4$	0.91	0.03
10/22/08	$4.5x10^5$	0.60	$1.3x10^5$	$6.0x10^5$	$6.2x10^4$	1.30	0.14
03/27/09	$3.5x10^5$	0.39	$2.3x10^5$	$1.3x10^6$	$5.6x10^4$	2.75	0.12
05/24/09	$3.2x10^5$	0.33	$1.7x10^5$	$7.5x10^5$	$3.2x10^5$	1.64	0.69
12/01/09	$4.0x10^5$	0.31	$3.4x10^5$	$1.1x10^6$	$0.0x10^0$	2.32	0.00
Mean	*$3.2x10^5$*	*0.49*	*$1.7x10^5$*	*$7.0x10^5$*	*$1.6x10^5$*	*1.53*	*0.35*
Std. Dev.	*$1.1x10^5$*	*0.17*	*$1.1x10^5$*	*$4.2x10^5$*	*$2.1x10^5$*	*0.91*	*0.45*
PC							
08/14/08	$1.4x10^5$	0.53	$3.5x10^4$	$9.2x10^4$	$1.2x10^5$	0.31	0.42
09/07/08	$1.1x10^5$	0.47	$4.0x10^4$	$1.9x10^5$	$2.9x10^4$	0.65	0.10
01/26/09	$2.4x10^5$	0.74	$1.1x10^4$	$7.2x10^4$	$3.7x10^3$	0.24	0.01
03/28/09	$2.3x10^5$	n.d.	n.d.	n.d.	n.d.	n.d.	n.d.
05/25/09	$3.7x10^5$	0.12	$3.3x10^5$	$1.6x10^6$	$1.7x10^5$	5.44	0.56
10/01/09	$1.8x10^5$	0.41	$9.8x10^4$	$4.7x10^5$	$5.3x10^4$	1.57	0.18
12/02/09	$3.5x10^5$	0.27	$2.0x10^5$	$1.5x10^6$	$1.6x10^5$	5.00	0.53
Mean	*$2.3x10^5$*	*0.43*	*$1.2x10^5$*	*$6.6x10^5$*	*$8.9x10^4$*	*2.20*	*0.30*
Std. Dev.	*$1.1x10^5$*	*0.21*	*$1.2x10^5$*	*$7.1x10^5$*	*$6.9x10^4$*	*2.39*	*0.23*

Date	Tidal Prism (m^3)	Return Flow b	GW Flux (m^3 day^{-1})	DIC Flux (mol day^{-1})	CH_4 Flux (mmol day^{-1})	DIC Flux (mol m^{-2} day^{-1})	CH_4 Flux (mmol m^{-2} day^{-1})
MH							
07/12/08	$6.4x10^6$	0.80	$2.7x10^5$	$7.6x10^5$	$7.9x10^4$	0.06	0.007
10/12/08	$1.3x10^7$	0.79	$2.6x10^5$	$7.8x10^5$	$3.1x10^4$	0.06	0.003
01/23/09	$7.1x10^6$	0.75	$1.9x10^5$	$7.5x10^4$	$1.2x10^4$	0.01	0.001
04/18/09	$6.8x10^6$	0.43	$6.4x10^4$	$1.1x10^5$	$3.4x10^3$	0.01	0.000
Mean	*$8.3x10^6$*	*0.69*	*$2.0x10^5$*	*$4.3x10^5$*	*$3.1x10^4$*	*0.04*	*0.003*
Std. Dev.	*$3.1x10^6$*	*0.18*	*$9.5x10^4$*	*$3.9x10^5$*	*$3.4x10^4$*	*0.03*	*0.003*

Table 5.5. Comparison of GHG fluxes from salt marshes via SGD and efflux to the atmosphere. Values are the mean flux plus or minus the standard deviation.

Site	DIC Flux (mol m^{-2} day^{-1})	CH_4 Flux (mmol m^{-2} day^{-1})	N_2O Flux (µmol m^{-2} day^{-1})	Reference
SGD-derived flux				
CI	0.27 ± 0.17	0.48 ± 0.44		This study
HN	1.53 ± 0.91	0.35 ± 0.45		This study
PC	2.2 ± 2.4	0.30 ± 0.23		This study
MH	0.04 ± 0.03	0.003 ± 0.003		This study
Okatee, South Carolina, USA	1.2	0.94	4.7	*Porubsky et al.* [2014]
North Inlet, South Carolina, USA	0.17			*Cai et al.* [2003]
Mean	0.90 ± 1.4	0.41 ± 0.84	4.7	
Sediment-atmosphere flux				
Dipper Harbour, Canada	0.22 ± 0.11	0.052 ± 0.115	1.1 ± 14	*Chmura et al.* [2011]
Kouchibouguacis Lagoon, Canada	0.26 ± 0.14	0.028 ± 0.087	7.1 ± 16	*Chmura et al.* [2011]
Plum Island, Massachusetts, USA	0.37 ± 0.10	0.74 ± 0.86	-32 ± 60	*Moseman-Valtierra et al.* [2011]
Dipper Harbour, Canada	0.059 ± 0.030	0.034 ± 0.025		*Magenheimer et al.* [1996]
Barataria Basin, Louisiana, USA			3	*Smith et al.* [1983]
Chesapeake Bay, Maryland, USA		2.7 ± 6.05		*Lipschultz* [1981]
Sapelo Island, Georgia, USA		0.075		*King and Wiebe* [1978]
Mean	0.23 ± 0.21	0.60 ± 2.80	-5.2 ± 68	

CHAPTER 6

CONCLUSIONS

The overarching goals of this work were to understand the influence of nitrogen and greenhouse gas cycling within coastal aquifers on the atmosphere and coastal ocean. A mass balance of N_2O revealed high rates of bioavailable nitrogen removal from permeable beach sand in **Chapter 2**. In **Chapter 3**, it was shown that the NO_3^- required to support this nitrogen removal was produced by nitrification that was made possible by the deep penetration of dissolved oxygen into beach sands. In **Chapter 4**, CH_4 production and consumption rates were measured along an entire groundwater flow path to demonstrate that methanotrophy controlled CH_4 export from a barrier island aquifer. Finally, in **Chapter 5**, groundwater-derived export of dissolved inorganic carbon, CH_4, and N_2O from salt marsh ecosystems was shown to rival the export of these gases via direct efflux to the atmosphere.

In **Chapter 2**, a hotspot of N_2O production was identified and the loss processes from this zone, including vertical diffusion and vertical and horizontal advection, were quantified. This mass balance showed that only a small fraction of the N_2O produced escaped to the atmosphere. The net N_2O production rate was estimated to be the sum of the measured loss rates: 47 $\mu mol\ m^{-2}\ day^{-1}$. This production was associated with NO_3^- consumption that removed bioavailable nitrogen from beach sand at a rate of 11 $mmol\ m^{-2}\ day^{-1}$. This rate rivals the highest denitrification rates reported for permeable coastal sediments [*Huettel et al.*, 2014].

In **Chapter 3**, daily oscillations in porewater dissolved oxygen concentrations from near 0% saturation at night to almost 100% saturation during the day were observed in the shallow aquifer beneath the upper beach on Cabretta Island, and were likely to be the result of benthic photosynthesis. Under oxic conditions, the net nitrification rate was 0.78 ± 0.26 mmol m^{-2} day^{-1}, while net NO_3^- removal was 1.2 ± 1.7 mmol m^{-2} day^{-1} when averaged across daily dissolved oxygen oscillations. These oscillations coupled nitrogen oxidation and reduction reactions, driving the removal of bioavailable nitrogen from beach sands.

The NO_3^- removal rate in **Chapter 3** was a factor of three lower than the same rate measured by a different approach in **Chapter 2**. The rate from **Chapter 3** was based on static bottle incubations, and denitrification rates are known to increase when porewater is advected through permeable sediment [*Huettel et al.*, 2014]. Therefore, the rate in **Chapter 2** that is more firmly rooted in in situ environmental conditions is likely to be a better estimate of the in situ NO_3^- removal rate. However, the nitrification rate reported in **Chapter 3** was too low to support the NO_3^- reduction rate measured in **Chapter 2**. Therefore, an additional nitrogen source, likely nitrogen fixation in shallower strata, was necessary to support the observed N_2O production. Taken together, these two chapters show that beach sand acts as a nitrogen filter that can mitigate some groundwater nitrogen loading to surface water bodies and simultaneously help to maintain them in nitrogen-limited states.

Potential methanogenesis rates of 22.2 ± 10.6 mmol m^{-2} day^{-1} were observed in the freshwater lens of the barrier island in **Chapter 4**. Very little of the CH_4 produced there was exported to the ocean, however, as rates of microbial methane consumption

were also elevated in beach sand (18 ± 2.1 mmol m^{-2} day^{-1}). CH_4 produced within the freshwater lens could not be exported to the ocean through the surficial beach aquifer as the approximately 160 day groundwater residence time in this system provided ample opportunity for the CH_4 to be consumed via methanotrophy. The more likely pathway for CH_4 export was the confined, sandy aquifer beneath the beach, but the much longer groundwater residence time there means that the rate of methanotrophy would have to be near zero for any CH_4 to escape consumption. This finding challenges the use of CH_4 as a tracer for submarine groundwater discharge [*Cable et al.*, 1996; *Kim and Hwang*, 2002]. While the presence of elevated CH_4 concentrations in coastal surface waters suggests groundwater discharge, this discharge can be present in the absence of CH_4 enrichment due to aquifer methanotrophy.

In **Chapter 5**, submarine groundwater discharge-derived fluxes of dissolved inorganic carbon, CH_4, and N_2O from salt marsh aquifers to adjacent tidal creeks were measured at four sites. These data were combined with other measurements from the literature to generate mean fluxes of 0.90 ± 1.4 mol m^{-2} day^{-1} for DIC, 0.41 ± 0.84 mmol m^{-2} day^{-1} for CH_4, and 4.7 μmol m^{-2} day^{-1} for N_2O. These fluxes ignore consumption processes such as methanotrophy that take place within the aquifer prior to groundwater discharge. The rate of methanotrophy in marsh soils is unlikely to be as high as it is in unsaturated beach sand, however, and flux calculations were carried out such the fluxes presented here are conservative estimates. Even so, more study is needed on microbial consumption of greenhouse gases at the interface between groundwater and surface water in salt marshes. For comparison, the mean efflux of greenhouse gases from the marsh soil surface to the atmosphere reported in the literature is 0.23 ± 0.21 mol m^{-2} day^{-1} for CO_2,

0.6 ± 2.8 mmol m^{-2} day^{-1} for CH_4, and -5.2 ± 68 mmol m^{-2} day^{-1} for N_2O. This comparison demonstrates that greenhouse gas export from salt marsh ecosystems by these two pathways are of the same order of magnitude, and that the submarine groundwater discharge-derived flux cannot be ignored when calculating the influence of these ecosystems on Earth's climate.

Eutrophication and climate change are the two greatest threats facing coastal communities and ecosystems. This work demonstrates that the processes taking place within coastal aquifers influence both of these threats. Permeable beach sand acts as a filter than can remove bioavailable nitrogen and greenhouse gases from the environment, efficiently consuming fixed nitrogen and methane that were produced elsewhere within a barrier island aquifer. The production of these materials supported active microbial communities capable of their consumption. In locations experiencing more human impact, this priming could cause shallow coastal aquifers to act as sinks for anthropogenic nitrogen and greenhouse gases. On the other hand, greenhouse gases produced within salt marsh soils can be exported from these systems via groundwater discharge as well as direct efflux to the atmosphere, roughly doubling the total greenhouse gas flux from these coastal wetlands.

LITERATURE CITED

Cable, J. E., G. C. Bugna, W. C. Burnett, and J. P. Chanton. 1996. Application of 222Rn and CH4 for assessment of groundwater discharge to the coastal ocean. Limnological Oceanography **41:** 1347-1353.

Huettel, M., P. Berg, and J. E. Kostka. 2014. Benthic Exchange and Biogeochemical Cycling in Permeable Sediments, p. 23-51. *In* C. A. Carlson and S. J. Giovannoni [eds.], Annual Review of Marine Science, Vol 6. Annual Review of Marine Science.

Kim, G., and D. W. Hwang. 2002. Tidal pumping of groundwater into the coastal ocean revealed from submarine ^{222}Rn and CH_4 monitoring. Geophysical Research Letters **29:** 1678.

REFERENCES

An, S., and S. Joye (2001), Enhancement of coupled nitrification-denitrification by benthic photosynthesis in shallow estuarine sediments, *Limnology and Oceanography*, *46*(1), 62-74.

Andersen, M. S., L. Baron, J. Gudbjerg, J. Gregersen, D. Chapellier, R. Jakobsen, and D. Postma (2007), Discharge of nitrate-containing groundwater into a coastal marine environment, *Journal of Hydrology*, *336*(1-2), 98-114.

Anschutz, P., T. Smith, A. Mouret, D. J., S. Bujan, D. Poirer, and P. Lecroart (2009), Tidal sands as biogeochemical reactors, *Estuarine, Coastal and Shelf Science*, *84*, 84-90.

Atkins, M. L., I. R. Santos, S. Ruiz-Halpern, and D. T. Maher (2013), Carbon dioxide dynamics driven by groundwater discharge in a coastal floodplain creek, *Journal of Hydrology*, *493*, 30-42.

Bange, H. W. (2006), Nitrous oxide and methane in European coastal waters, *Estuarine Coastal and Shelf Science*, *70*(3), 361-374.

Bange, H. W. (2008), Gaseous nitrogen compounds (NO, N_2O, N_2, NH_3) in the ocean, in *Nitrogen in the Marine Environment*, edited by D. G. Capone, D. A. Bronk, M. R. Mulholland and E. J. Carpenter, pp. 51-94, Elsevier, Burlington, MA.

Bendschneider, K., and R. J. Robinson (1952), A new spectrophotometric method for the determination of nitrite in sea water, *Journal of Marine Research*, *11*(1), 87-96.

Boehm, A. B., G. G. Shellenbarger, and A. Paytan (2004), Groundwater discharge: potential association with fecal indicator bacteria in the surf zone, *Environmental science & technology*, *38*(13), 3558-3566.

Boudreau, B. P., M. Huettel, S. Forster, R. A. Jahnke, A. McLachlan, J. J. Middelburg, P. Nielsen, F. Sansone, G. Taghon, and W. Van (2001), Permeable marine sediments: overturning an old paradigm, *EOS, Transactions American Geophysical Union*, *82*(11), 133-140.

Bourke, M. F., A. J. Kessler, and P. L. M. Cook (2014), Influence of buried Ulva lactuca on denitrification in permeable sediments, *Marine Ecology Progress Series*, *498*, 85-U420.

Braeckman, U., M. Y. Foshtomi, D. Van Gansbeke, F. Meysman, K. Soetaert, M. Vincx, and J. Vanaverbeke (2014), Variable importance of macrofaunal functional biodiversity for biogeochemical cycling in temperate coastal sediments, *Ecosystems*, *17*(4), 720-737.

Broecker, W. S., and T. H. Peng (1974), Gas-exchange rates between air and sea, *Tellus*, *26*(1-2), 21-35.

Brotas, V., A. Amorim-Ferreira, C. Vale, and F. Catarino (1990), Oxygen profiles in intertidal sediments of Ria Formosa (S. Portugal), *Hydrobiologia*, *207*(1), 123-130.

Brown, A. C. (2001), Biology of sandy beaches, *Encyclopedia of Ocean Sciences*, *5*, 2496-2504.

Bugna, G. C., J. P. Chanton, J. E. Cable, W. C. Burnett, and P. H. Cable (1996), The importance of groundwater discharge to the methane budgets of nearshore and continental shelf waters of the northeastern Gulf of Mexico, *Geochimica et Cosmochimica Acta*, *60*(23), 4735-4746.

Burnett, W. C., H. Bokuniewicz, M. Huettel, W. S. Moore, and M. Taniguchi (2003), Groundwater and pore water inputs to the coastal zone, *Biogeochemistry*, *66*(1-2), 3-33.

Cable, J. E., G. C. Bugna, W. C. Burnett, and J. P. Chanton (1996), Application of 222Rn and CH4 for assessment of groundwater discharge to the coastal ocean, *Limnological Oceanography*, *41*(6), 1347-1353.

Cai, W. J., Y. C. Wang, J. Krest, and W. S. Moore (2003), The geochemistry of dissolved inorganic carbon in a surficial groundwater aquifer in North Inlet, South Carolina, and the carbon fluxes to the coastal ocean, *Geochimica Et Cosmochimica Acta*, *67*(4), 631-639.

Canion, A., J. E. Kostka, T. M. Gihring, M. Huettel, J. E. E. van Beusekom, H. Gao, G. Lavik, and M. M. M. Kuypers (2014), Temperature response of denitrification and anammox reveals the adaptation of microbial communities to in situ temperatures in permeable marine sediments that span 50 degrees in latitude, *Biogeosciences*, *11*(2), 309-320.

Cardoso, R. B., R. Sierra-Alvarez, E. R. Flores, J. Gómez, and J. A. Field (2006), Sulfide oxidation under chemolithoautotrophic conditions, *Biotechnology and Bioengineering*, *95*(6), 1148-1157.

Carini, S. A., B. N. Orcutt, and S. B. Joye (2003), Interactions between methane oxidation and nitrification in coastal sediments, *Geomicrobiology Journal*, *20*(4), 355-374.

Casciotti, K. L., and C. Buchwald (2012), Insights on the marine microbial nitrogen cycle from isotopic approaches to nitrification, *Frontiers in Microbiology*, *3*.

Charbonnier, C., P. Anschutz, D. Poirier, S. Bujan, and P. Lecroart (2013), Aerobic respiration in a high-energy sandy beach, *Marine Chemistry*, *155*, 10-21.

Charette, M., R. Splivallo, and C. Herbold (2003), Salt marsh submarine groundwater discharge as traced by radium isotopes, *Marine Chemistry*.

Charette, M. A., and K. O. Buesseler (2004), Submarine groundwater discharge of nutrients and copper to an urban subestuary of Chesapeake Bay (Elizabeth River), *Limnology and Oceanography*, *49*(2), 376-385.

Chmura, G. L., L. Kellman, and G. R. Guntenspergen (2011), The greenhouse gas flux and potential global warming feedbacks of a northern macrotidal and microtidal salt marsh, *Environmental Research Letters*, *6*(4).

Chmura, G. L., S. C. Anisfeld, D. R. Cahoon, and J. C. Lynch (2003), Global carbon sequestration in tidal, saline wetland soils, *Global Biogeochemical Cycles*, *17*(4).

Ciais, P., et al. (2013), Carbon and other biogeochemical cycles, in *Climate Change 2013: The Physical Science Basis. Contribution of Working Group I to the Fifth Assessment Report of the Intergovernmental Panel on Climate Change*, edited by T. F. Stocker, D. Qin, G.-K. Plattner, M. Tignor, S. K. Allen, J. Boschung, A. Nauels, Y. Xia, V. Bex and P. M. Midgley, Cambridge University Press, Cambridge, United Kingdom and New York, NY, USA.

Cicerone, R. J., and R. S. Oremland (1988), Biogeochemical aspects of atmospheric methane, *Global Biogeochemical Cycles*, *2*(4), 299-327.

Cline, J. D. (1969), Spectrophotometric determination of hydrogen sulfide in natural waters, *Limnology and Oceanography*, *14*(3), 454-458.

Clough, T. J., R. R. Sherlock, and D. E. Rolston (2005), A review of the movement and fate of N_2O in the subsoil, *Nutrient Cycling in Agroecosystems*, *72*, 3-11.

Collins, W. H., and D. H. Easley (1999), Fresh-water lens formation in an unconfined barrier-island aquifer, *Journal of the American Water Resources Association*, *35*(1), 1-21.

Conrad, R. (1996), Soil microorganisms as controllers of atmospheric trace gases (H_2, CO, CH_4, OCS, N_2O, and NO), *Microbiological reviews*, *60*(4), 609-640.

Croteau, P., E. L. Atlas, S. M. Schauffler, D. R. Blake, G. S. Diskin, and K. A. Boering (2010), Effect of local and regional sources on the isotopic composition of nitrous oxide in the tropical free troposphere and tropopause layer, *Journal of Geophysical Research-Atmospheres*, *115*.

de Beer, D., F. Wenzhöfer, T. G. Ferdelman, S. E. Boehme, M. Huettel, J. E. E. van Beusekom, M. E. Böttcher, N. Musat, and N. Dubilier (2005), Transport and mineralization rates in north sea sandy intertidal sediments, Sylt-Rømø basin, Wadden sea, *Limnology and Oceanography*, *50*(1), 113-127.

Deborde, J., P. Anschutz, F. Guerin, D. Poirier, D. Marty, G. Boucher, G. Thouzeau, M. Canton, and G. Abril (2010), Methane sources, sinks and fluxes in a temperate tidal Lagoon: the Arcachon lagoon (SW France), *Estuarine Coastal and Shelf Science*, *89*(4), 256-266.

Deurer, M., C. von der Heide, J. Böttcher, W. H. M. Duijnisveld, D. Weymann, and R. Well (2008), The dynamics of N_2O near the groundwater table and the transfer of N_2O into the unsaturated zone: a case study from a sandy aquifer in Germany, *Catena*, *72*(3), 362-373.

Domenico, P. A., and F. W. Schwartz (1998), *Physical and chemical hydrogeology*, Wiley New York.

Dulaiova, H., R. Camilli, P. B. Henderson, and M. A. Charette (2010), Coupled radon, methane and nitrate sensors for large-scale assessment of groundwater discharge and non-point source pollution to coastal waters, *Journal of Environmental Radioactivity*, *101*, 553-563.

Ehrenhauss, S., and M. Huettel (2004), Advective transport and decomposition of chain-forming planktonic diatoms in permeable sediments, *Journal of Sea Research*, *52*(3), 179-197.

Frame, C. H., and K. L. Casciotti (2010), Biogeochemical controls and isotopic signatures of nitrous oxide production by a marine ammonia-oxidizing bacterium, *Biogeosciences*, *7*(9), 2695-2709.

Galloway, J. N., et al. (2004), Nitrogen cycles: past, present, and future, *Biogeochemistry*, *70*(2), 153-226.

Gao, H., F. Schreiber, G. Collins, M. M. Jensen, J. E. Kostka, G. Lavik, D. de Beer, H.-Y. Zhou, and M. M. Kuypers (2010), Aerobic denitrification in permeable Wadden Sea sediments, *The ISME Journal*, *4*, 417-426.

Gao, H., et al. (2012), Intensive and extensive nitrogen loss from intertidal permeable sediments of the Wadden Sea, *Limnology and Oceanography*, *57*(1), 185-198.

Gihring, T. M., A. Canion, A. Riggs, M. Huettel, and J. E. Kostka (2010), Denitrification in shallow, sublittoral Gulf of Mexico permeable sediments, *Limnology and Oceanography*, *55*(1), 43-54.

Goodfriend, G. A., and H. B. Rollins (1998), Recent barrier beach retreat in Georgia: dating exhumed salt marshes by aspartic acid racemization and post-bomb radiocarbon, *Journal of Coastal Research*, *14*(3), 960-969.

Grossman, E. L., B. K. Coffman, S. J. Fritz, and H. Wada (1989), Bacterial production of methane and its influence on groundwater chemistry in east-central Texas aquifers, *Geology*, *17*(6), 495-499.

Grunwald, M., O. Dellwig, M. Beck, J. W. Dippner, J. A. Freund, C. Kohlmeier, B. Schnetger, and H. Brumsack (2009), Methane in the southern North Sea: sources, spatial distribution and budgets, *Estuarine Coastal and Shelf Science*, *81*(4), 445-456.

Heyer, J., and U. Berger (2000), Methane emission from the coastal area in the southern Baltic Sea, *Estuarine Coastal and Shelf Science*, *51*(1), 13-30.

Hladik, C., and M. Alber (2012), Accuracy assessment and correction of a LIDAR-derived salt marsh digital elevation model, *Remote Sensing of Environment*, *121*, 224-235.

Hoagland, P., and S. Scatasta (2006), The economic effects of harmful algal blooms, in *Ecology of harmful algae*, edited, pp. 391-402, Springer.

Houston, J. R. (2008), The economic value of beaches—a 2008 update, *Shore & Beach*, *76*(3), 22-26.

Howarth, R. W. (1988), Nutrient limitation of net primary production in marine ecosystems, *Annual Review of Ecology and Systematics*, *19*, 89-110.

Huettel, M., P. Berg, and J. E. Kostka (2014), Benthic Exchange and Biogeochemical Cycling in Permeable Sediments, in *Annual Review of Marine Science, Vol 6*, edited by C. A. Carlson and S. J. Giovannoni, pp. 23-51.

Huettel, M., W. Ziebis, S. Forster, and G. W. Luther (1998), Advective transport affecting metal and nutrient distributions and interfacial fluxes in permeable sediments, *Geochimica et Cosmochimica Acta*, *62*(4), 613-631.

Jacinthe, P. A., and W. A. Dick (1993), Use of silicone tubing to sample nitrous oxide in the soil atmosphere, *Soil Biology and Biochemistry*, *28*(6), 721-726.

Jakobsen, R., and D. Postma (1999), Redox zoning, rates of sulfate reduction and interactions with Fe-reduction and methanogenesis in a shallow sandy aquifer, Romo, Denmark, *Geochimica Et Cosmochimica Acta*, *63*(1), 137-151.

Jansen, S., E. Walpersdorf, U. Werner, M. Billerbeck, M. E. Bottcher, and D. de Beer (2009), Functioning of intertidal flats inferred from temporal and spatial dynamics of O_2, H_2S and pH in their surface sediment, *Ocean Dynamics*, *59*(2), 317-332.

Jorgensen, B. B., and R. J. Parkes (2010), Role of sulfate reduction and methane production by organic carbon degradation in eutrophic fjord sediments (Limfjorden, Denmark), *Limnology and Oceanography*, *55*(3), 1338-1352.

Joye, S. B. (2002), Denitrification in the marine environment, in *Encyclopedia of Environmental Microbiology*, edited by G. Bitton, Wiley, New York, NY.

Joye, S. B., and I. C. Anderson (2008), Nitrogen cycling in coastal sediments, in *Nitrogen in the Marine Environment, 2nd Edition*, edited by D. G. Capone, D. A. Bronk, M. R. Mulholland and E. J. Carpenter, pp. 686-902, Elsevier.

Joye, S. B., S. V. Smith, J. T. Hollibaugh, and H. W. Paerl (1996), Estimating denitrification rates in estuarine sediments: A comparison of stoichiometric and acetylene based methods, *Biogeochemistry*, *33*(3), 197-215.

Kim, G., and D. W. Hwang (2002), Tidal pumping of groundwater into the coastal ocean revealed from submarine ^{222}Rn and CH_4 monitoring, *Geophysical Research Letters*, *29*(14), 1678.

King, G. M. (1997), Responses of atmospheric methane consumption by soils to global climate change, *Global Change Biology*, *3*(4), 351-362.

King, G. M., and W. J. Wiebe (1978), Methane release from soils of a Georgia salt marsh, *Geochimica Et Cosmochimica Acta*, *42*(4), 343-348.

Konhauser, K. (2007), *Introduction to Geomicrobiology*, Blackwell Publishing, Malden, MA.

Krest, J. M., W. S. Moore, L. R. Gardner, and J. T. Morris (2000), Marsh nutrient export supplied by groundwater discharge: evidence from radium measurements, *Global Biogeochemical Cycles*, *14*(1), 167-176.

Kroeger, K. D., P. W. Swarzenski, W. J. Greenwood, and C. Reich (2007), Submarine groundwater discharge to Tampa Bay: nutrient fluxes and biogeochemistry of the coastal aquifer, *Marine Chemistry*, *104*(1), 85-97.

Kuwae, T. (2003), Effect of emersion and immersion on the porewater nutrient dynamics of an intertidal sandflat in Tokyo Bay, *Estuarine, Coastal and Shelf Science*, *57*(5-6), 929-940.

Lam, P., M. M. Jensen, G. Lavik, D. F. McGinnis, B. Muller, C. J. Schubert, R. Amann, B. Thamdrup, and M. M. M. Kuypers (2007), Linking crenarchaeal and bacterial

nitrification to anammox in the Black Sea, *Proceedings of the National Academy of Sciences of the United States of America*, *104*(17), 7104-7109.

LaMontagne, M. G., R. Duran, and I. Valiela (2003), Nitrous oxide sources and sinks in coastal aquifers and coupled estuarine receiving waters, *The Science of the Total Environment*, *309*, 139-149.

Laursen, A. E., and S. P. Seitzinger (2002), The role of denitrification in nitrogen removal and carbon mineralization in Mid-Atlantic Bight sediments, *Continental Shelf Research*, *22*(9), 1397-1416.

Le Mer, J., and P. Roger (2001), Production, oxidation, emission and consumption of methane by soils: a review, *European Journal of Soil Biology*, *37*(1), 25-50.

Lipschultz, F. (1981), Methane release from a brackish intertidal salt-marsh embayment of Chesapeake Bay, Maryland, *Estuaries*, *4*(2), 143-145.

Magenheimer, J. F., T. R. Moore, G. L. Chmura, and R. J. Daoust (1996), Methane and carbon dioxide flux from a macrotidal salt marsh, Bay of Fundy, New Brunswick, *Estuaries*, *19*(1), 139-145.

Maher, D. T., I. R. Santos, L. Golsby-Smith, J. Gleeson, and B. D. Eyre (2013), Groundwater-derived dissolved inorganic and organic carbon exports from a mangrove tidal creek: The missing mangrove carbon sink?, *Limnology and Oceanography*, *58*(2), 475-488.

Martens, C. S., D. B. Albert, and M. J. Alperin (1998), Biogeochemical processes controlling methane in gassy coastal sediments - Part 1. A model coupling organic matter flux to gas production, oxidation and transport, *Continental Shelf Research*, *18*(14-15), 1741-1770.

McIlvin, M. R., and K. L. Casciotti (2010), Fully automated system for stable isotopic analyses of dissolved nitrous oxide at natural abundance levels, *Limnology and Oceanography-Methods*, *8*, 54-66.

McLeod, E., G. L. Chmura, S. Bouillon, R. Salm, M. Bjork, C. M. Duarte, C. E. Lovelock, W. H. Schlesinger, and B. R. Silliman (2011), A blueprint for blue carbon: toward an improved understanding of the role of vegetated coastal habitats in sequestering CO2, *Frontiers in Ecology and the Environment*, *9*(10), 552-560.

Meyer, R. L., D. E. Allen, and S. Schmidt (2008), Nitrification and denitrification as sources of sediment nitrous oxide production: a microsensor approach, *Marine Chemistry*, *110*(1-2), 68-76.

Middelburg, J. J., and J. Nieuwenhuize (2000), Nitrogen uptake by heterotrophic bacteria and phytoplankton in the nitrate-rich Thames estuary, *Marine Ecology Progress Series*, *203*.

Middelburg, J. J., G. Klaver, J. Nieuwenhuize, R. M. Markusse, T. Vlug, and F. J. W. A. van der Nat (1995), Nitrous oxide emissions from estuarine intertidal sediments, *Hydrobiologia*, *311*, 43-55.

Millero, F. J. (2006), *Chemical Oceanography*, Third ed., CRC Press, Taylor & Francis Group, Boca Raton.

Mizota, C., K. Noborio, and Y. Mori (2012), The Great Cormorant (*Phalacrocorax carbo)* colony as a "hot spot" of nitrous oxide (N_2O) emission in central Japan, *Atmospheric Environment*, *57*, 29-34.

Moore, W. S. (1999), The subterranean estuary: a reaction zone of ground water and sea water, *Marine Chemistry*, *65*, 111-125.

Moore, W. S. (2007), Seasonal distribution and flux of radium isotopes on the southeastern U.S. continental shelf, *Journal of Geophysical Research*, *112*(C10), 1-16.

Moore, W. S., and A. M. Wilson (2005), Advective flow through the upper continental shelf driven by storms, buoyancy, and submarine groundwater discharge, *Earth and Planetary Science Letters*, *235*(3), 564-576.

Moore, W. S., and T. J. Shaw (2008), Fluxes and behavior of radium isotopes, barium, and uranium in seven Southeastern US rivers and estuaries, *Marine Chemistry*, *108*(3), 236-254.

Moore, W. S., J. O. Blanton, and S. B. Joye (2006), Estimates of flushing times, submarine groundwater discharge, and nutrient fluxes to Okatee Estuary, South Carolina, *Journal of Geophysical Research*, *111*, C09006.

Moore, W. S., J. M. Krest, G. Taylor, E. Roggenstein, S. B. Joye, and R. Lee (2002), Thermal evidence of water exchange through a coastal aquifer: Implications for nutrient fluxes, *Geophysical Research Letters*, *29*(14), 1704.

Moseman-Valtierra, S., R. Gonzalez, K. D. Kroeger, J. W. Tang, W. C. Chao, J. Crusius, J. Bratton, A. Green, and J. Shelton (2011), Short-term nitrogen additions can shift a coastal wetland from a sink to a source of N2O, *Atmospheric Environment*, *45*(26), 4390-4397.

Myhre, G., et al. (2013), Anthropogenic and natural radiative forcing, in *Climate Change 2013: The Physical Science Basis. Contribution of Working Group I to the Fifth*

Assessment Report of the Intergovernmental Panel on Climate Change, edited by T. F. Stocker, D. Qin, G.-K. Plattner, M. Tignor, S. K. Allen, J. Boschung, A. Nauels, Y. Xia, V. Bex and P. M. Midgley, Cambridge University Press, Cambridge, United Kingdom and New York, NY, USA.

Neale, C. N., J. B. Hughes, and C. H. Ward (2000), Impacts of unsaturated zone properties on oxygen transport and aquifer reaeration, *Groundwater*, *38*(5), 784-794.

Nielsen, M., A. Gieseke, D. de Beer, and N. P. Revsbech (2009), Nitrate, nitrite, and nitrous oxide transformations in sediments along a salinity gradient in the Weser Estuary, *Aquatic Microbial Ecology*, *55*(1), 39-52.

Niencheski, L., H. Windom, and W. S. Moore (2007), Submarine groundwater discharge of nutrients to the ocean along a coastal lagoon barrier, …, *Marine Chemistry*.

Nixon, S. W. (1995), Coastal marine eutrophication: a definition, social causes, and future concerns, *Ophelia*, *41*, 199-219.

Oremland, R. S., and S. Polcin (1982), Methanogenesis and sulfate reduction - competitive and noncompetitive substrates in estuarine sediments, *Applied and Environmental Microbiology*, *44*(6), 1270-1276.

Paerl, H. W. (1997), Coastal eutrophication and harmful algal blooms: Importance of atmospheric deposition and groundwater as" new" nitrogen and other nutrient sources, *Limnology and oceanography*, *42*(5), 1154-1165.

Paerl, H. W., R. L. Dennis, and D. R. Whitall (2002), Atmospheric deposition of nitrogen: implications for nutrient over-enrichment of coastal waters, *Estuaries*, *25*(4B), 677-693.

Parkes, R. J., F. Brock, N. Banning, E. R. C. Hornibrook, E. G. Roussel, A. J. Weightman, and J. C. Fry (2012), Changes in methanogenic substrate utilization and communities with depth in a salt-marsh, creek sediment in southern England, *Estuarine Coastal and Shelf Science*, *96*, 170-178.

Pilkey, O. H., J. A. G. Cooper, and D. A. Lewis (2009), Global distribution and geomorphology of fetch-limited barrier islands, *Journal of Coastal Research*, *25*(4), 819-837.

Porubsky, W. P. (2008), Nutrient-replete benthic microalgae as a source of dissolved organic carbon to coastal waters, *Estuaries and Coasts*, *31*(5), 860-876.

Porubsky, W. P., S. B. Joye, W. S. Moore, K. Tuncay, and C. Meile (2010), Field measurements and modeling of groundwater flow and biogeochemistry at Moses Hammock, a backbarrier island on the Georgia coast, *Biogeochemistry*, *104*, 69-70.

Porubsky, W. P., N. B. Weston, W. S. Moore, C. Ruppel, and S. B. Joye (2014), Dynamics of submarine groundwater discharge and associated fluxes of dissolved nutrients, carbon, and trace gases to the coastal zone (Okatee River estuary, South Carolina), *Geochimica et Cosmochimica Acta*, *131*, 81-97.

Post, W. M., and K. C. Kwon (2000), Soil carbon sequestration and land‐use change: processes and potential, *Global change biology*, *6*(3), 317-327.

Ragotzkie, R. A., and R. A. Bryson (1955), Hydrography of the Duplin River, Sapelo Island, Georgia, *Bulletin of Marine Science of the Gulf and Caribbean*, *5*(4), 297-314.

Rao, A. M. F., M. J. McCarthy, W. S. Gardner, and R. A. Jahnke (2007), Respiration and denitrification in permeable continental shelf deposits on the South Atlantic Bight: rates of carbon and nitrogen cycling from sediment column experiments, *Continental Shelf Research*, *27*(13), 1801-1819.

Rao, A. M. F., M. J. McCarthy, W. S. Gardner, and R. A. Jahnke (2008), Respiration and denitrification in permeable continental shelf deposits on the South Atlantic Bight: N-2 : Ar and isotope pairing measurements in sediment column experiments, *Continental Shelf Research*, *28*(4-5), 602-613.

Robinson, C., L. Li, and D. A. Barry (2007), Effect of tidal forcing on a subterranean estuary, *Advances in Water Resources*, *30*(4), 851-865.

Sáenz, J. P., E. C. Hopmans, D. Rogers, P. B. Henderson, M. A. Charette, S. Schouten, K. L. Casciotti, J. S. Sinninghe Damsté, and T. I. Eglinton (2012), Distribution of anaerobic ammonia-oxidizing bacteria in a subterranean estuary, *Marine Chemistry*, *136*, 7-13.

Samarkin, V. A., M. T. Madigan, M. W. Bowles, K. L. Casciotti, J. C. Priscu, C. P. Mckay, and S. B. Joye (2010), Abiotic nitrous oxide emission from the hypersaline Don Juan Pond in Antarctica, *Nature Geoscience*, *3*(5), 341-344.

Sanford, R. A., et al. (2012), Unexpected nondenitrifier nitrous oxide reductase gene diversity and abundance in soils, *Proceedings of the National Academy of Sciences of the United States of America*, *109*(48), 19709-19714.

Santoro, A. E. (2010), Microbial nitrogen cycling at the salwater-freshwater interface, *Hydrogeology Journal*, *18*, 187-202.

Santos, I. R., W. C. Burnett, J. P. Chanton, and B. Mwashote (2008), Nutrient biogeochemistry in a Gulf of Mexico subterranean estuary and groundwater-derived fluxes to the coastal ocean, *Limnology and Oceanography*.

Santos, I. R., W. C. Burnett, T. Dittmar, I. G. N. A. Suryaputra, and J. P. Chanton (2009a), Tidal pumping drives nutrient and dissolved organic matter dynamics in a Gulf of Mexico subterranean estuary, *Geochimica et Cosmochimica Acta*, *73*(5), 1325-1339.

Santos, I. R., N. Dimova, R. N. Peterson, B. Mwashote, J. P. Chanton, and W. C. Burnett (2009b), Extended time series measurements of submarine groundwater discharge tracers (^{222}Rn and CH_4) at a coastal site in Florida, *Marine Chemistry*, *113*(1), 137-147.

Schippers, A., and B. B. Jørgensen (2002), Biogeochemistry of pyrite and iron sulfide oxidation in marine sediments, *Geochimica et Cosmochimica Acta*, *66*(1), 85-92.

Schlesinger, W. H. (2009), On the fate of anthropogenic nitrogen, *Proceedings of the National Academy of Sciences*, *106*(1), 203-208.

Schultz, G., and C. Ruppel (2002), Constraints on hydraulic parameters and implications for groundwater flux across the upland-estuary interface, *Journal of Hydrology*, *260*, 255-269.

Schutte, C. A., K. Hunter, P. McKay, D. Di Iorio, S. B. Joye, and C. Meile (2013), Patterns and controls of nutrient concentrations in a southeastern United States tidal creek, *Oceanography*, *26*(3), 132-139.

Segarra, K. E. A., C. Comerford, J. Slaughter, and S. B. Joye (2013), Impact of electron acceptor availability on the anaerobic oxidation of methane in coastal freshwater and brackish wetland sediments, *Geochimica Et Cosmochimica Acta*, *115*, 15-30.

Seitzinger, S. P., and S. W. Nixon (1985), Eutrophication and the rate of denitrification and N_2O production in coastal marine sediments, *Limnology and Oceanography*, *30*(6), 1332-1339.

Slomp, C. P., and P. Van Cappellen (2004), Nutrient inputs to the coastal ocean through submarine groundwater discharge: controls and potential impact, *Journal of Hydrology*, *295*, 64-86.

Smith, C. J., R. D. Delaune, and W. H. Patrick (1983), Nitrous oxide emission from Gulf Coast wetlands, *Geochimica Et Cosmochimica Acta*, *47*(10), 1805-1814.

Solorzano, L. (1969), Determination of ammonia in natural waters by the phenolhypochlorite method, *Limnology and Oceanography*, *14*(5), 799-801.

Steppe, T. F., and H. W. Paerl (2005), Nitrogenase activity and nifH expression in a marine intertidal microbial mat, *Microbial Ecology*, *49*(2), 315-324.

Strickland, J. D. H., and T. R. Parsons (1972), *A practical handbook of seawater analysis*, 2nd ed., Bulletin of the Fisheries Research Board of Canada.

Stutz, M. L., and O. H. Pilkey (2001), A review of global barrier island distribution, *Journal of Coastal Research*(Special Issue 34), 15-22.

Tamimi, A., E. B. Rinker, and O. C. Sandall (1994), Diffusion coefficients for hydrogen sulfide, carbon dioxide, and nitrous oxide in water over the temperature range 293-368 K, *Journal of Chemical and Engineering Data*, *39*(2), 330-332.

Thang, N. M., V. Bruchert, M. Formolo, G. Wegener, L. Ginters, B. B. Jorgensen, and T. G. Ferdelman (2013), The Impact of Sediment and Carbon Fluxes on the Biogeochemistry of Methane and Sulfur in Littoral Baltic Sea Sediments (Himmerfjarden, Sweden), *Estuaries and Coasts*, *36*(1), 98-115.

Treude, T., and W. Ziebis (2010), Methane oxidation in permeable sediments at hydrocarbon seeps in the Santa Barbara Channel, California, *Biogeosciences*, *7*(10), 3095-3108.

Ueda, S., C.-S. U. Go, M. Suzumura, and E. Sumi (2003), Denitrification in a seashore sandy deposit influenced by groundwater discharge, *Biogeochemistry*, *63*(2), 187-205.

Voss, C. I., and A. M. Provost (2002), A model for saturated-unsaturated, variable-density ground-water flow with solute or energy transport, *U.S. Geological Survey Water Resources Investigations Report*, 02-4231.

Walther, G.-R., E. Post, P. Convey, A. Menzel, C. Parmesan, T. J. C. Beebee, J.-M. Fromentin, O. Hoegh-Guldberg, and F. Bairlein (2002), Ecological responses to recent climate change, *Nature*, *416*(6879), 389-395.

Werner, U., M. Billerbeck, L. Polerecky, U. Franke, M. Huettel, J. E. E. van Beusekom, and D. de Beer (2006), Spatial and temporal patterns of mineralization rates and oxygen distribution in a permeable intertidal sand flat (Sylt, Germany), *Limnology and Oceanography*, *51*(6), 2549-2563.

Weston, N. B., J. T. Hollibaugh, and S. B. Joye (2009), Population growth away from the coastal zone: thirty years of land use change and nutrient export in the Altamaha River, GA, *Science of the Total Environment*, *407*(10), 3347-2256.

Weston, N. B., W. P. Porubsky, V. A. Samarkin, M. Erickson, S. E. Macavoy, and S. B. Joye (2006), Porewater stoichiometry of terminal metabolic products, sulfate, and dissolved organic carbon and nitrogen in estuarine intertidal creek-bank sediments, *Biogeochemistry*, *77*(3), 375-408.

Wilson, A. M., and L. R. Gardner (2006), Tidally driven groundwater flow and solute exchange in a marsh: numerical simulations, *Water Resources Research*, *42*(1).

Wilson, A. M., W. S. Moore, S. B. Joye, J. L. Anderson, and C. A. Schutte (2011), Storm-driven groundwater flow in a salt marsh, *Water Resources Research*, *47*(2), W02535.

Yamamoto, S., J. B. Alcauskas, and T. E. Crozier (1976), Solubility of methane in distilled water and seawater, *Journal of Chemical and Engineering Data*, *21*(1), 78-80.